

## **INFORMATION TO USERS**

**This manuscript has been reproduced from the microfilm master. UMI films the text directly from the original or copy submitted. Thus, some thesis and dissertation copies are in typewriter face, while others may be from any type of computer printer.**

**The quality of this reproduction is dependent upon the quality of the copy submitted. Broken or indistinct print, colored or poor quality illustrations and photographs, print bleedthrough, substandard margins, and improper alignment can adversely affect reproduction.**

**In the unlikely event that the author did not send UMI a complete manuscript and there are missing pages, these will be noted. Also, if unauthorized copyright material had to be removed, a note will indicate the deletion.**

**Oversize materials (e.g., maps, drawings, charts) are reproduced by sectioning the original, beginning at the upper left-hand corner and continuing from left to right in equal sections with small overlaps. Each original is also photographed in one exposure and is included in reduced form at the back of the book.**

**Photographs included in the original manuscript have been reproduced xerographically in this copy. Higher quality 6" x 9" black and white photographic prints are available for any photographs or illustrations appearing in this copy for an additional charge. Contact UMI directly to order.**

# **UMI**

A Bell & Howell Information Company  
300 North Zeeb Road, Ann Arbor, MI 48106-1346 USA  
313:761-4700 800:521-0600



**Characterization and modulation of ionic  
conductances in cultured rabbit  
retinal pigment epithelial (RPE) cells**

By

Qianping Tao

Submitted to the Faculty of Graduate Studies  
in partial fulfillment of the requirements  
for the degree of Doctor of Philosophy

at

Dalhousie University  
Halifax, Nova Scotia,  
Canada

(March, 1997)

© Copyright by Qianping Tao, 1997



National Library  
of Canada

Acquisitions and  
Bibliographic Services

395 Wellington Street  
Ottawa ON K1A 0N4  
Canada

Bibliothèque nationale  
du Canada

Acquisitions et  
services bibliographiques

395, rue Wellington  
Ottawa ON K1A 0N4  
Canada

*Your file Votre référence*

*Our file Notre référence*

The author has granted a non-exclusive licence allowing the National Library of Canada to reproduce, loan, distribute or sell copies of this thesis in microform, paper or electronic formats.

The author retains ownership of the copyright in this thesis. Neither the thesis nor substantial extracts from it may be printed or otherwise reproduced without the author's permission.

L'auteur a accordé une licence non exclusive permettant à la Bibliothèque nationale du Canada de reproduire, prêter, distribuer ou vendre des copies de cette thèse sous la forme de microfiche/film, de reproduction sur papier ou sur format électronique.

L'auteur conserve la propriété du droit d'auteur qui protège cette thèse. Ni la thèse ni des extraits substantiels de celle-ci ne doivent être imprimés ou autrement reproduits sans son autorisation.

0-612-24762-7

Canada

**DALHOUSIE UNIVERSITY**

**FACULTY OF GRADUATE STUDIES**

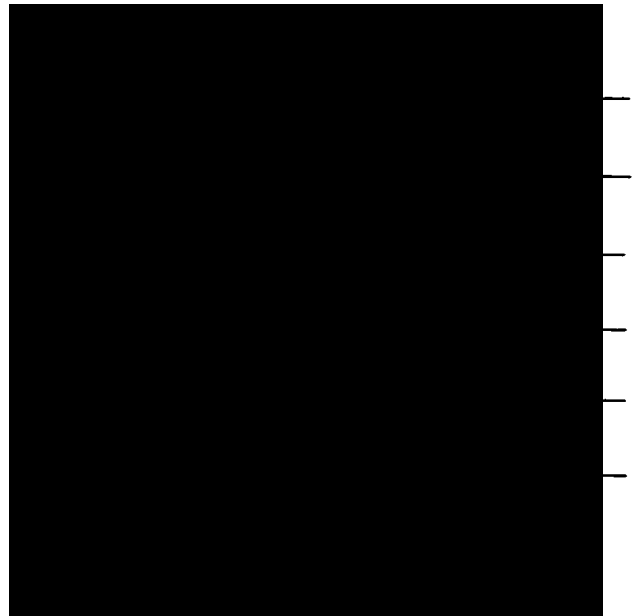
The undersigned hereby certify that they have read and recommend to the Faculty of Graduate Studies for acceptance a thesis entitled “Characterization and Modulation of Ionic Conductances in Cultured Rabbit Retinal Pigment Epithelial (RPE) Cells”

by Qian Ping Tao

in partial fulfillment of the requirements for the degree of Doctor of Philosophy.

Dated: March 27, 1997

External Examiner  
Research Supervisor  
Examining Committee



# Dalhousie University

Date: March 1997

Author: Qianping Tao

Title : Characterization of ionic conductances and their modulation in  
cultured rabbit retinal pigment epithelial (RPE) cells

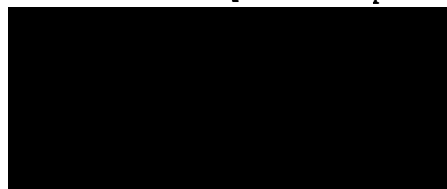
Department or School: Department of Pharmacology,

Faculty of Medicine

Degree: Ph.D.

Convocation: May Year: 1997

Permission is herewith granted to Dalhousie University to circulate and to have copied for non-commercial purposes, at its discretion, the above title upon the request of individuals or institutions.



Signature of Author

The author reserves other publication rights, and neither the thesis nor extensive extracts from it may be printed or otherwise reproduced without the author's written permission.

The author attests that permission has been obtained for the use of any copyrighted material appearing in this thesis (other than brief excerpts requiring only proper acknowledgment in scholarly writing), and that all such use is clearly acknowledged.

This thesis is dedicated to my parents  
for their consistent moral support.

此论文献给我父母，  
为他们自始至终的精神支助。

# Table of Contents

Page #

---

|  |          |
|--|----------|
| List of Figures .....  | x        |
| List of Tables .....   | xiii     |
| Abstract .....   | xiv      |
| Publications .....   | xv       |
| List of Abbreviations .....  | xvi      |
| Acknowledgements .....   | xix      |
| <b>1 Introduction .....</b>  | <b>1</b> |
| 1. Processing of visual images .....   | 4        |
| 2. General structure and functions of the RPE .....  | 6        |
| 2.1 Basal plasma membrane .....  | 7        |
| 2.2 Apical plasma membrane .....   | 8        |
| 2.3 Lateral plasma membrane .....  | 10       |
| 2.4 Unusual features of cytoplasmic organelles .....   | 11       |
| 2.5 Other functions of the RPE .....   | 11       |
| 3. Transport and membrane properties of the RPE .....  | 12       |
| 3.1 Light induced electrical response of the RPE .....   | 13       |
| 3.2 Electrogenic, electroneutral transport systems and passive ion<br>conductances in the RPE .....              | 16       |
| 3.3 Ionic transport mechanisms underlying the RPE membrane potential<br>changes in response to light onset ..... | 18       |



|          |   |           |
|----------|---|-----------|
| 3.4      | Regulation of ion channels within RPE cells .....   | 20        |
| 4.       | Experimental rationale and objectives .....   | 26        |
| 4.1      | Specific objectives .....   | 27        |
| 4.1.1    | To establish and identify viable primary rabbit RPE cell<br>cultures .....  | 27        |
| 4.1.2    | To characterize K <sup>+</sup> conductances in isolated and cultured<br>rabbit RPE cells .....  | 27        |
| 4.1.3    | To examine $\alpha_1$ -adrenergic modulation of maxi-K <sub>Ca</sub> currents<br>(I <sub>K(Ca)</sub> ) in cultured rabbit RPE cells ..... | 28        |
| 5.       | Techniques used in this study: Patch-clamp recording .....  | 29        |
| 5.1.     | Whole-cell voltage patch-clamp recording .....  | 29        |
| 5.2.     | Single-channel recording .....  | 31        |
| <b>2</b> | <b>Materials and Methods</b> .....  | <b>33</b> |
| 1.       | Materials .....   | 33        |
| 1.1      | Materials for cell preparation .....  | 33        |
| 1.2      | Materials for immunocytochemical and fluorescent experiments ..   | 33        |
| 1.3      | Solutions and chemicals for the electrophysiological experiments .  | 35        |
| 2.       | Methods .....   | 36        |
| 2.1      | Cell dissociation and culture .....   | 36        |
| 2.2      | Trypan blue exclusion test for cell viability .....   | 38        |
| 2.3      | Immunocytochemical and Immunofluorescent experiments .....  | 39        |
| 2.4      | Superfusion system .....  | 41        |

|          |   |           |
|----------|---|-----------|
| 2.5      | Fabrication of recording electrodes .....   | 43        |
| 2.6      | Electrophysiological recording techniques .....   | 44        |
| 2.7      | Data analysis and figure construction .....   | 49        |
| <b>3</b> | <b>Results</b> .....  | <b>51</b> |
| 1.       | Establishment of rabbit RPE cell culture .....  | 51        |
| 2.       | Cell identification .....   | 54        |
| 3.       | Whole-cell currents and membrane properties in cultured rabbit RPE cells ..   | 56        |
| 4.       | Characterization of outward current in cultured rabbit RPE cells .....  | 60        |
| 4.1      | Outward current is $K^+$ selective .....  | 60        |
| 4.2.     | Voltage-dependence and kinetics of the outward $K^+$ current .....  | 63        |
| 4.3      | Effects of $K^+$ channel blockers on the outward $K^+$ current .....  | 70        |
| 4.4      | Fast-inactivating outward $K^+$ current .....   | 76        |
| 4.5      | The inwardly rectifying current in rabbit RPE cells is selective for $K^+$<br>.....   | 84        |
| 4.6.     | Barium ( $Ba^{2+}$ ) and cesium ( $Cs^+$ ) block the inward rectifier .....   | 88        |
| 4.7.     | Time-dependent decay of the inward rectifier at negative potentials<br>.....  | 93        |
| 5.       | Evidence for the presence of large conductance $Ca^{2+}$ -activated $K^+$ (maxi- $K_{Ca}$ )<br>channels in rabbit RPE cells ..... | 95        |
| 5.1      | Whole-cell recording .....  | 95        |
| 5.1.1    | Increases in $[Ca^{2+}]_i$ enhance voltage-dependent outward $K^+$<br>current ( $I_K$ ) .....                                     | 95        |

|          |  |     |
|----------|--|-----|
| 5.1.2    | Dependence of the outward $K^+$ current upon $[Ca^{2+}]_i$ . . . . .   | 104 |
| 5.1.3    | Sensitivity of $I_K$ to selective maxi- $K^+$ channel blockers . .   | 105 |
| 5.2      | Single-channel recording . . . . .   | 109 |
| 6.       | $\alpha_1$ -Adrenergic modulation of maxi- $K_{Ca}$ channels in rabbit RPE cells . . . . .                               | 120 |
| 6.1      | Whole-cell recording . . . . .   | 120 |
| 6.1.1    | Phenylephrine (PhE) increases the macroscopic outwardly<br>rectifying $K^+$ current . . . . .                            | 120 |
| 6.1.2    | The outward $K^+$ current induced by PhE was sensitive to the<br>specific maxi- $K_{Ca}$ channel blocker, IbTX . . . . . | 124 |
| 6.1.3    | PhE-induced increases in maxi- $K_{Ca}$ current ( $I_{K(Ca)}$ ) involve<br>$\alpha_1$ -adrenergic receptors . . . . .    | 127 |
| 6.1.4    | Effect of internal application of $IP_3$ . . . . .   | 129 |
| 6.2      | Single-channel recording . . . . .   | 132 |
| <b>4</b> | <b>Discussion</b> . . . . .  | 136 |
| 1.       | Membrane properties of rabbit RPE cells in primary culture . . . . .   | 136 |
| 2.       | Voltage-dependent $K^+$ currents in rabbit RPE cells: Comparison<br>with other cell types . . . . .                      | 137 |
| 2.1.     | Delayed rectifier . . . . .  | 137 |
| 2.2.     | Fast-inactivating outward rectifier . . . . .  | 139 |
| 2.3.     | Inward rectifier . . . . .   | 140 |
| 3.       | Calcium-activated $K^+$ current in rabbit RPE cells . . . . .  | 141 |
| 4.       | Modulation of maxi- $K_{Ca}$ channel activity by $\alpha_1$ -adrenergic receptors . . . . .                              | 146 |

|   |            |
|---|------------|
| 5. Other currents in rabbit RPE cells .....   | 147        |
| 6. Heterogeneity of K <sup>+</sup> channel type expression .....  | 148        |
| 7. Functions of various K <sup>+</sup> conductances observed in rabbit RPE cells .....                                    | 150        |
| 8. Physiological implications of maxi-K <sub>Ca</sub> channel modulation by α <sub>1</sub> -adrenergic<br>receptors ..... | 155        |
| 8.1. Subretinal ion and fluid absorption .....  | 156        |
| 8.2. Phagocytosis .....   | 157        |
| <b>5 Future directions .....</b>  | <b>159</b> |
| <b>6 Appendices .....</b>   | <b>161</b> |
| <b>7 References .....</b>   | <b>163</b> |

# List of Figures

Page #

|      |  |    |
|------|--|----|
| 1-1. | Cross section of the eye. ....   | 5  |
| 1-2. | Cross section of the neurosensory retina and the RPE. ....   | 5  |
| 1-3. | RPE cells, surface view. ....  | 7  |
| 1-4. | RPE cell, cross-sectional view. ....   | 8  |
| 1-5. | A DC-ERG (cat) in response to 5-min illumination. ....   | 14 |
| 1-6. | Diagrammatic summary of current knowledge of the $\alpha_1$ -adrenergic receptor activation cascade leading to $PIP_2$ breakdown. .... | 23 |
| 2-1. | Simplified schematic diagram of rabbit RPE cell dissociation procedure<br>.....  | 38 |
| 2-2. | Schematic diagram of different patch clamping configurations. ....   | 45 |
| 2-3. | Schematic diagram for whole-cell patch clamp recording. ....   | 47 |
| 2-4. | Patch-clamp recording, cell attached configuration. ....   | 50 |
| 3-1. | Photomicrographs of rabbit RPE explant and compact patches derived from confluent monolayer cultures. ....                             | 52 |
| 3-2. | Morphology of isolated rabbit RPE cells in culture. ....   | 53 |
| 3-3. | Immunocytochemical staining of cultured rabbit RPE cells. ....   | 55 |
| 3-4. | Voltage-dependent currents in rabbit RPE cells. ....   | 58 |
| 3-5. | Outward currents in rabbit RPE cells are carried by $K^+$ ions. ....   | 62 |
| 3-6. | Activation of outward $K^+$ current in rabbit RPE cells. ....  | 65 |
| 3-7. | Inactivation of outward $K^+$ current. ....  | 69 |
| 3-8. | Effect of external TEA on the outward $K^+$ current in rabbit RPE cells. .   | 72 |

| LIST OF FIGURES |   | Page # |
|-----------------|---|--------|
| 3-9.            | Effect of external 4-AP on the outward $K^+$ current. ....  | 75     |
| 3-10.           | Activation of the fast-inactivating outward $K^+$ current in rabbit RPE cells<br>.....                          | 78     |
| 3-11.           | Inactivation of the fast-inactivating outward $K^+$ current. ....   | 80     |
| 3-12.           | Quinine blocks the fast-inactivating outward current. ....  | 83     |
| 3-13.           | The inwardly rectifying current in rabbit RPE cells is dependent on $[K^+]_o$<br>.....                          | 86     |
| 3-14.           | Effect of external $Ba^{2+}$ on the inwardly rectifying $K^+$ current . ....                                    | 90     |
| 3-15.           | Effect of external $Cs^+$ on the inward rectifier. ....   | 92     |
| 3-16.           | $[Na^+]_o$ -dependent relaxation of the inwardly current at negative potentials<br>.....                        | 94     |
| 3-17.           | Ionomycin enhances and quinine blocks the outward $K^+$ current. ....   | 97     |
| 3-18.           | The effect of ionomycin on the outward $K^+$ current. ....  | 100    |
| 3-19.           | Ionomycin has no effect on $I_{K1}$ . ....  | 102    |
| 3-20.           | Outward $K^+$ currents are $Ca^{2+}$ -sensitive. ....   | 104    |
| 3-21.           | IbTX and CTX block the outward $K^+$ currents. ....   | 108    |
| 3-22.           | Identification of a large-conductance voltage-dependent $K^+$ channel. ...                                      | 111    |
| 3-23.           | The effect of ionomycin on the activity of the large conductance channel<br>.....                               | 112    |
| 3-24.           | The large-conductance channel is $Ca^{2+}$ -activated and $K^+$ selective. ...                                  | 115    |
| 3-25.           | The effect of $[Ca^{2+}]_i$ and cytosolic $Ba^{2+}$ on the open probability of the<br>$K_{(Ca)}$ channels. .... | 118    |
| 3-26.           | PhE increased macroscopic $I_K$ . ....  | 123    |
| 3-27.           | IbTX blocked PhE's effect on the $I_K$ . ....   | 126    |

## LIST OF FIGURES

|   | Page # |
|---|--------|
| 3-28. Prazosin inhibited the effect of PhE on $I_{K(Ca)}$ .....                             | 128    |
| 3-29. The effect of internal application of $IP_3$ on the $I_{K(Ca)}$ .....                 | 131    |
| 3-30. The PhE-induced current is due to the activation of a large conductance channel. .... | 133    |
| 3-31. The large-conductance channel activated by PhE is $K^+$ -selective. ....              | 134    |
| 4-1. Model of RPE ion transport mechanism. ....   | 151    |
| 4-2. Phagocytotic function of cultured rabbit RPE cells. ....                               | 154    |

# List of Tables

Page #

---

|      |  |    |
|------|--|----|
| 1-1  | Summary of RPE responses and their mechanisms upon light onset<br>.....                                | 19 |
| 3-1. | Summary of membrane properties and currents recorded from rabbit<br>RPE cells in primary culture. .... | 59 |



# ABSTRACT

---

The retinal pigment epithelium (RPE) is a monolayer of cuboidal cells which lies in close association with the photoreceptors of the neural retina. This epithelium is an indispensable component of the retina and has diverse functions which are essential for the maintenance of retinal viability. The RPE participates in both regulation of the ionic concentration within the subretinal space as well as the maintenance of the homeostasis of the microenvironment surrounding the photoreceptors.

In this study, membrane potential and ionic conductances as well as their modulation by adrenergic agonists were studied in cultured rabbit RPE cells using whole-cell, perforated-patch, and single-channel patch-clamp recording techniques. RPE cells had a mean membrane capacitance of  $27.0 \pm 0.8$  pF (SE,  $n=294$ ). The resting membrane potential averaged  $-31.0 \pm 1.4$  mV (SE,  $n=110$ ), but was as high as  $-60$  mV in some cells. When  $K^+$  was the principal cation in the recording electrode, depolarizing voltage steps from a holding potential of  $-60$  mV activated outwardly rectifying currents. These depolarization-activated outward currents were apparent in 80% of cells studied. Tail current analysis revealed that the outward currents were primarily  $K^+$  selective. The outwardly rectifying  $K^+$  current ( $I_K$ ) was the most frequently observed conductance in RPE cells and resembled the delayed rectifying  $K^+$  current described in other cells.  $I_K$  was blocked by tetraethylammonium ions ( $TEA^+$ ) and barium ( $Ba^{2+}$ ) and reduced by 4-aminopyridine (4-AP). In a small number of cells (7%), depolarization to  $-50$  mV or more positive potentials evoked a fast-inactivation outward  $K^+$  current ( $I_{Kf}$ ). An inwardly rectifying  $K^+$  current ( $I_{Ki}$ ) was also present in 40% of cells.  $I_{Ki}$  was blocked by extracellular  $Ba^{2+}$  or cesium ( $Cs^+$ ) and exhibited time-dependent decay at negative potentials, due to  $Na^+$  blockage.

The manipulation of cytosolic free  $Ca^{2+}$  ( $[Ca^{2+}]_i$ ) revealed a  $Ca^{2+}$ -activated component of  $I_K$ . Studies of  $Ca^{2+}$ -activated  $K^+$  current ( $I_{K(Ca)}$ ) were carried out by increasing the extracellular  $Ca^{2+}$  concentration ( $[Ca^{2+}]_o$ ) in the presence of a  $Ca^{2+}$  ionophore, ionomycin.  $I_{K(Ca)}$  was blocked by iberiotoxin (IbTX), a specific maxi- $K_{Ca}$  channel blocker. Single channel recording from cell-attached and excised membrane patches confirmed the presence of large conductance  $Ca^{2+}$ -activated  $K^+$  channels which could be classified as maxi- $K_{Ca}$  channels based on: 1) the large unitary conductance ( $>220$  pS with 130 mM  $K^+$ ), 2) the voltage dependence, 3) the dependence of the current reversal potential on the transmembrane  $K^+$  gradient, and 4) the  $[Ca^{2+}]_i$  dependence. Further experiments demonstrated that maxi- $K_{Ca}$  channels in rabbit RPE cells are modulated by the activation of  $\alpha_1$ -adrenoceptor coupled signalling pathway(s). Calcium released from intracellular stores by  $IP_3$  following  $\alpha_1$ -adrenoceptor activation, enhanced maxi- $K_{Ca}$  channel activity.

The  $K^+$  conductances reported here may provide conductive pathways which are important for maintaining ion and fluid homeostasis within the subretinal space, and may be also involved in other important cellular functions vital to the photoreceptors. This study also provides evidence for a role for  $\alpha_1$ -adrenoceptors in the modulation of maxi- $K_{Ca}$  channels in rabbit RPE cells. The modulation of maxi- $K_{Ca}$  channels may contribute to the physiological regulation of  $K^+$  transport and other important functions in this cell type.

# PUBLICATIONS

---

Parts of this thesis have been published in the following peer-reviewed journals:

**Tao, Qianping** and Kelly, M.E.M., 1996. Calcium-activated potassium currents in cultured rabbit RPE cells. *Curr. Eye. Res.* **15**:237-246

**Tao, Qianping**, Rafuse, P.E. and Kelly, M.E.M., 1994. Potassium currents in cultured rabbit retinal pigmented epithelial cells. *J. Memb. Biol.* **141**:123-138

**Tao, Qianping** and Kelly, M.E.M., 1995. Calcium-activated potassium currents in cultured rabbit RPE cells. *Invest. Ophthalmol. Vis. Sci. Suppl.* **36**: 2720

**Tao, Qianping**, Poyer, J.F. and Kelly, M.E.M., 1994. The pharmacology of potassium channels in mammalian retinal pigment epithelial cells. *Invest. Ophthalmol. Vis. Sci. Suppl.* **35**: 1455

**Tao, Qianping**, Poyer, P.F and Kelly, M.E.M., 1994. Ionic currents in rabbit retinal pigment epithelial cells. *Biophys J.* **66**: A440.

**Tao, Qianping**, Rafuse, P.E. and Kelly, M.E.M., 1993. Potassium and anion currents in rabbit retinal pigment epithelium. *Invest. Ophthalmol. Vis. Sci. Suppl.* **34**: 847.

# List of Abbreviation

---

The subscript 'i' or 'o' refers to intracellular/inward or extracellular/outward effects, respectively; and the bracket [ ] stands for the concentration (e.g.  $[K^+]_i$  = intracellular  $K^+$  concentration;  $I_{ki}$  = inward  $K^+$  current). Most of the abbreviations listed below are defined as they appear in the text.

|         |  |
|---------|--|
| 4-AP:   | 4-aminopyridine  |
| ABC:    | Avidin and Biotinylated horseradish peroxidase macromolecular Complex                                    |
| AMD:    | age-related macular degeneration   |
| cAMP:   | cyclic adenosine monophosphate   |
| cGMP:   | cyclic guanosine monophosphate   |
| CSR:    | central serous retinopathy   |
| CTX:    | charybdotoxin  |
| DAB:    | 3,3'-diaminobenzidine  |
| DAG:    | diacylglycerol   |
| DIDS:   | diisothiocyano-2-2 disulfonic acid stilbene  |
| DMEM:   | Dulbecco's Modified Eagle's Medium   |
| DMSO:   | dimethylsulphoxide   |
| EGTA:   | Ethylene Glycol-bis ( $\beta$ -Aminoethyl Ether) N,N,N',N'-Tetraacetic Acid ( $Ca^{2+}$ chelating agent) |
| $E_k$ : | equilibrium potential for potassium ion  |

|                     |  |
|---------------------|--|
| EPI:                | epinephrine  |
| ER:                 | endoplasmic reticulum  |
| $E_{rev}$ :         | reversal potential   |
| ERG:                | electroretinogram  |
| GDP:                | guanosine 5'-diphosphate   |
| GTP:                | guanosine 5'-triphosphate  |
| GTPtS:              | guanosine 5'- <i>O</i> -(3-thio)triphosphate (non-hydrolysable GTP analogue)                           |
| G protein:          | guanine nucleotide regulatory binding protein  |
| HEPES:              | N-(2-hydroxyethyl)piperazine-N'-(2-ethanesulphonic acid) (buffer, $pK_a = 7.5$ at $25^\circ\text{C}$ ) |
| IbTX:               | iberiotoxin  |
| IF:                 | intermediate filament  |
| $IP_3$ :            | inositol(1,4,5)-triphosphate   |
| IPM:                | interphotoreceptor matrix  |
| NE:                 | norepinephrine   |
| NMDG <sup>+</sup> : | N-methyl-D-glucamine <sup>+</sup>  |
| PBS:                | phosphate buffered saline  |
| PhE:                | phenylephrine  |
| PLC:                | phospholipase C  |
| PNMT:               | phenylethanolamine-N-methyltransferase   |
| $PIP_2$ :           | phosphatidylinositol-4,5-bisphosphate  |

|            |   |
|------------|---|
| RCS:       | Royal College of Surgeons                               |
| RMP:       | resting membrane potential                              |
| ROS:       | rod outer segments                                      |
| RP:        | retinitis pigmentosa                                    |
| RPE:       | retinal pigment epithelium                              |
| SD:        | standard deviation                                      |
| SE:        | standard error  |
| SITS:      | 4-acetamido-4'isothiocyanostibene-2,2'-disulphonic acid |
| TEA:       | tetraethylammonium                                      |
| TEP:       | transepithelial potential                               |
| $V_{ap}$ : | apical membrane potential                               |
| $V_{ba}$ : | basal membrane potential                                |

# Acknowledgements

---

I am deeply grateful to Dr. Mel Kelly for providing me with this challenging project and for her guidance and support during the course of my research. Her belief in my abilities has been a great encouragement. I will always remember that tenacity pays off.

I am indebted to Christine Jollimore for her friendship and professional technical assistance, especially in immunocytochemical assays. I acknowledge my co-students in the lab, Robert Gilbert and Jennifer Ryan for their friendship and helpful discussion. Special thanks also goes to Dr. John Poyer who was a postdoctoral fellow during part of my program and who provided me with the pictures of rabbit RPE phagocytosis.

I hereby extend my sincere thanks to Dr. Ken Renton who is the chairman of my committee and was the Department head during the first 3.5 years of my program. I benefitted immensely from his encouragement and support which enabled me to pull through a very difficult time.

I would also like to express appreciation to every single support staff in the departmental office: Janet Murphy, Luisa Vaughan, Karen Machan and Sandi Leaf, for all their help in the administrative work, and all the faculty members and my fellow students in the department who helped during my study. I would especially like to thank Dr. Greg Ferrier who has always been very helpful and patient in answering my numerous electrophysiology questions.

Finally, I would like to thank this department, the Killam Trust Fund of Dalhousie University and the Canadian Retinitis Pigmentosa Eye Research Foundation for their financial support.

# 1

## Introduction

---

**The retinal pigment epithelium (RPE)** is a monolayer of specialized epithelial cells situated between the choroidal blood supply and the neurosensory retina. The RPE is vital for the integrity of the photoreceptors and carries out a number of functions which are essential for the processing of incoming light rays.

Due to its key location and specific anatomy, the RPE acts as an important part of the blood-retinal barrier. The tight junctions of the RPE together with the endothelium of the choriocapillaris and the retinal blood vessels form the blood-retinal barrier, which restricts the exchange of certain substances between the neural retina and the choroid vascular system (Clark, 1986; Bok, 1993). The RPE regulates the transport of nutrients and co-factors from the choroid to the neural retina, and removes metabolic wastes in the opposite direction. Additionally, the RPE is responsible for the net movement of ions and water in the retinal to choroidal direction (Bok, 1988 & 1993; Clark, 1986; Steinberg and Miller, 1979; Zinn and Benjamin-Henkind, 1979). The capacity of the RPE to move water out of the subretinal space between the photoreceptor outer segments and the apical processes of the RPE, is important for maintaining the neurosensory retina in a proper state of dehydration and optical clarity (Bok, 1988). It is also the major factor responsible for neural retinal adhesion to the RPE layer (Bok, 1993; Clark, 1986; Steinberg and Miller, 1979; Zinn and Benjamin-Henkind, 1979). Additional contributions of the RPE to retinal adhesion include the close physical envelopment of the photoreceptor outer

segments by the apical processes of the epithelial cells and secretion of the interphotoreceptor matrix (IPM), a very thin layer of extracellular matrix material which separates the plasma membrane of the photoreceptor and the RPE cell (Zinn and Benjamin-Henkind, 1979; Bird, 1989; Marmor, 1989). Other functions of the RPE include storage, conversion and transport of vitamin A esters for incorporation into rhodopsin as the visual chromophore; phagocytosis and digestion of detached distal portions of the photoreceptor outer segments; and protection of the photoreceptors from light scatter and damaging levels of radiation (Bok, 1993 & 1988; Zinn and Benjamin-Henkind, 1979).

Once differentiated, the RPE does not renew itself by cell division, it continues to carry out its versatile functions throughout the lifetime of the individual unless such processes are lost due to disease. Because of the diverse functions of the RPE and its importance for retinal integrity, any alterations in the normal functioning of the RPE may result in either visual impairment or blindness. Alterations in RPE function may occur either as a result of diseases which specifically affect the RPE, such as age-related macular degeneration (AMD) (Tso, 1988) and central serous retinopathy (CSR) (Chuang et al., 1987), or due to secondary changes resulting from many retinal diseases including retinitis, retinitis pigmentosa (RP) (Chader, Aguirre and Sanyal, 1988) and proliferative vitreoretinopathy (Machemer and Laqua, 1975; Topping, Abrams and Machemer, 1979). In the case of CSR, it is widely held that the pathogenesis of this disease involves a dysfunction in the ion and fluid transport activities of the RPE. This results in an accumulation of subretinal fluid between the neural retina and the RPE, thereby leading to the eventual detachment of the neural retina (Bird, 1989; Chuang et al., 1987; Jalkh et



al., 1984).

Experimental evidence suggests that the fluid movement across the RPE may be due to the combination of three forces: hydrostatic, osmotic and active pumping. Among these, the latter two seem to be more significant (Steinberg, 1986). However, our overall knowledge of fluid transport in both normal and diseased retina is limited. It has been shown that ion and fluid movement can change as a function of 1) light and dark transition in normal retina, 2) release of transmitters and other molecules by neural retinal cells, and 3) changes in the total surface area of the RPE membrane, which may occur following retinal detachment. Changes in surface area will affect the number of ion channels and transport sites located on the RPE cell membrane.

It is the purpose of my thesis project to further identify the electrophysiological properties of the mammalian RPE. In particular, the processes leading to passive ion diffusion via ion channels and the modulation of ion channels by receptor coupled signaling pathways. This work will increase our understanding of the mechanisms underlying ion and fluid transport in the RPE, and the function of this epithelium in regulating ionic concentrations in the subretinal space. Further information on ion transport by the RPE may eventually contribute to the overall efforts made towards developing new, more selective pharmacological means to treat sight-threatening conditions such as CSR and other ocular diseases which result from, or give rise to, alterations in RPE function.

The subsequent sections will briefly introduce the processing of visual images. The general structure and functions of the RPE will be summarized, and the role of the

RPE in the visual cycle will be briefly described where appropriate. A review of relevant work done previously in other laboratories will be included, and the rationale and specific objectives of the research presented in this thesis will be outlined. Finally, justification for the techniques used in this study will be addressed.

## **1. Processing of visual images**

Visual image formation may be divided into two processes: encoding and decoding. Encoding starts in the retina and continues in the lateral geniculate nucleus and visual cortex (Hubel and Wiesel, 1961 & 1962), whereas decoding takes place in the brain where the exact location is still unknown (Wu, 1988). The vertebrate retina, like other regions of the central nervous system is embryologically derived from the neural tube which then forms the optic cup. It is composed of the neurosensory retina and the RPE, both of which are differentiated from the inner wall and the outer wall of the optic cup respectively (Dowling, 1987). The neural retina is a thin layer of nervous tissue lining the back of the eye where the image is formed (Wu, 1988) (Fig. 1-1 & 1-2). Its primary function is to absorb light and to encode visual images as patterns of nerve impulses that can then be conveyed to and understood by the brain. The light receiving units of the retina are the rods and cones, also called photoreceptors. Each photoreceptor detects a tiny part of the image which is projected on it and produces a small electrical signal. These discrete electrical signals are further transmitted through the retinal network consisting of innumerable secondary-order neurons (horizontal cells, bipolar cells, amacrine cells, and ganglion cells) and synapses through a process called

INTRODUCTION

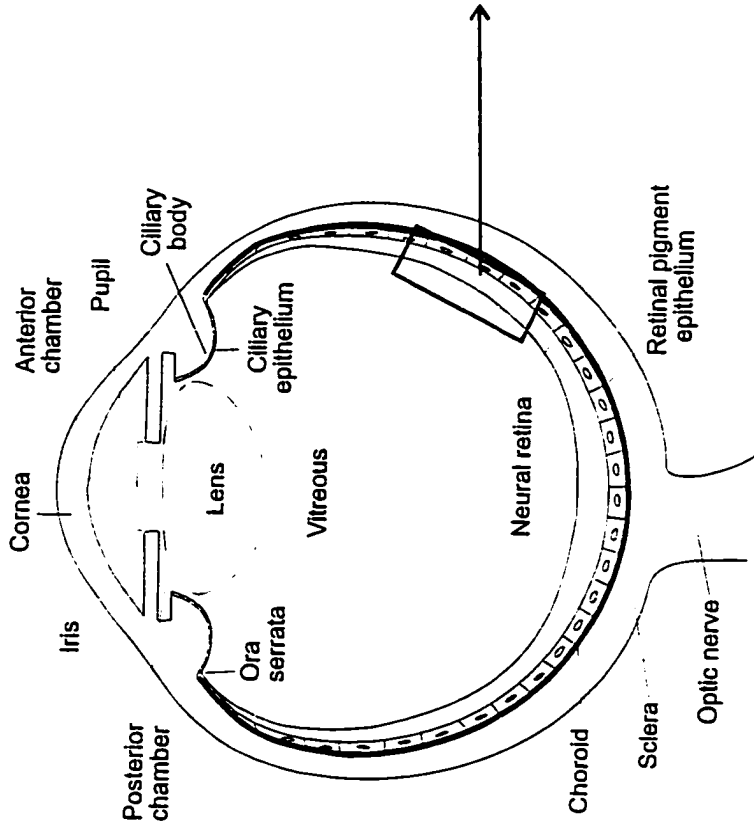


Fig. 1-1. Cross section of the eye.

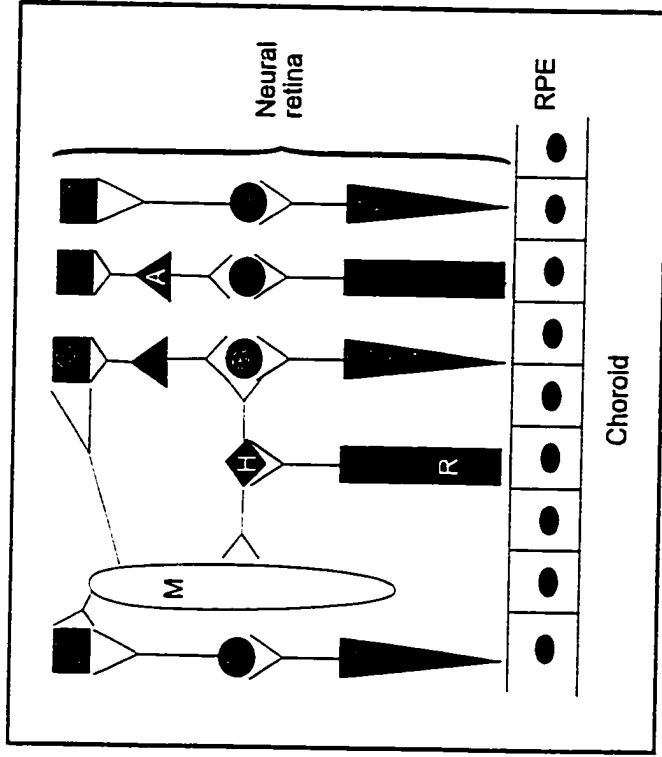


Fig. 1-2. Cross section of the neurosensory retina and the RPE. (R=rods; C=cones; A=amacrine cells; B=bipolar cells; H=horizontal cells; G=ganglion cells; M=müller cells).

phototransduction.

The process of phototransduction consists of an enzyme cascade including a visual pigment (rhodopsin), a GTP-binding protein (transducin) and an enzyme hydrolyzing cyclic GMP (cGMP) (cGMP-phosphodiesterase), leading to a decrease in cGMP (Kawamura, 1995). In the dark, a cGMP-activated steady inward cation current (~80% Na<sup>-</sup>/20%Ca<sup>2+</sup>) flows in the outer segment of the photoreceptor. The current is blocked in the light due to the decrease of cGMP so that the cell elicits a hyperpolarizing response, which is the primary phototransduction signal (Kawamura, 1995). All retinal neurons except ganglion cells use graded potentials to encode visual information. Elements of visual images are stored as amplitudes of voltage signals. These signals are gathered and translated into frequency-modulated signals by ganglion cells, and then transmitted to the higher levels in the visual system in the form of action potentials via the axons of these cells, where the visual signals are further modified. When the decoding area in the brain receives these signals, it decodes them and interprets them as an image (Wu, 1988).

## **2. General structure and functions of the RPE**

The structure of the RPE is uniquely adapted to many of its complex functions. As the outer portion of the vertebrate retina, the RPE sits between the photoreceptors of the neurosensory retina and the choroidal blood supply. Histologically, the RPE consists of a continuous monolayer of cells beginning at the edge of the optic nerve head and extending peripherally to the ora serrata. Anterior to the ora serrata, the RPE continues as

the ciliary pigment epithelium (Fig. 1-1). The cell body of the RPE has a cuboidal configuration. When viewed in a flat preparation, the RPE cells are tightly packed with little extracellular space between neighbouring cells (Zinn and Benjamin-Henkind, 1979, Fig. 1-3). The plasma membrane and cytoplasmic contents of RPE cells are highly polarized. This polarity is essential for the many vectorial transport functions that the RPE cell carries out.

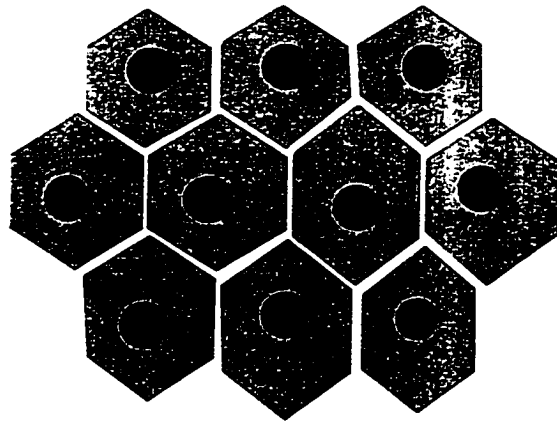


Fig. 1-3. RPE cells, surface view.

## 2.1 Basal plasma membrane

As shown in figure 1-4, the basal plasma membrane of the RPE cell has numerous infoldings and lies on a basement membrane which is secreted by the RPE cell itself (Clark, 1986; Zinn and Benjamin-Henkind, 1979). These infoldings are very useful for facilitating the ion movement in transporting epithelia such as the RPE, as they increase the surface area of the cell. The basal surface of the RPE is functionally linked to the choroid via Bruch's membrane, a fibroelastic layer which separates the photoreceptor-RPE unit from its blood supply derived from the choriocapillaris (Clark, 1986; Zinn and

Benjamin-Henkind, 1979). Bruch's membrane is permeable to small molecules and some macromolecules, and is thought to contribute to the blood-retinal barrier (Pino and Essner, 1981; Pino, Essner and Pino, 1982).

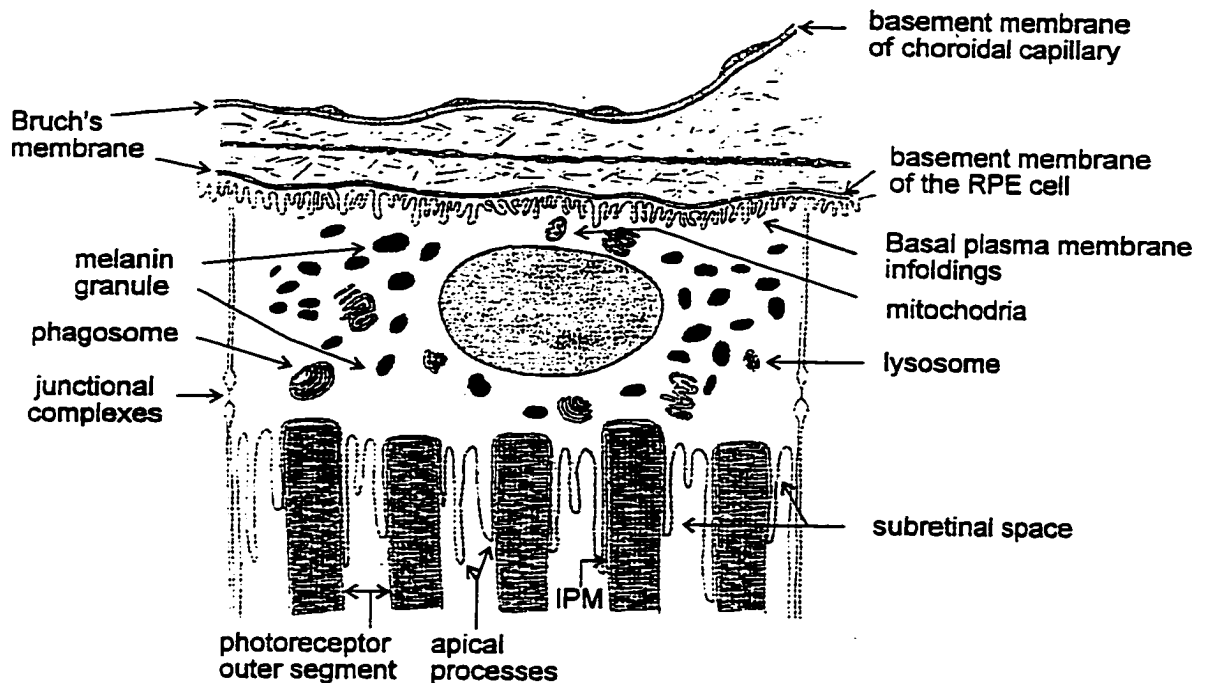


Fig. 1-4. RPE cell, cross section (modified from Clark, 1986, with permission from Academic Press, Inc.).

## 2.2 Apical plasma membrane

The apical surfaces of RPE cells face the photoreceptors, and contain both long and short microvilli (Fig. 1-4). These microvillus processes interdigitate with the outer segment tips of the photoreceptors across the subretinal space. The close proximity of the large surface areas of both the photoreceptor and RPE cell plasma membranes aids in the exchange of nutrients and metabolites between these two cell types. Although there is no direct contact between the apical processes of RPE cells and the photoreceptor outer

segments (Clark, 1986; Steinberg, 1986; Dowling, 1987), they adhere to each other and functionally communicate across the subretinal space. The apical surface of the RPE, as well as the rod and cone outer segments are coated with an extracellular matrix, the interphotoreceptor matrix (IPM) which is secreted in part, by the RPE cells (Zinn and Benjamin-Henkind, 1979; Clark, 1986). It is believed that the IPM may play a minor role in the adhesion of neurosensory retina to the RPE by acting as a "glue" (Clark, 1986; Marmor, 1989). The IPM may also serve as a medium for the exchange of metabolites between the outer segments of the photoreceptors and the RPE (Clark, 1986). Due to the lack of tight attachment between the neural retina and the RPE, the neural retina can become detached from the RPE under certain conditions. Detachment seriously disrupts the photoreceptors and RPE, and can eventually lead to the loss of vision.

The apical membrane of the RPE is also rich in  $\text{Na}^+/\text{K}^+$  ATPase which, together with other ionic transport mechanisms, moves water out of the subretinal space. The apical location of the  $\text{Na}^+/\text{K}^+$  ATPase (along with the epithelium of the choroid plexus) is a unique feature among epithelia, as this pump is normally located on the basal membrane (Bok, 1993; Ernst, Palacios and Siegel, 1986). This apical pump is mainly responsible for absorptive fluid movement from the apical to the basal membrane of the RPE. The removal of subretinal fluid by the RPE is thought to provide the major motive force for adhesion of the neural retina to the RPE (Zauberman, 1979; Clark, 1986; Bok, 1988; Bird, 1989; Marmor, 1989).

As part of the photoreceptor renewal process, the apical processes of the RPE continually phagocytize the distal portions of the outer segments of rods and cones.

These photoreceptor outer segments are shed into the subretinal space, in a specific receptor-mediated manner that is not yet well defined (Bok, 1993). Once internalized by the RPE, the phagosomes are then quickly digested by the lysosomal system in the cytoplasm of RPE cells (Bok, 1988). Each of these outer segments is renewed by new membrane assembly at the photoreceptor proximal ends. This process of shedding, phagocytosis and renewal of the photoreceptors follows a circadian rhythm (Bok, 1993). It has been observed that the close approximation of the photoreceptors to the RPE is required before this process can take place (Williams and Fisher, 1987).

### **2.3 Lateral plasma membrane**

Unlike its basal and apical counterparts, the lateral plasma membrane of the RPE cell lacks infoldings (Fig. 1-4). The basal and lateral membranes are usually referred as a single functional unit, called *basolateral*. The RPE cell interacts with its neighbours laterally through junctional complexes which begin about halfway down the lateral surface at the apical end of each cell. These are composed of gap junctions located apically, adhering junctions which occur more basally and tight junctions which overlap the others (Bok, 1988). Among these complexes, it is the tight junctions which help to form the blood-retina barrier. Neither the gap junctions nor the adhering junctions contribute to the barrier function of the junctional complexes. Instead, the gap junctions represent low electrical resistance pathways and sites for metabolic cooperation between neighbouring cells (Steinberg and Miller, 1979; Bok, 1988).



## 2.4 Unusual features of cytoplasmic organelles

In addition to the standard organelles within an epithelial cell, the RPE cell contains two types of pigment granules: melanin and lipofuscin. These two pigment granules tend to be intermixed within the apical two thirds of the cell, and melanin granules occupy apical microvilli (Bok, 1988). The melanin granules synthesized by the RPE cells allow the RPE to absorb excess photons, thereby reducing their scatter and reflection which would otherwise degrade the visual image. This effect increases the efficiency of the photoreceptors, protects them from damaging levels of radiation, and helps to improve the resolution of images (Bok, 1993). Lipofuscin, on the other hand, is a residual material derived from phagocytic and autophagic activity, therefore, it can be the result of either the incomplete digestion of intracellular organelles or outer segments of photoreceptors (Bok, 1988).

## 2.5 Other functions of the RPE

As one of its transport functions, the RPE cell acts as a mediator in the transport of dietary retinoids (retinol or vitamin A, and its derivatives) from the liver to the photoreceptors through the bloodstream with the aid of specialized serum (or plasma) retinoid-binding proteins (synthesized and secreted in the liver) as carriers. The isomer of retinoids, 11-*cis*-retinaldehyde (11-*cis*-retinal) serves as the chromophore, an essential component of rhodopsin, the light-capturing pigment, in the outer segments of the photoreceptors. Following a series of events after the entry of retinoids into the RPE cells (isomerization and oxidation), the final product, 11-*cis* retinal is eventually released from

the apical membrane of the RPE, across the subretinal space and into the photoreceptors (Saari, 1990) for incorporation into rhodopsin during the visual cycle. If the retinoids are not required by the photoreceptors immediately, they are esterified to a relatively inert form and stored in the RPE (Clark, 1986; Bok, 1988 & 1993). Retinoid uptake occurs at both the basolateral and apical surfaces of the RPE by separate binding proteins and through different receptor-mediated processes (Bok, 1993).

The visual cycle involves the repeated movement of retinoid back and forth between the photoreceptors and the RPE. The purpose of the cycle is to regenerate 11-*cis* retinal. The RPE is the cellular site at which the regeneration of 11-*cis* retinal takes place (Bernstein, Law and Rando, 1987). The first step in phototransduction occurs when photons trigger isomerization and reduction of 11-*cis* retinal back to the all-*trans* form in the photoreceptor outer segments. In order to reutilize the endogenous retinoid, all-*trans* retinol must first leave the photoreceptors and re-enter the RPE, where it is converted to 11-*cis* retinal, and then it must return to the photoreceptors (Bok, 1993).

Finally, due to its absorptive-vectorial transport functions (from the retina to choroid), the RPE also participates in regulating ionic concentrations in the subretinal space, thus playing an important role in maintaining the homeostasis of the extracellular fluid surrounding the retinal photoreceptors (Steinberg and Miller, 1979; Immel and Steinberg, 1986; La Cour, Lund-Andersen and Zeuthen, 1986). Further details of the transporters and ion transport mechanisms found in the RPE are described below.

### **3. Transport and membrane properties of the RPE**

During the visual process, light passes through the entire neural retina layer and strikes the photoreceptors, thereby initiating the phototransduction cascade which leads to alterations in photoreceptor and secondary neuron activity within the neural retina. The light-induced changes in retinal activity alter the chemical composition in the subretinal space and produce decreases in the subretinal  $[K^+]_o$ . These alterations are sufficient to change the membrane voltage and conductance at both the apical and basolateral membranes of the RPE, thereby modulating the transport of ions, fluid, and metabolites across the RPE (Joseph and Miller, 1991).

Cell membrane potential change results from ionic current flow via electrogenic and electroneutral transporters and through individual channel proteins in the membrane of cells. The ion transport mechanisms of the RPE have now been extensively studied in a variety of vertebrate species including toad, frog, cat, chicken, rabbit and bovine retinae. The studies have been carried out in order to provide a model of RPE transport which links these electrical events to cellular mechanisms, including changes in ion concentrations, metabolites and water transport between the RPE and the blood or the RPE and the neural retina. The following section provides a brief review of previous research which was carried out towards understanding how the potentials, including those in electroretinogram (ERG) and transepithelial potential (TEP) are generated in the RPE and how ion transport mechanisms are implicated in these voltage changes.

### **3.1 Light induced electrical response of the RPE**

Field or gross potentials are usually recorded from the surface of a tissue. They

reflect the summed electrical activity of populations of cells. When a low-resistance electrode is placed on the corneal surface of an eye and a reference electrode is positioned elsewhere on the head, voltage changes are recorded upon light stimulation. Field potentials recorded in this way from the eye are called an electroretinogram (ERG). An ERG monitors the electrical consequences of light and dark interactions between the photoreceptors and RPE. The ERG waves originating from events in the RPE and neural retina, have proved to be a very useful tool for the evaluation of retinal and visual function. The direct-current ERG (DC-ERG) is a modified measure of ERG and is designed to record slower electrical responses originating from the RPE.

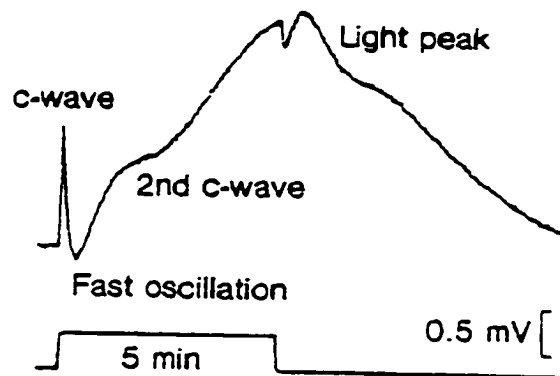


**Fig. 1-5.** A DC-ERG (cat) in response to 5-min illumination (Modified from Linsenmeier and Steinberg 1984, with permission from *J. Gen. Physiol.*).

Absorption of light by the photoreceptors results in changes in both the membrane potential and the resistance of the RPE (Adorante and Miller, 1990; Joseph and Miller 1991; Quinn and Miller, 1992). These changes contribute to three DC-ERG components

including: c-wave, fast oscillation, and light peak (see figure 1-5) (Linsenmeier and Steinberg, 1984).

Studies have confirmed that the c-wave is the sum of two components (Rodieck, 1972). One of which is generated by the RPE (Noell, 1954; Brown and Wiesel, 1961; Steinberg, Schmidt and Brown, 1970; Niemeyer, 1976). It has been shown that photoreceptor activation upon light onset causes a decrease in  $[K^+]_o$  in the subretinal space. In response to this fall in  $[K^+]_o$ , the apical membrane of the RPE cell hyperpolarizes, which in turn, induces an increase in TEP and is recorded as the RPE component of the c-wave in DC-ERG, called TEP c-wave (Oakley and Green, 1976; Oakley, 1977; Steinberg, 1988). TEP is the difference between the apical and basal membrane potentials of the RPE, therefore, it is determined by the potentials of both membranes of the RPE. An apical membrane hyperpolarization and/or basal membrane depolarization will increase TEP. It has been suggested that the change in  $[K^+]_o$  in the subretinal space has a direct effect on the  $K^+$  equilibrium potential of the apical membrane (Miller and Steinberg, 1977a; Oakley, 1977). The fast-oscillation of the RPE is generated primarily in the delayed basal membrane response (hyperpolarization) of the RPE, which decreases the TEP (Steinberg, 1988). Another mechanism which contributes to the decrease of the TEP during fast oscillation is the reaccumulation of  $[K^+]_o$  in the subretinal space which occurs during sustained light after an initial period of decrease (Oakley and Steinberg, 1982). This reaccumulation causes recovery of the apical membrane from hyperpolarization. The light peak originates solely in the basal membrane of the RPE, and is due to a basal membrane depolarization, which in turn

results in an increase of the TEP thereby producing a light peak in the DC-ERG (Steinberg, Linsenmeier and Griff, 1983). Light offset initiates a repetition of the above sequence but the responses have the opposite polarity from those recorded during light onset. The ion transport mechanisms responsible for these potential changes during light onset are discussed later in section 3.3.

### **3.2 Electrogenic, electroneutral transport systems and passive ion conductances in the RPE**

The electrogenic and electroneutral transport mechanisms, as well as the passive ion conductances in the RPE respond to changes in both the chemical composition of the choriocapillaris blood supply and the microenvironment surrounding the photoreceptors (subretinal space). These mechanisms work together giving a net absorptive KCl flow across the RPE (from apical to basal membrane).

Transepithelial isotope flux, microelectrode and  $\text{pH}_i$  measurement experiments using isolated RPE-choroid tissue have made some inferences concerning the localization of the electrogenic and electroneutral transport mechanisms in the RPE. The major transport mechanisms (both electrogenic and electroneutral) which have been demonstrated in the apical RPE membrane include: 1) an ouabain-sensitive  $\text{Na}^+/\text{K}^+$ -ATPase [Miller and Steinberg, 1977b & 1982 (frog); Tsuboi, Manabe and Iizuka, 1986 (dog); Frambach and Misfeldt, 1983 (chicken); Frambach, Valentine and Weiter, 1988a (rabbit); Joseph and Miller, 1991 (bovine)]; 2) an apical  $\text{Na}^+/\text{K}^+/\text{Cl}^-$  cotransporter, which is sensitive to bumetanide [Miller and Edelman, 1990; Joseph and Miller, 1991 (bovine);

Frambach and Misfeldt, 1983 (chicken); Tsuboi et al., 1986 (dog)]; 3) an apical membrane  $\text{Na}^{\text{-}}\text{-HCO}_3^{\text{-}}$ -cotransporter, which is inhibited by the anion transport inhibitors diisothiocyano-2,2-disulphonic acid stilbene (DIDS) and 4-acetamido-4'-isothiocyano-stibene-2,2'-disulphonic acid (SITS) [Adorante, Hughes and Miller, 1988; La Cour, 1989 & 1991; Hughes et al., 1989; Lin and Miller, 1991a (frog)]; 4) an amiloride-sensitive apical  $\text{Na}^{\text{-}}\text{-H}^{\text{+}}$  exchanger [Kenyon, Lin and Miller, 1991 (human)]; and 5) an apical  $\text{Na}^{\text{-}}\text{-Ca}^{2+}$  exchange mechanism [Fujisawa, Ye and Zadunaisky, 1992 (dogfish and bovine)]. In the basolateral membrane of RPE, a pH-sensitive,  $\text{Na}^{\text{-}}$ -independent  $\text{Cl}^{\text{-}}\text{-HCO}_3^{\text{-}}$  exchanger has been identified (Miller and Steinberg, 1977b; Lin and Miller, 1992).

Recently, a more detailed understanding of the properties of ion channels has been obtained through the use of patch-clamp recording techniques. In frog and mammalian RPE, intracellular microelectrode experiments have demonstrated that a  $\text{Ba}^{2+}$ -sensitive  $\text{K}^{\text{-}}$  conductance is present in the apical membrane and that both a  $\text{K}^{\text{-}}$  and a stilbene sensitive  $\text{Cl}^{\text{-}}$  conductance are present in the basal membrane (Fujii et al., 1992; Quinn and Miller, 1992; Joseph and Miller, 1991; Miller and Edelman, 1990; Gallemore and Steinberg, 1989; Miller et al., 1988; La Cour et al., 1986). Patch-clamp recordings from freshly dissociated RPE cells derived from both frog and turtle RPE have revealed that these cells express several populations of  $\text{K}^{\text{-}}$  channels which include inwardly and outwardly rectifying voltage-dependent  $\text{K}^{\text{-}}$  currents (Hughes and Steinberg, 1990; Fox and Steinberg, 1992). Single channel recordings from the apical membranes of cultured human RPE cells have also revealed several different  $\text{K}^{\text{-}}$  selective channels. However, none of these channels showed any voltage-dependence (Fox, Pfeffer and Fain, 1988).

More recently, several reports have described whole-cell voltage-dependent  $\text{Ca}^{2+}$  and  $\text{K}^+$  currents in freshly isolated and cultured rat RPE cells (Ueda and Steinberg, 1993; Strauß & Weinrich, 1992) and in fresh and cultured primate RPE cells (Strauß, Richard and Weinrich, 1993; Wen, Lui and Steinberg, 1993). These studies demonstrated that, like amphibian RPE cells, mammalian RPE cells may exhibit several different voltage-dependent  $\text{K}^+$  currents. Further comparative studies are required in order to resolve the functional implications of these different ion channels.

### **3.3 Ionic transport mechanisms underlying the RPE membrane potential changes in response to light onset**

The active and passive ionic transport mechanisms which underlie the response of RPE cells to light onset are summarized in Table 1-1. The first light-evoked event of the RPE recorded in the DC-ERG is the TEP C-wave, which is results from an increase in TEP. Light onset induces decreases in the subretinal  $[\text{K}^+]$  which in turn causes a  $\text{K}^+$  efflux through  $\text{K}^+$  conductive channels and inhibits the  $\text{Na}^+/\text{K}^+$  ATPase activity at the apical RPE membrane. Of these two effects, the first one is greater than the second resulting in a net hyperpolarization of the apical membrane which accounts for an increase in TEP, hence the TEP C-wave. The fast-oscillation trough following the C-wave in the DC-ERG is given by a decrease of the TEP which is thought to primarily result from the basal  $\text{Cl}^-$  transporter. The light-induced decrease of subretinal  $[\text{K}^+]_o$  also decreases the inward driving force on the  $\text{Na}^+-\text{K}^+-2\text{Cl}^-$  cotransporter at the apical membrane and slows the influx of  $\text{Cl}^-$ . This reduction in  $[\text{Cl}^-]_i$  could decrease the



INTRODUCTION

**Table 1-1. Summary of RPE responses and their mechanisms upon light onset**  
(Steinberg, 1988; Gallemore & Steinberg 1989; Joseph & Miller, 1991).

| Phase | Subretinal $[K^+]_o$ | RPE  |                                 |   |  | TEP<br>( $V_{ba} - V_{ap}$ ) | DC-ERG           |
|-------|----------------------|--|---------------------------------|---|--|------------------------------|------------------|
|       |                      | Apical membrane  |                                 | Basolateral membrane  |  |                              |                  |
|       |                      | Mechanisms   | $V_{ap}^*$                      | Mechanisms  | $V_{ba}^{**}$  |                              |                  |
| I     | ↓                    | Na <sup>+</sup> /K <sup>+</sup> ATPase ↓<br>K <sup>+</sup> efflux via its channels ↓ ↓                       | Hyperpolarization               |   |  | ↓                            | TEP C-wave       |
| II    | Reaccumulation       | Na <sup>+</sup> -K <sup>+</sup> -Cl <sup>-</sup> cotransporter ↓<br>K <sup>+</sup> efflux via its channels ↓ |                                 | (1) a <sub>Cl</sub> <sup>-</sup> ↓ → Cl <sup>-</sup> efflux via its channels ↓<br>(2) shunting from hyperpolarized $V_{ap}^{***}$ | Hyperpolarization  | ↓                            | Fast oscillation |
| III   | Level-off            |  | Recovery from hyperpolarization |   | (1) Cl <sup>-</sup> channel activity ↓<br>(2) Metabolic events ? | ↓                            | Light-peak       |

\*  $V_{ap}$ : apical membrane potential of the RPE; \*\*  $V_{ba}$ : basolateral membrane potential of the RPE;

\*\*\* Shunting is the effect of passive cell membrane voltage drops produced by current flow across the shunt resistance. It reduces the magnitude of the voltage at the membrane generating it and produces a smaller voltage of the same polarity at the opposite membrane.

basolateral  $\text{Cl}^-$  conductance, thereby generating a delayed basal membrane hyperpolarization (Joseph and Miller, 1991). In addition, the recovery of the apical membrane from the initial hyperpolarization, due to the reaccumulation of subretinal space  $[\text{K}^+]_o$ , also contributes to decreases in the TEP. The light-peak following the fast-oscillation trough has been demonstrated to be generated by the depolarization of the basal membrane of the RPE. This depolarization may originate as an increase in basal membrane  $\text{Cl}^-$  conductance (Gallemore and Steinberg, 1989).

### **3.4 Regulation of ion channels within RPE cells**

Ion channels in the cell membrane may either be controlled by transmembrane potentials and/or modulated by a number of substances including neurotransmitters, hormones, cytosolic messengers, fatty acids and metabolites. These compounds can act in a variety of ways, for example they may directly act on the channels (cyclic nucleotides and fatty acids) (Latorre et al., 1991; Ordway et al., 1989) or may indirectly mediate their actions via specific receptors and receptor coupled guanine nucleotide regulatory binding proteins (G-proteins). There is evidence that G-proteins may directly couple to ionic channels, (Cole and Sanders, 1989; Toro, Romos-Franco and Stefani, 1990; Brown et al., 1991; Kume, Graziano and Kotlikoff, 1992) or they may activate cytoplasmic enzyme systems including the adenylate cyclase system, the guanylate cyclase system or the membrane-bound phosphoinositol-specific phospholipase C (PLC), which in turn may generate other second messengers. Ultimately, the ion channels may be activated or inhibited via either the direct actions of G-proteins and second messengers, or through

phosphorylation (Toro and Stefani, 1991).

Intracellular free  $\text{Ca}^{2+}$  has long been recognized as a major second messenger which regulates a number of cellular events. The free  $[\text{Ca}^{2+}]$  in the cytosol of any cell is maintained at extremely low levels ( $\leq 100$  nM), whereas its concentration in extracellular fluid and in the endoplasmic reticulum (ER) is relative high. Thus, there is a large gradient tending to drive  $\text{Ca}^{2+}$  into the cytosol across both the plasma membrane and the ER membrane. When a signal opens either  $\text{Ca}^{2+}$ -channels in the plasma membrane and/or  $\text{Ca}^{2+}$ -releasing channels in the ER membrane,  $\text{Ca}^{2+}$  enters into the cytosol, increasing the local  $[\text{Ca}^{2+}]$  and activating  $\text{Ca}^{2+}$ -responsive proteins in the cell, including ion channels (Alberts et al., 1994).

$\alpha_1$ -Adrenergic receptors are members of a G-protein-coupled receptor superfamily. In a wide variety of systems, they control cytosolic  $\text{Ca}^{2+}$  by stimulating the hydrolysis of inositol phospholipids, which are thought to be located within the inner half of the plasma membrane lipid bilayer.  $\alpha_1$ -Adrenergic receptors are membrane glycoproteins with several common structural features including seven membrane-spanning domains with an extracellular amino terminus and an intracellular carboxyl terminus. Multiple subtypes have been identified using molecular ( $\alpha_{1a/d}$ ,  $\alpha_{1b}$  and  $\alpha_{1c}$ ) and pharmacological ( $\alpha_{1A}$ ,  $\alpha_{1B}$  and  $\alpha_{1L}$ ) techniques. The pharmacological differentiation of these multiple subtypes is based on their different ratios of affinities for the  $\alpha_1$ -adrenoceptor antagonists prazosin and WB4101, and to the degree of susceptibility to inactivation by the alkylating agent chlorethylclonidine (Ford et al., 1994). However, due to the lack of highly selective drugs for all of these subtypes, their pharmacological

characterization remains incomplete. The fact that most tissues express more than one subtype, further complicates this characterization (Graham et al., 1995). The cloned  $\alpha_{1c}$  subtype has been suggested to represent the pharmacological  $\alpha_{1A}$  subtype (Ford et al., 1994; Price et al., 1994). The cloned  $\alpha_{1b}$  subtype is identical to the pharmacologically-characterised  $\alpha_{1B}$  subtype (Graham et al., 1995). All three cloned  $\alpha_1$ -receptor subtypes have been shown to mobilize intracellular  $Ca^{2+}$ , and to activate PLC and  $PLA_2$  (Schwinn et al., 1991; Perez, Young and Graham, 1993). For PLC activation, receptor coupling may involve the  $G_q$ -protein family (Wu et al., 1992). A novel  $G_h$ -protein has recently been shown to be involved in polyphosphoinositide turnover in mediating  $\alpha_{1B}$  receptor effect (Nakaoka et al., 1994).

Figure 1-6 is a schematic diagram of the chain of events of activation of  $\alpha_1$ -adrenoceptors leading to phosphatidyl-inositol-4,5-bisphosphate ( $PIP_2$ ) breakdown. Initial events involve the binding of an agonist to the  $\alpha_1$ -receptor. The  $\alpha_1$ -receptor is linked to a trimeric G-protein located on the cytoplasmic face of the plasma membrane. The activation of the  $\alpha_1$ -receptor stimulates the G-protein by triggering the exchange of GDP (guanosine 5'-diphosphate) with GTP, which in turn activates PLC. The activated PLC enzyme then cleaves  $PIP_2$  into two second messengers: inositol (1,4,5)-triphosphate ( $IP_3$ ) and diacylglycerol (DAG). From this point the signal transduction pathway divides into two branches with the stimulation of  $IP_3$  receptors and the release of  $Ca^{2+}$  from the ER into the cytosol, and the translocation and activation of protein kinase C by DAG.  $IP_3$  is a small water soluble molecule which leaves the plasma membrane and diffuses rapidly through the cytosol.  $IP_3$  mobilizes  $Ca^{2+}$  from the ER by interacting with a specific

INTRODUCTION

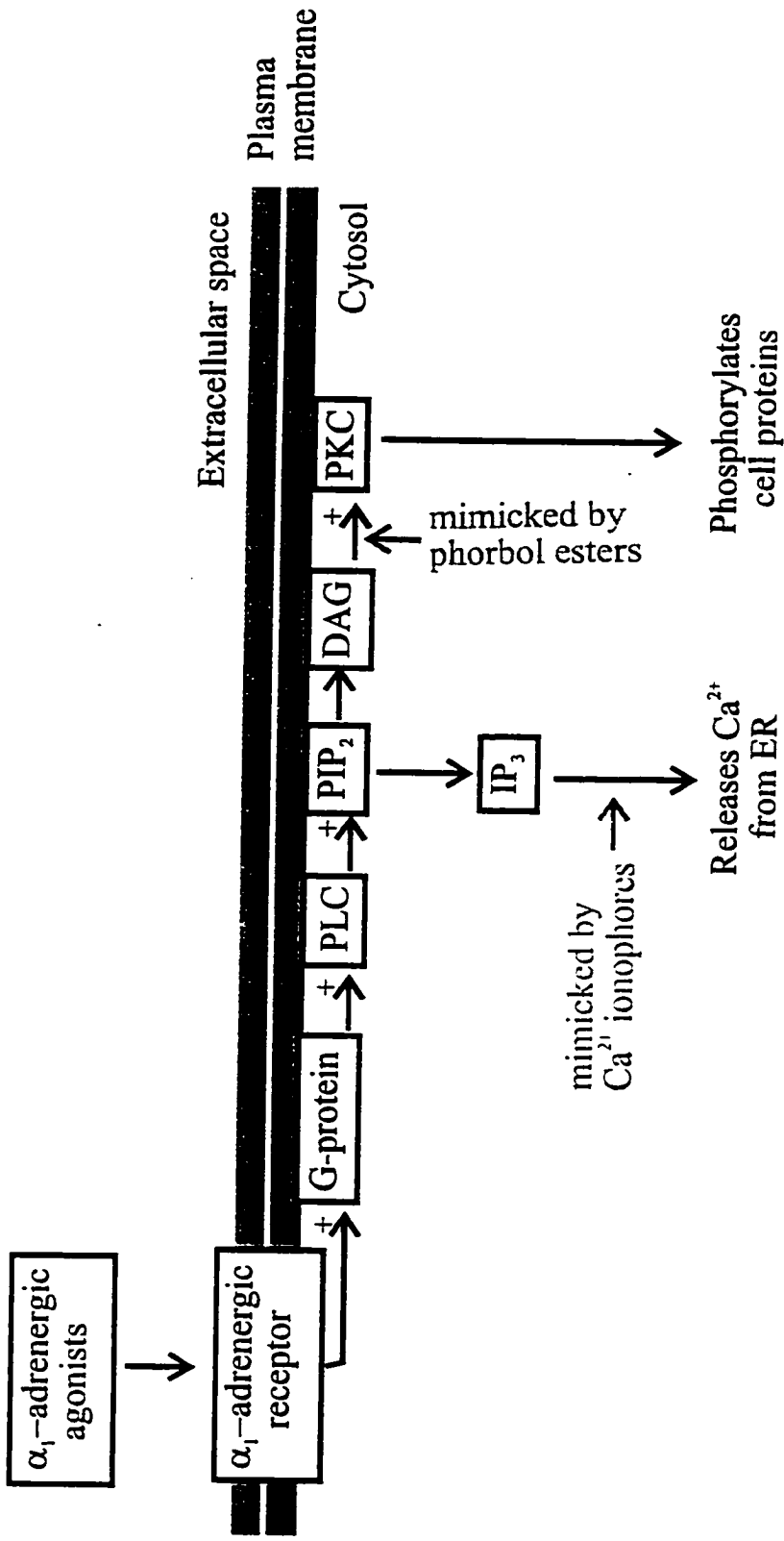


Fig. 1-6. Diagrammatic summary of current knowledge of the  $\alpha_1$ -adrenergic receptor activation cascade leading to PIP<sub>2</sub> breakdown. (See text for details)

receptor, which is a  $\text{Ca}^{2+}$ -releasing channel found in the ER membrane. As indicated in figure 1-6, the effect of the  $\text{IP}_3$  pathway may be mimicked by using a  $\text{Ca}^{2+}$  ionophore (a small hydrophobic molecule acting as a mobile carrier or forming a channel), such as ionomycin, which allows  $\text{Ca}^{2+}$  to move into the cytosol from the extracellular fluid (Alberts et al., 1994).

Biochemical and physiological studies of RPE function have revealed that the list of effective agents include adrenergic (Frambach, Valentine and Weiter, 1988b; Frambach et al., 1990; Quinn and Miller, 1992; Joseph and Miller, 1992), muscarinic (Heth and Marescalchi, 1994) and purinergic receptors (Gregory, Abrams and Hall 1994) as well as cyclic adenosine monophosphate (cAMP) (Miller, Hughes and Machen, 1982; Hughes, Miller and Machen, 1984; Hughes et al., 1988; Frambach et al., 1990; Gregory et al., 1994) and  $\text{Ca}^{2+}$  (Joseph and Miller, 1992).

Studies on frog RPE have shown that apical cAMP stimulates the  $\text{Na}^+/\text{K}^+$  ATPase (Hughes et al., 1988) and inhibits the overall transport of ions and fluid across the RPE (Hughes et al., 1984). In rabbit and bovine RPE, ion transport studies have shown that epinephrine (EPI) stimulates fluid absorption across the RPE by acting on apical  $\alpha_1$ -adrenoreceptors. This effect involves an apical  $\text{Na}^+/\text{K}^+/\text{2Cl}^-$  co-transporter, as well as a transient elevation in intracellular  $\text{Ca}^{2+}$  concentration ( $[\text{Ca}^{2+}]_i$ ) which in turn, probably increases a  $\text{Cl}^-$  conductive pathway at the basolateral membrane. The basolateral membrane  $\text{Cl}^-$  conductance may also be accompanied by coupled  $\text{K}^+$  exit (Frambach et al., 1988b; Edelman and Miller, 1991; Lin and Miller, 1991b; Edelman and Miller, 1992; Joseph and Miller, 1992; Quinn and Miller, 1992). The actions of muscarinic and

purinergic agonists on ion and fluid transport in the mammalian RPE remain unclear, however in certain studies the activation of these receptors and their respective intracellular signalling pathways have been demonstrated to modulate other functions of the RPE, including phagocytosis. For example, it has been reported that muscarinic stimulation, with increases in  $IP_3$ , stimulates photoreceptor outer segment phagocytosis by rat RPE cells (Heth and Marescalchi, 1994), whereas activation of  $A_2$  receptors by adenosine agonists with the concurrent stimulation of cAMP, inhibits the ingestion of photoreceptor outer segments by rat RPE cells (Gregory et al., 1994). It remains to be defined whether adrenergic stimulation plays a role other than regulating transepithelial ion and fluid transport within the retina.

Biochemical studies have identified catecholamine-containing neurons in the retina of many species (Starr, 1977). Hadjiconstantinou and co-workers (1983 & 1984) found that the majority of norepinephrine (NE) is present within the sympathetic neurons which innervate the vascular region of the choroid and retina, whereas epinephrine (EPI) as well as phenylethanolamine-*N*-methyltransferase (PNMT) is associated with elements intrinsic to the retina. The sympathetic neurons innervating the eye are found in the superior cervical ganglia, and PNMT is the enzyme which converts NE into EPI by substituting the amino group with methyl. The intrinsic EPI-containing neuron system within the retina is responsive to light stimulation; upon light stimulation (for 1 hour) EPI content increases (2 fold) for more than 2 hours [Hadjiconstantinou et al., 1983 (rat)]. While intrinsic EPI-containing neurons (amacrine cells) in mammalian retina have been well established (Osborne and Nesselhut, 1982; Park et al., 1986), the NE-containing

neurons within retina. remains unclear [Nesselhut and Osborne, 1982 (bovine)].

The basal surface of the RPE and the choriocapillaris, and the apical surface of the RPE and the retinal photoreceptors are physically very closely related, therefore ion channels in the RPE are subjected to modulation by substances released from both the choroid and the retina. Given these facts, it is possible that NE and EPI emanating from the choroidal and retinal blood supply may act as endocrine signals. Similarly, NE and EPI released by retinal neurons may act as paracrine signals for the RPE by diffusing to the apical membrane, thereby regulating transepithelial responses.

#### **4. Experimental rationale and objectives**

RPE cells help to control the exchange of nutrients and metabolites between the photoreceptors and choroid, therefore they are essential for both the nourishment. They also play an important role in promoting neural retina adhesion, and renewal of the photoreceptors. Ion transport is closely related to these functions. For this reason, the molecular mechanisms by which ions are transported across the RPE are vital for our understanding of retinal functions.

The rabbit is extensively used as one of the animal models for ocular disorders such as age-related macular degeneration (AMD), central serous retinopathy (CSR), retinitis pigmentosa, and other retinal pathologies involving the RPE and photoreceptors. Therefore information on the passive ionic conductances in this species is essential in order to facilitate interpretation of transport data and also to extrapolate data between different animal models. The overall goal of this study is to provide information on the



ion channels involved in transepithelial ion transport in rabbit RPE cells and the regulation of ion channels by adrenergic receptor-coupled pathways.

#### 4.1 Specific objectives

##### *4.1.1 To establish and identify viable primary rabbit RPE cell cultures*

In order to study ion channels at both the cellular and molecular level using patch-clamp technology, the cells must be dissociated. The first objective of the present study was to establish a viable primary culture system of rabbit RPE cells to use for electrophysiological recordings, and to confirm that the cells isolated and recorded from were indeed RPE cells. The RPE cells were identified by their morphological characteristics as well as by using immunocytochemistry.

##### *4.1.2 To characterize $K^+$ conductances in isolated and cultured rabbit RPE cells*

The photoreceptors and the RPE have a common ionic environment, thus they can alter the activity of one another by causing ion or metabolite changes in the subretinal space. Changes in  $[K^+]_o$  in the subretinal space as a result of photoreceptor activation affect transepithelial transport by altering the RPE membrane potentials and the rates of active transport. The RPE, in turn, may also serve to regulate  $[K^+]_o$  both passively, by acting as a spatial buffer, and actively, through the transport of  $K^+$  (Oakley, 1977; Steinberg and Miller, 1979; La Cour et al., 1986; Immel and Steinberg, 1986). Transport studies in the vertebrate RPE suggest that the RPE apical membrane is primarily permeable to  $K^+$  ions and that the apical  $K^+$  conductances are of fundamental importance

for changes in both TEP and subretinal  $[K^+]$  which occur as a result of photoreceptor activity (La Cour et al., 1986). Although voltage-clamp studies carried out using isolated RPE cells and tissue have confirmed that  $K^+$  channels are present on the apical membrane (Fox et al., 1988) and that both  $K^+$  and  $Cl^-$  channels are present on the basal membrane (Miller and Steinberg, 1982; Frambach et al., 1990; La Cour et al., 1986), further information on the properties and regulation of individual channel types is required in order to define the role of these channels in RPE ion transport.

In this study the different types of  $K^+$  currents present in isolated and cultured rabbit RPE cells and their pharmacology was examined using whole-cell and single channel patch-clamp recording methods.

#### *4.1.3 To examine $\alpha_1$ -adrenergic modulation of maxi- $K_{Ca}$ currents ( $I_{K(Ca)}$ ) in cultured rabbit RPE cells*

Modulation of the activity of membrane ion channels is of fundamental importance for the regulation of cellular activity. Understanding the mechanisms which regulate ion channels in the RPE is essential in order to further define their roles in the maintenance of ion and fluid homeostasis in the subretinal space and for predicting the actions drugs and ligands may play on RPE transport.

A number of neurotransmitters and hormones have been shown to modulate  $K_{Ca}$  channel activity. These transmitters usually exert their actions via changes in intracellular free  $Ca^{2+}$  or cAMP levels (Toro and Stefani, 1991). Since  $\alpha_1$ -adrenergic receptors have been identified in rabbit RPE cells (Frambach et al., 1988b), and transepithelial studies

have shown that EPI and  $\alpha_1$ -adrenergic agonists modulate ionic and fluid transport across the RPE in the bovine retina (Edelman and Miller, 1991; Lin and Miller, 1991b; Edelman and Miller, 1992; Joseph and Miller, 1992; Quinn and Miller, 1992), the role of  $\alpha_1$ -adrenergic receptor coupled pathways in modulating  $K^+$  channels in rabbit RPE was examined.

## **5. Techniques used in this study: Patch-clamp recording**

The development of the patch-clamp recording technique not only made direct measurements of membrane channels possible, it also enabled researchers to apply voltage-clamp methodology to small cells and to trace their signalling pathways by controlling the intracellular environment. This technique has now been applied to several different ocular epithelial cell types. It is a versatile technique which can be used in a number of configurations. These configurations will be described in further detail in chapter 2, Material and Methods (see section 2.4 - 2.6). The following section will outline some of the advantages and disadvantages of patch-clamp recording in relation to other methodologies for examining RPE ion transport.

### **5.1. Whole-cell voltage patch-clamp recording**

Whole-cell patch-clamp recording measures the summed currents which flow through ion channels located in the entire cell membrane regardless of their position, thus detailed biophysical and pharmacological properties of channels can then be measured. The whole-cell patch-clamp has the following advantages: 1) The pipette filling solution

is continuous with the cell interior in this configuration, therefore one can directly modify cytosolic pathways during current recording by adding test molecules to the cell interior via the pipette solution. 2) The cell capacitance can be measured and used to determine total cell surface area since the membrane area is proportional to capacitance. 3) It allows quantitation of macroscopic conductances in cells too small to be voltage-clamped by conventional means, this feature is especially important in epithelial cells. 4) It provides more artifact-free voltage measurements than intracellular microelectrode recording does. In a discontinuous voltage clamp (dSEVC) intracellular microelectrode recording, one electrode passes current and records voltage alternately. "Ripple" in the membrane potential during a switching cycle may cause an error in the membrane voltage measurement. In addition, only slow events with respect to the switching frequency can be detected and controlled appropriately. 5) In whole-cell recordings, the specific cell type from which the recordings are made is known (Rae, 1993).

The disadvantage of the whole-cell patch clamp is that it requires cells to be dissociated. Dissociation of epithelial cells usually results in the loss of syncytial interaction with neighbouring cells which occurs through lateral junctions. It is clear that one cannot measure transepithelial transport by this technique, however the whole-cell recording method does provide an accurate measure of whole-cell currents. Although the exchange between the pipette filling solution and the interior of the cell can result in the loss of small molecules from the cell which may be important for the regulation of cell membrane transporters, this washout may be avoided by using the "perforated patch" approach (see Material and Methods, section 2.6 for details).

## 5.2. Single-channel recording

The single-channel recording configuration allows direct measurement of the conductance of individual membrane-bound channel proteins. Single-channel recording can be made from non-dissociated tissue. In this case, the particular part of the cell from which recordings are made is known, thereby providing spatial localization of the channel as well as information about the distribution of the channels on the cell membrane.

In cell-attached configuration, substances and structures inside the cell which regulate channel proteins remain intact and are able to exert their influence. The disadvantage of this configuration is that it is difficult to change the solution on either side of the patch of membrane and the membrane potential of the cell is not known.

In inside-out patch configuration, the outer membrane surface of the patch faces the electrode solution whereas the inner surface is exposed to the bath. In this configuration, the bath solution can be repeatedly changed, exposing the cytosolic membrane surface of the patch to different ions and chemicals. In addition, since the membrane patch is the same one which was excised when the pipette was sealed to the cell, the same channels found in the cell-attached mode should still be apparent in the inside-out mode. This allows the comparison of the behaviour of the channel(s) on and off the cell. This comparison is very important as some channels are dependent on intracellular messengers to regulate their activity. These cytosolic components are lacking in inside-out configuration, and thus channel activity may be changed.

**In summary**, regardless of the pitfalls which are currently present, patch clamp

recording provides reasonable means to determine both the single channel conductance, and the ionic selectivity of individual channels. Whole cell patch-clamp recording allows the characterization of the macroscopic conductances of entire cells by substituting both the inside and outside ion constituents of the cell. Thus, the application of the patch-clamp technique provides information about channel proteins and their regulation, and is a more sophisticated and direct method for investigating the role of ionic channels in epithelial cells as compared to other conventional methodologies.

# 2

## Materials and Methods

---

### 1. Materials

#### *1.1 Materials for cell preparation*

Pigmented rabbits between 4 to 8 weeks of age and weighing between 1.2-1.8 kg were obtained from a local resource in Burlington (Nova Scotia, Canada).

Sodium-pentobarbital ethanol, was purchased from MTC pharmaceuticals (Cambridge, ONT, Canada) and was used at a dose of 1 ml/5 kg from an original stock concentration of 540 mg/ml. For cell culture, Dulbecco's Modified Eagle's Medium (DMEM), fetal calf serum, penicillin-streptomycin and Nunclon tissue culture dishes were obtained from Gibco BRL. (Burlington, ONT, Canada). Ethylene glycol -bis ( $\beta$ -aminoethyl ether) N,N,N',N'-tetraacetic acid (EGTA) and trypan blue were obtained from Sigma Chemical Co. (St. Louis, Mo, USA). Phosphate buffered saline (PBS) was prepared using the following compositions (in mM): NaCl 140, KCl 2.7, Na<sub>2</sub>HPO<sub>4</sub> 8.0, KH<sub>2</sub>PO<sub>4</sub> 1.5. All chemicals used in preparing PBS were obtained from Sigma Chemical Co. and were dissolved in millipore purified water. Glass coverslips were obtained from Fisher Scientific Ltd. (Ottawa, ONT, Canada).

#### *1.2 Materials for immunocytochemical and fluorescent experiments*

Anti-cytokeratin pan 8.13 (Sigma ImmunoChemicals) and monoclonal anti-

epithelial keratin - AE1/AE3 mixture (ICN Biomedicals, Inc., Costa Mesa, CA., USA) (both made in mouse) were used for cytokeratin staining. These antibodies were chosen for the following reasons: Anti-cytokeratin pan 8.13 reacts specifically with a wide variety of epithelial tissues and cultured epithelial cells (Gigi et al., 1982). It binds to an epitope present in a large number of cytokeratins without staining cells of non-epithelial origin. For monoclonal anti-epithelial keratin - AE1/AE3 mixture, the AE1 antibody recognizes most of the acidic (Type I) keratins, whereas the AE3 antibody recognizes all known basic (Type II) keratins (Tseng, et al., 1982; Sun, et al., 1983). Since each epithelium contains at least one acidic and one basic keratin, these two antibodies are broadly reactive and positively stain almost all epithelia (Tseng, et al., 1982).

Monoclonal mouse anti-swine vimentin (DAKO-Vimentin, V9) was obtained from Dimension Laboratories (Mississauga, ON, Canada). It reacts with vimentin, the 57 kD intermediate filament protein present in cells of mesenchymal origin. No reaction has been found with other closely related intermediate filament proteins, such as desmin, keratin, neurofilament or glial fibrillary acid protein.

Normal (nonimmune) horse serum, biotinylated anti-mouse secondary antibody (made in horse) and Vectastain *Elite* ABC reagents containing Avidin DH and biotinylated horseradish peroxidase H, which were used for visualizing the immunocytochemical reaction. These were purchased in the form of a kit from Dimension Laboratories (Mississauga, ONT, Canada). Also purchased from Dimension Labs were the colouring reagent, 3,3'-diaminobenzidine (DAB) substrate kit and normal sheep serum. Fluorescein Rhodamine (TRITC) - conjugated anti-mouse (made in sheep)



secondary antibody was used for immunofluorescent staining of the epithelial cells and was obtained from Jackson ImmunoResearch Laboratories, Inc. (West Grove, PA, USA). Triton X-100 used to enhance membrane permeabilization was obtained from Sigma Chemical Co.; Fluomount and methanol were purchased from BDH Inc. (Toronto, ONT, Canada).

### *1.3 Solutions and chemicals for the electrophysiological experiments*

The standard external Ringer solution was composed of (in mM): NaCl, 130; KCl, 5; CaCl<sub>2</sub>, 2.5; MgSO<sub>4</sub>, 1; Na<sub>2</sub>HCO<sub>3</sub>, 25; HEPES, 5; Glucose, 10; the pH was adjusted to 7.4 with 1M NaOH or 1N HCl. The electrode filling (internal) solution which was used for all whole-cell, perforated-patch, and cell-attached recordings was composed of (in mM): KCl, 130; CaCl<sub>2</sub>, 0.4; EGTA, 1; HEPES, 20; ATP (Mg), 1; GTP(Na<sub>2</sub>), 0.1; and the pH was adjusted to 7.4 with 1M KOH. The free Ca<sup>2+</sup> and Mg<sup>2+</sup> levels of the intracellular solution were calculated using a computer software program and were 40 nM and 0.95 mM respectively, close to the corresponding physiological levels of  $\leq 100$  nM and 1 mM (Hille, 1992). Solution osmolarities were determined by freezing point depression using an osmometer (Osmette A, Fisher Scientific, Nepean, Ont.).

For perforated-patch recording, nystatin was dissolved in dimethylsulphoxide (DMSO) (50 mg/ml) and diluted to a final concentration of 0.1 mg/ml in internal solution. The DMSO-nystatin solution was sonicated in an ultrasonicator to enhance solubilization. Since the nystatin stock solution tends to lose activity upon prolonged storage and freezing, it was used within one week and the final solution was prepared

fresh each time.

N-methyl-D-glucamine<sup>+</sup> (NMDG<sup>+</sup>) was used to replace Na<sup>+</sup> in the external perfusion solution in some experiments. Potassium channel blockers and other drugs including tetraethylammonium (TEA); 4 aminopyridine (4-AP); quinine; charybdotoxin (CTX); iberiotoxin (IbTX); barium (Ba<sup>2+</sup>); cesium (Cs<sup>+</sup>), phenylephrine (PE), and inositol(1,4,5)-trisphosphate (IP<sub>3</sub>) were dissolved in Millipore water and made into concentrated stocks. Stock solutions were then diluted with the standard external solution to desired concentrations before use. Ionomycin and prazosin were first dissolved in DMSO, then made into concentrated stocks with millipore water and diluted to desired concentrations with standard external solution before use. IbTX stock was lyophilized for storage due to the fact that it will hydrolyse in solution. All stocks were kept at -20°C. IbTX was obtained from Peninsula Lab. Inc. (Belmont, CA. USA) and CTX was from Accurate Chemicals & Scientific Corp. (Westbury, NY, USA); ionomycin was purchased from Rose Scientific Ltd. (Edmonton, Albert, Canada); DMSO was from J. T. Baker Inc. (Phillipsburg, NJ. USA). All other chemicals were from Sigma Chemical Co. The final concentration of DMSO in all solutions used was less than 0.05% (vol/vol). DMSO itself at this concentration does not significantly affect the electrical properties of cells (Joseph and Miller, 1992).

## 2. Methods

### 2.1 Cell dissociation and culture

Four to eight week old pigmented rabbits were used for the preparation of isolated

MATERIALS AND METHODS

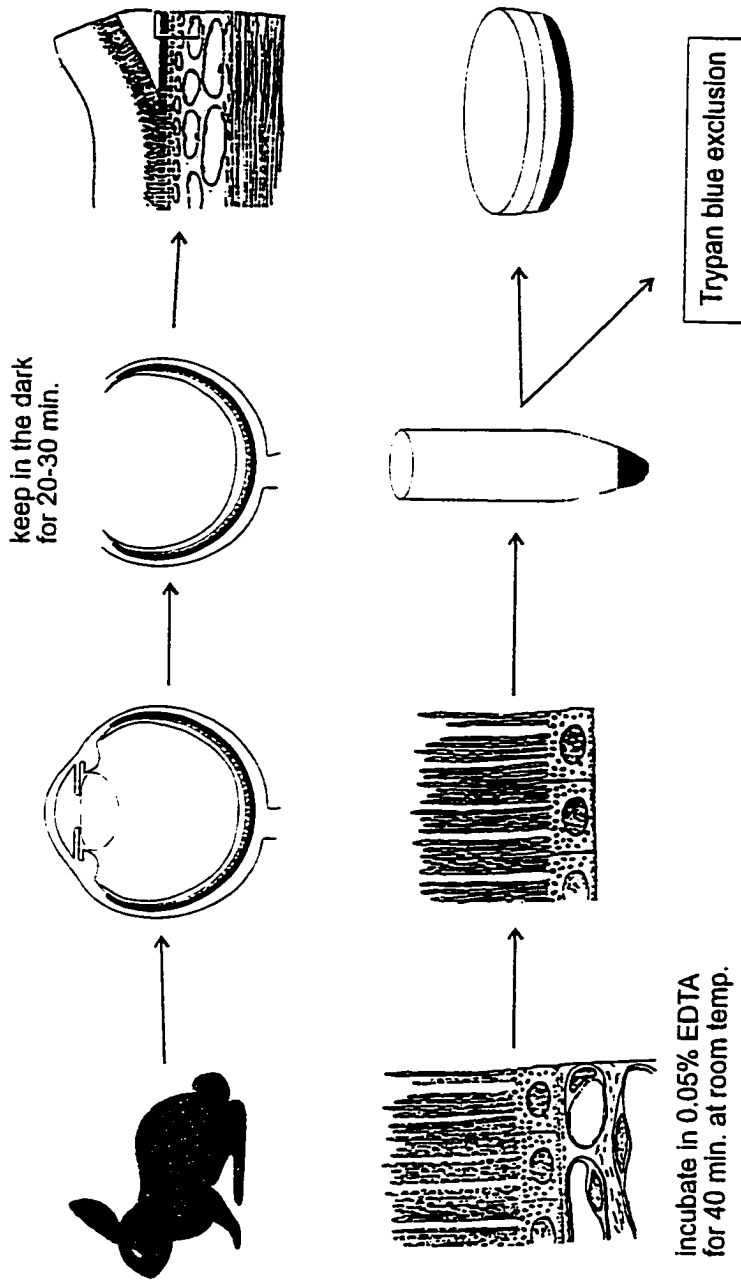


Fig. 2-1. Simplified schematic diagram of rabbit RPE cell dissection procedure (see text for details).

RPE cells. Animals were euthanized with sodium-pentobarbital and the eyes were removed (in accordance with the Association for Research in Vision and Ophthalmology guidelines for the use of animals in biomedical research). Following enucleation, the eyes were placed in PBS and kept in the dark. Using aseptic conditions, the globes were hemisected below the ora serrata and the anterior segment and vitreous were removed. The neural retina was then gently peeled off using forceps and the posterior eye cups were incubated in sterile PBS containing 0.05% EGTA for 40 min at room temperature. Eye-cups were then irrigated with fresh EDTA-free PBS and separated RPE sheets were obtained by gentle aspiration. The RPE tissue was triturated through a narrow-bore glass pipette to yield a single cell suspension. Isolated cells were washed and resuspended in DMEM plus 10% fetal calf serum and 0.1% Penicillin-Streptomycin. Cell viability was estimated by exclusion of trypan blue (discussed below), and was generally greater than 95% ( $95.75 \pm 5.74\%$ , mean  $\pm$  SD,  $n=17$ ). Cells were seeded onto glass coverslips (12 mm diameter) in 35 mm plastic petri dishes at a density of  $0.5 \times 10^5$  -  $1.5 \times 10^5$  cells/dish, and placed in a 37°C incubator in a humidified atmosphere with 5% CO<sub>2</sub>/95% O<sub>2</sub>. Cells generally attached to the coverslips within 24 hours. Cells were maintained in primary culture for 2-5 days and were identified by morphological criteria, the presence of melanin, and by immunocytochemical and fluorescent staining for cytokeratins and vimentin (see Results, section 2). The dissection procedure is illustrated in figure 2-1.

### *2.2 Trypan blue exclusion test for cell viability*

Cells which remain viable throughout the dissociation will have intact membranes

and will be impermeable to trypan blue. To assess the permeability to trypan blue, 10  $\mu\text{l}$  of 2.5% trypan blue and 90  $\mu\text{l}$  of cell suspension were mixed thoroughly and 20  $\mu\text{l}$  of the mixture was transferred immediately to a hemocytometer chamber and left at room temperature for 2 min. Cells were counted within 4 1- $\text{mm}^2$  areas under a binocular microscope with a 10x objective. Cells which stained blue were designated as non-viable. Cells which remained impermeable to the stain were considered viable. The cell concentration was derived from the following equation:

$$c = n/v \quad (1)$$

where  $c$  is the cell concentration (cells/ml),  $n$  is the number of cells counted, and  $v$  is the volume counted (ml). Since only one 1  $\text{mm}^2$  area is used and the depth of the chamber is 0.1 m, therefore  $v=0.1 \text{ mm}^2$  or  $10^4 \text{ ml}$ ,  $n=\text{total cells counted}/4$ . Since 90% of the mixture was cell suspension, the actual cell concentration was corrected by dividing 90%. So formula (1) becomes:

$$c=n/4 \times 10^4 \times 100/90 \quad (2)$$

Cell counts were carried out in triplicate in each experiment and the average of these values was recorded. Cell viability was expressed as the number of unstained cells as a percentage of the total cells.

### 2.3 *Immunocytochemical and Immunofluorescent experiments*

The immunocytochemical staining procedure was a modification of the ABC technique (instructions provided with the Vectastain *Elite* ABC kit from Vector Labs).

This technique employs an unlabeled primary antibody, which is followed by a

biotinylated secondary antibody and then a preformed avidin and biotinylated horseradish peroxidase macromolecular complex (ABC). The following procedure was used: The culture media was removed, the cells were washed in PBS three times for 10 min each and then fixed in methanol for 5 - 10 min at  $-20^{\circ}\text{C}$ . All subsequent steps were carried out at room temperature unless otherwise stated. The fixed cells were incubated with 0.3%  $\text{H}_2\text{O}_2$  + 0.03% Triton X-100 for 10 min to quench endogenous peroxidases and to enhance membrane permeabilization to the antibodies, respectively. The cells were then treated for 1 hour with 10% nonimmune horse serum (a serum from the species in which the secondary antibody was made) to block non-specific immunoglobulin binding sites. Cells were then incubated for 1 hour at  $37^{\circ}\text{C}$  or overnight at  $4^{\circ}\text{C}$  with the primary antibodies [anticytokeratin pan 8.13 (1:100 dilution in PBS) or AE1/AE3 mixture (1:200 dilution)]. After washing in PBS, the cells were then incubated for 1 hour in a biotinylated anti-mouse secondary antibody (made in horse, 1:500 dilution). The secondary antibody was removed and the cells were washed with PBS after which they were incubated in the ABC reagent (1:500) for 45 min. After extensive washing, cytokeratin pan/ AE1/AE3 positive stained cells were visualized using DAB substrate (= 10 min incubation). Stained cells on coverslips were then washed with distilled water for 15 min and mounted onto glass slides with aqueous mount (PBS/glycerol, 1:3).

When staining for vimentin, the procedure was the same as above except the primary antibody used was DAKO-Vimentin, V9 (1:25 dilution in PBS).

For immunofluorescent staining, the same procedure was used except the blocking serum was 10% normal sheep serum and the secondary antibody was a

fluorescein Rhodamine (TRITC) - conjugated anti-mouse in sheep (1:50 dilution). Cells were incubated with the fluorescein secondary for 1 hour at 37°C. Positively stained cells were mounted onto glass slides with Fluomount.

In all experiments, a control coverslip was used in which the primary antibodies were replaced by PBS. All other steps remained the same. This was done in order to detect any non-specific background staining of the cells.

#### *2.4 Superfusion system*

Cells, attached to glass coverslips, were placed in a shallow recording chamber and positioned on the stage of a Nikon inverted microscope. Cells were superfused (1-2 ml/min) with standard physiological solution. External solutions (see material section 1.3 for composition), equilibrated with 95% O<sub>2</sub> and 5% CO<sub>2</sub>, were gravity-fed into the recording chamber from elevated reservoirs and were selected by a series of switches designed to maintain a constant flow. In experiments where pharmacological blockade of ionic currents was studied, test solutions were applied by bath superfusion or by pneumatic pressure ejection from micropipettes (tip diameter 1-2 μm). When test substances were applied by bath superfusion, the flow rate (1-2 ml/min) was kept constant and the test solution was selected using a switching valve. It was determined that it took ≈ 30 sec for the solution to flow into the bath from the reservoirs at this constant flow rate. Test solutions were applied for a minimum of five and usually for ten complete (1 ml) bath exchanges. For application of test substances by pressure ejection, micropipettes were positioned 50-100 μm from the cell and ≈ 2-5 lb/in<sup>2</sup> pressure was

applied to the back of the micropipette using a Picospritzer II (General Valve Corp., Fairfield, NJ, USA). For those experiments where external  $K^+$  was increased, NaCl was replaced with equimolar amounts of KCl to a final concentration of 25 or 50 mM  $K^+$ . In experiments which investigated time-dependent decay of the whole-cell inward current at negative potentials,  $Na^+$  was substituted with NMDG $^+$ . The composition of the electrode filling solution is listed in the materials section 1.3. Free  $[Ca^{2+}]_i$  in the internal solution was estimated to be  $\approx 100$  nM. When investigating  $K_{Ca}$  channels and their  $\alpha_1$ -adrenergic modulation, most of the  $Cl^-$  was replaced with aspartate in both the external and internal Ringers in order to minimize the contribution of the  $Cl^-$  current. Low  $Ca^{2+}$  (100nM) external Ringer was used to minimize  $K_{Ca}$  channel activity under control conditions in order that an increase in current due to an increase in  $[Ca^{2+}]_i$  after application of an  $\alpha_1$ -adrenergic agonist could be clearly observed. The EGTA concentration in the internal Ringer was also reduced from 1mM to 0.5mM in order to observe any effects of increased  $[Ca^{2+}]_i$ . The electrode filling solution was filtered using a 0.22  $\mu$ m filter (Millipore Products Division, Bedford, MA). External solutions had a final osmolarity of between 330-340 mOsm.kg $^{-1}$  and the osmolarity of internal solutions was 320 mOsm.kg $^{-1}$ . The use of a slightly hyperosmotic external solution was found to be effective for eliminating any transient changes in ionic conductances, which occurred as a result of osmotic changes during the initial period of time following attainment of whole-cell recording configuration. Because during the initial period of recording, the cell is being dialysed with internal pipette solution whose osmolarity is different from cell interior, some osmotic changes may happen as the cell attempts to equilibrate. If the cell swells, it



might transiently activate other conductances such as  $\text{Cl}^-$  conductances. Using slightly hyperosmotic external solution prevents cell swelling and reduces the possibility of swelling-induced ion channel activation.

In cell-attached patch or inside-out patch single-channel recordings, 130 mM  $\text{K}^+$  was used for both external and internal solutions. In cell-attached configuration, 130 mM  $\text{K}^+$  was used to zero the cell membrane potential (assuming the  $[\text{K}^+]_i$  of the rabbit RPE cells is close to 130mM) so that it could be clamped as desired during the experiment (discussed in section 2.7).

### *2.5 Fabrication of recording electrodes*

Patch electrodes were pulled from borosilicate glass micropipettes with a 1.5 mm outside diameter and a 1.1 mm inside diameter (Sutter Instruments, Novato, CA, USA) on a two-stage vertical microelectrode puller (Narishige, PP83, Tokyo, Japan). The electrodes were coated with beeswax, a hydrophobic substance, to within about 50 -100  $\mu\text{m}$  of the tip leaving the tip uncoated. This was done in order to minimize the background noise by preventing the creep of bath fluid and reducing the pipette-bath capacitance (Rae and Levis, 1984). The electrode tips were first filled with a small amount of internal solution and then back-filled using a syringe fitted with a 0.22  $\mu\text{m}$  filter and a 30 gauge needle. Bubbles in the shank of the electrode were removed by tapping the electrode. The electrodes had resistances of 2 to 3  $\text{M}\Omega$  when filled with the internal solution and placed in the bath solution.

When the perforated-patch technique was used, the electrode tips were filled with

nystatin-free internal solution and back-filled with nystatin-containing solution. This step was necessary due to the fact that nystatin interferes with seal formation.

### *2.6 Electrophysiological recording techniques*

The cell-attached, inside-out patch and whole-cell configurations of the patch-clamp recording technique (Hamill et al., 1981), as well as the nystatin perforated patch method (Horn and Marty, 1988), were used in this study. Figure 2-3 summarizes these different patch-clamp recording configurations. By pressing a patch pipette against the membrane of a cell and applying gentle suction to the back of the pipette, a giga-seal can be formed around a small patch of the cell membrane (cell-attached). Here, the electrode records the activity of any ion channels which are active in the small patch of the membrane under the electrode. In this mode, the outside of the cell membrane faces the pipette solution and the inside of the membrane faces the cytoplasm of the cell. By withdrawing the pipette from the cell after seal formation, an isolated patch of the membrane sealed to the pipette can be torn off the cell resulting in "inside out" patch recording configuration. In this configuration, the cytoplasmic membrane surface faces the bath solution thereby, allowing easy control of the cytosolic environments. From cell-attached mode, a brief application of stronger suction can rupture the patch of membrane but leave the giga-seal intact (whole-cell). In this configuration the electrode interior is directly connected to the cell interior, and the whole-cell current is recorded. In the whole-cell recording configuration the cytoplasmic constituents can be exchanged with the pipette filling solution, thereby allowing experimental control of the intracellular

MATERIALS AND METHODS

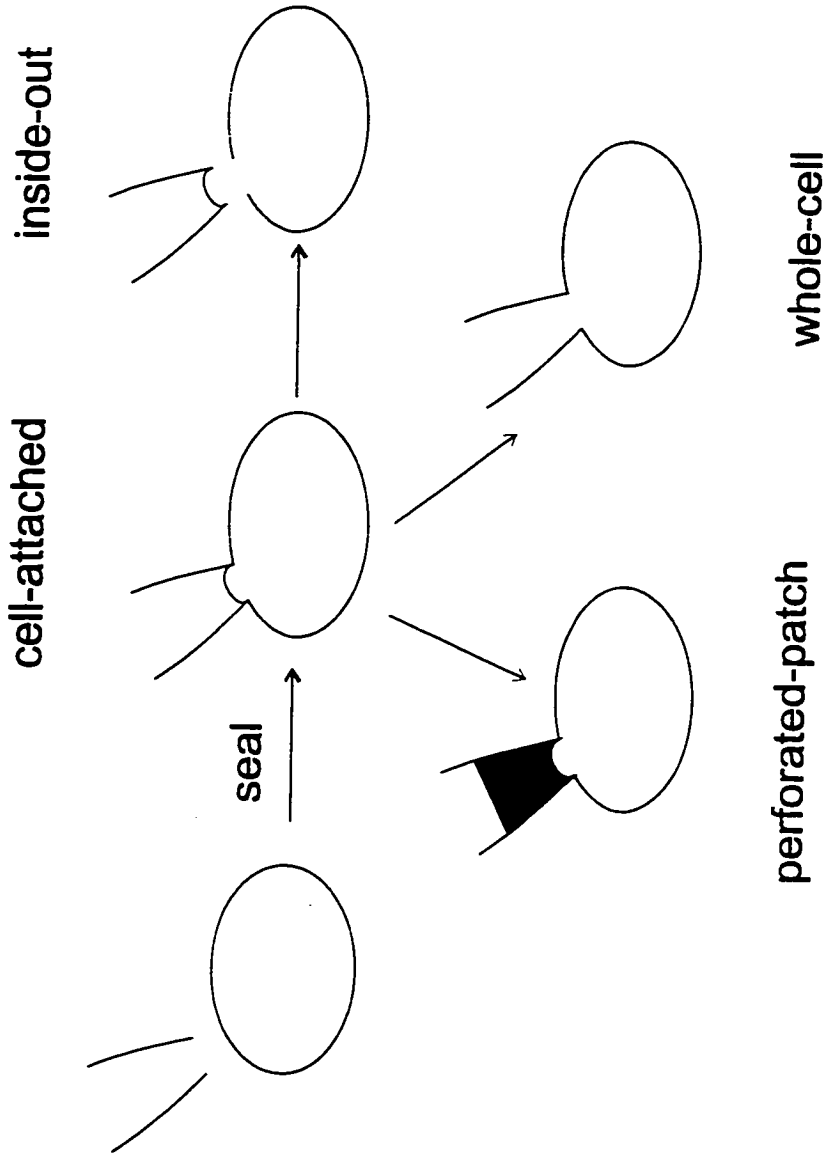
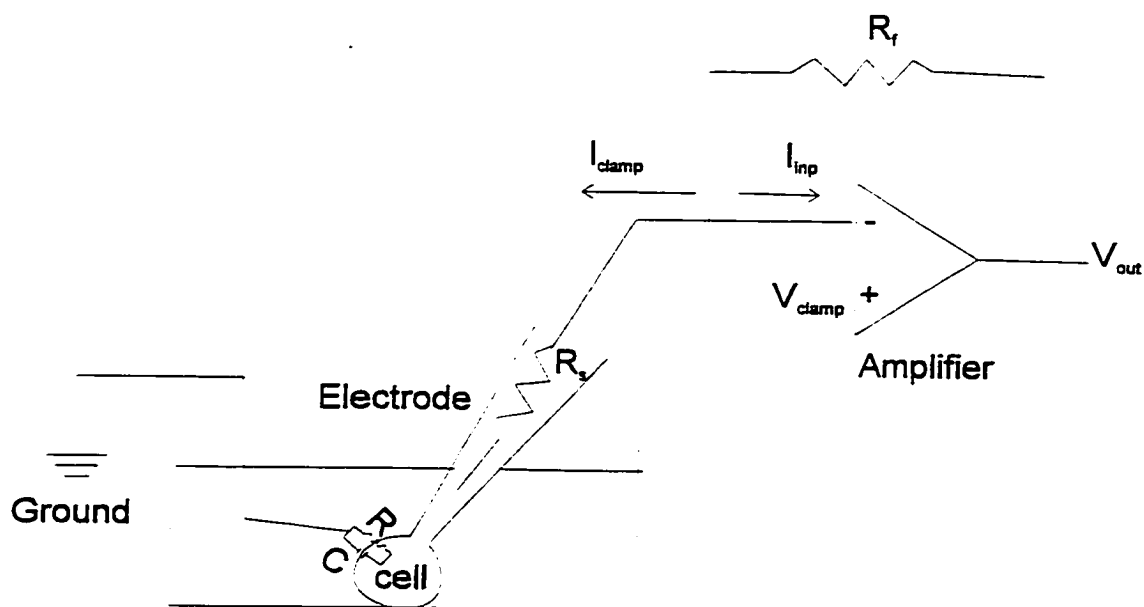


Fig. 2-2. Schematic diagram of different patch clamp configurations used in this study.

See text for details.

constituents. However, it also dialyses the cytoplasmic ions, nucleotides and other diffusible constituents in the pipette. The introduction of the "perforated-patch" method improves this drawback. In this method, the pore-forming antibiotic nystatin is included in the electrode filling solution. Following attainment of the cell-attached configuration, over a period of some 10 - 20 min, nystatin incorporates itself into the patch membrane and provides a low access resistance pathway from the pipette to the cell interior. The channels formed by nystatin are permeable to monovalent cations and  $\text{Cl}^-$  but exclude multivalent ions including divalent cations as well as large organic molecules and proteins. This minimizes the cellular dialysis so that the physiologically relevant second-messenger cascades and mechanisms important to cell signaling and channel regulation remain operative during the recording. This method was used for identifying  $\text{Ca}^{2+}$ -activated  $\text{K}^+$  currents and examining  $\alpha_1$ -adrenergic modulation of these currents.

Figure 2-3 shows the arrangement of a patch clamp experiment in whole-cell configuration. The bath solution was connected to the reference electrode by a 3 M KCl-2% agar bridge. Offset potentials were nulled using the amplifier circuitry before seals were made on cells. Liquid junction potentials of 1-2 mV for standard external and internal solutions which arose due to different ionic compositions of the bath and the patch-clamp electrode, were not corrected in the data shown unless otherwise noted. Membrane potential and ionic currents were recorded with an Axopatch 1D amplifier (Axon Instruments Inc., Foster City, CA, USA). Data were filtered with a 4-pole lowpass Bessel filter (-3 dB at 1 kHz) to eliminate both extraneous noise and any signals above the bandwidth of interest, so that the interpretation of the data would be enhanced. Data



**Fig. 2-3.** Schematic diagram for whole-cell patch clamp recording. The electrode forms a tight seal with the cell membrane, so the cytoplasm is electrically continuous with the saline in the pipette. Ionic currents flow through the open channels which are located in the cell membrane, then flow out of the pipette which is connected to the negative input of the operational amplifier. The amplifier serves two functions: it is an ammeter to measure the ionic currents and it is also a variable clamp battery. The clamping current which is used to impose a voltage on the cell membrane also flows into the cell via the pipette. The bath is grounded via the reference electrode (Modified and reproduced from Armstrong and Gilly, 1992).  $R_f$ : feedback resistor;  $R_s$ : series resistance;  $R$ : cell input resistance;  $V_{out}$ : output voltage;  $V_{clamp}$ : clamp-battery voltage;  $I_{inp}$ : current flowing through the inputs;  $I_{clamp}$ : clamp current;  $C$ : cell capacitance.

were digitized at a sampling frequency of 5 kHz using pClamp software (Axon Instruments Inc.) and were displayed on a Gould TA240 chart recorder and stored on computer disc. Values for cell capacitance were obtained from the capacitance compensation circuitry on the amplifier or by integration of the uncompensated current transient (obtained using 10 mV voltage commands). In the later case, cell capacitance was derived from the total charge  $Q$  displaced during the 10 mV step command, according to  $C = Q/V$ . Measures of series resistance ( $R_{\text{access}}$ ) were obtained directly from the amplifier and were generally less than 15 M $\Omega$ . Eighty percent series resistance compensation was used in most cases. All experiments were conducted at room temperature (21-22°C). At this temperature, the effect on channel conductance would be expected to be negligible, the channel kinetics may be slowed as compared to that observed at 37°C (Hille, 1975).

### *2.7 Data analysis and figure construction*

Data were recorded using appropriate acquisition parameters (sampling rate, filtering) as mentioned above (section 2.6). Fitting functions to sets of data points were performed using either CLAMPFIT (Axon pClamp Ver 5.5.1 software program) or Sigmaplot, a graphing software program (Jandel Scientific, San Rafael, CA, USA). The function of exponential time-dependent decline of currents was fitted with respect to the relevant set of data. This fitting was made using the CLAMPFIT program to decide how well the data followed the best fit function and to extract the time constant. The relationship of the reversal potentials of the whole-cell tail currents and  $[K^+]_o$  was

determined by linear regression analysis and was performed using the Sigmaplot program. Boltzmann equation fittings were done in Sigmaplot in order to describe the behaviour of sets of data. All the fitting functions will be described in the results chapter, where appropriate. All graphs of experimental data were made using Sigmaplot Ver 5.1 for DOS or Ver 2.0 for Windows. The final figures were constructed using an illustrative computer program package, Coreldraw (Corel Corp., Ontario, Canada). Values of currents reported in the figures are averages of 10 to 50 points. In some cells current records were corrected for a linear leakage current (resistance values were calculated from linear regression of the I-V relations for the leak currents measured at hyperpolarized potentials). Where currents have been leak subtracted the resistance value is stated in the figure legend.

In the cell-attached or inside-out patch configuration, the patch potential is the negative of the pipette potential. In cell-attached mode, the cell membrane remains intact, therefore:

$$V_m = RMP - V_p \quad (3)$$

where  $V_m$  is the clamped potential across the membrane patch, RMP is cell resting membrane potential, and  $V_p$  is the pipette potential (see Fig. 2-4).  $V_m \approx -V_p$  when RMP is close to 0 mV. Whereas in inside-out configuration, because the cytoplasmic surface faces the bath solution and the bath is grounded, the voltage across the patch of the membrane equals to the voltage in the electrode in the opposite polarity ( $V_m \approx -V_p$ ).

In cases where voltage-ramp commands were used to generate current-voltage relationships the current was sampled every 500  $\mu$ s and was smoothed using a 4-point

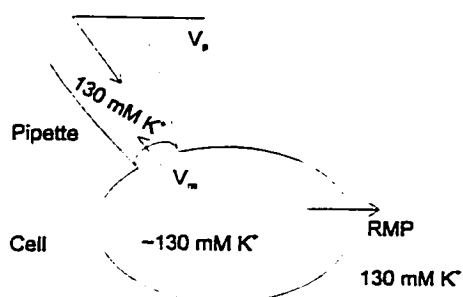


Fig. 2-4. Patch-clamp recording, cell attached configuration.

averaging method which decreased the number of data points to facilitate display. Current traces recorded using ramp commands were corrected for leakage via the subtraction of null sweeps which contained no channel openings. The conductance values of the channels were calculated from the slope of their current-voltage relationship fitted by linear regression. Current-voltage (I-V) plots were obtained either from current ramps or from unitary single channel currents measured at different holding potentials. The probability of the channel being open ( $P_o$ ) was determined in patches containing only a single channel type, from the average current above the baseline divided by the unitary current amplitude and the number of channels in the patch (using pCLAMP analysis programs).  $P_o$  values were calculated for 4 or 8 second periods of channel activity. In patches where many channels were open simultaneously, channel activity was expressed as  $NP_o$ , where  $N$  is the number of channels in the patch and  $P_o$  is the opening probability (Carl and Sanders, 1990).

The data difference between control and test conditions was analyzed by Student's paired or unpaired  $t$  test ( $P < 0.05$ ). Data are presented as mean  $\pm$  SE unless indicated otherwise.



# 3

## Results

---

### 1. Establishment of rabbit RPE cell culture

Primary rabbit RPE cell cultures were established using 4-8 week old pigmented rabbit eyes. Mechanical dissociation of RPE explants was used to yield isolated cells. The typical yield was about  $1-3 \times 10^5$  cells per eye with viabilities ranging from 80 to 100%, estimated using trypan blue exclusion test. Figure 3-1A shows a freshly dissociated RPE explant before mechanical trituration. Hexagonal shaped RPE cells were tightly packed and contained pigment granules. Figure 3-2A shows freshly isolated RPE cells. The isolated cells were heavily pigmented and still maintained their hexagonal shape. Figures 3-2B and C show representative single cells used for recording. They have been growing in primary culture for 3 days. Cells usually attached to the plastic culture dish and started growing as early as 24 hours after being plated. In figure 3-2B, the apical portion of the cell is readily distinguished by the presence of pigment granules as well as cellular processes. Cells growing for longer periods of time in primary culture became more spindle-shaped, and formed confluent monolayers. Cells grown for even longer periods of time ( $> 6$  weeks) also formed raised patches of monolayers (Fig. 3-1B). Similar characteristics have been described previously in human and monkey RPE cells, and have been suggested to be an indication that RPE cells in monolayer culture continue

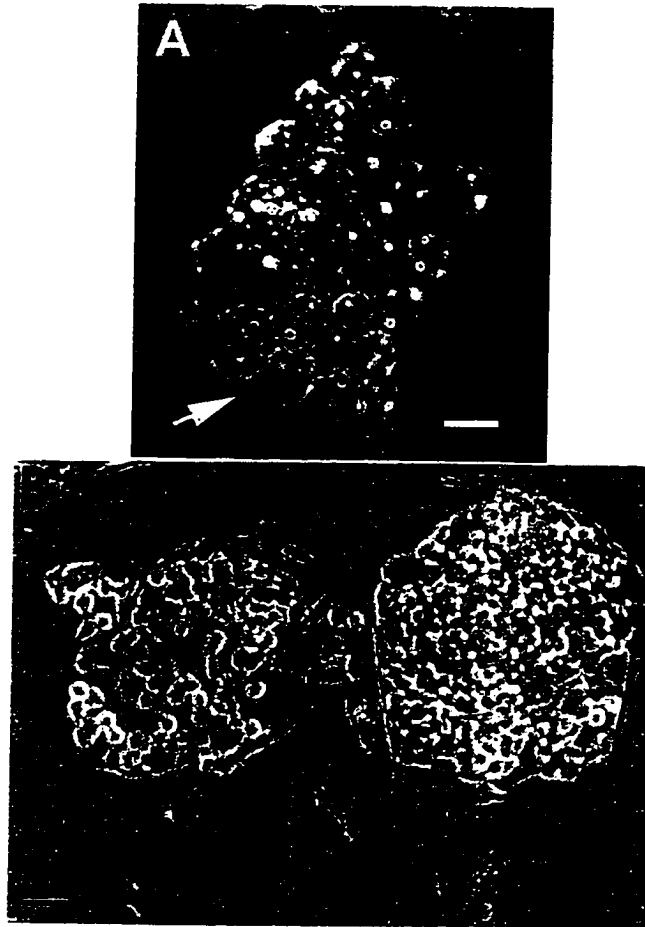


**Fig. 3-1.** (A) Photomicrograph of a freshly dissociated RPE explant. Cells are hexagonal and heavily pigmented (arrow). (B) Compact patches of rabbit RPE cells derived from confluent monolayer culture (arrows) six weeks after plating. Scale bars equal 10  $\mu\text{m}$  for (A) and 20  $\mu\text{m}$  for (B).



**Fig. 3-2.** Morphology of rabbit RPE cells in culture (phase-contrast photomicrograph)  
(A) Freshly isolated rabbit RPE cells (arrows). (B & C) Representative RPE cells used  
for recording. Apical portion of the cell (arrow in B). Cells have been growing for 3  
days in primary culture. Scale bars are equal to 20  $\mu\text{m}$  in (A) and 10  $\mu\text{m}$  for (B) and (C).

to carry out unidirectional transport of ions and water (Pfeffer and Newsome, 1983; Aronson, 1983). A similar finding has also been reported in cultured intestinal epithelial cells which are capable of unidirectional movement of water to the basal cell membrane (Misfeldt, Hamamoto and Pitelka, 1976).

## **2. Cell identification**

RPE cells were identified by their morphological characteristics and by immunocytochemical staining. The morphological characteristics of RPE cells include a polygonal shape and the presence of melanin granules (see Fig. 3-1A, Fig. 3-2). Rabbit RPE cells in primary culture exhibited positive staining for cytokeratins (see Fig. 3-3A). Cytokeratins represent a family of intermediate filament (IF) proteins which are present in all epithelial cells. Typically, a given epithelial cell contains several types of cytokeratins (Corwin and Gown, 1989). Cytokeratins appear to be only expressed in true epithelia (Travo, Weber and Osborn, 1982). Antibodies which recognize cytokeratins CK8 and CK18, including those used in this study have been reported as useful markers of RPE cells (Hiscott, Grierson and McLeod, 1984; Owaribe et al., 1988; Fuchs, Kivelä and Tarkkanen, 1991). Rabbit RPE cells also stained positive for vimentin (Fig. 3-3B), the intermediate filament protein expressed in nearly all mesenchymal cells (Corwin and Gown, 1989). It has been reported that mammalian RPE cells express either CK8 and CK18 alone or together with vimentin IFs (Owaribe et al., 1988).

For electrophysiological recordings, cells were generally used at 2-5 days in

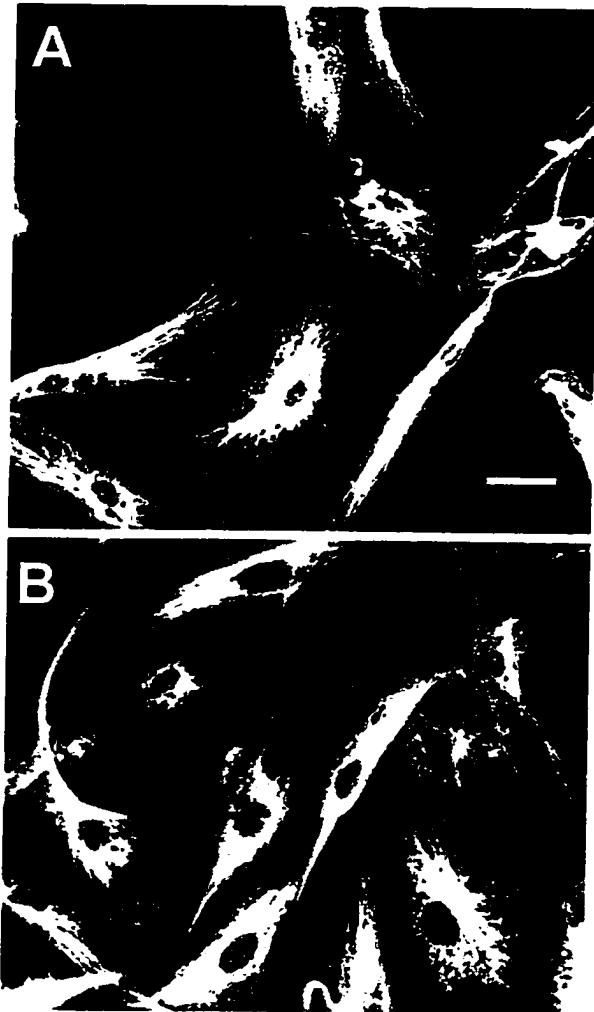


**Fig. 3-3.** Immunocytochemistry of rabbit RPE cells grown in culture for approximate two weeks. (A) Positive cyokeratin staining in cultured rabbit RPE cells. (B) Positive vimentin staining in cultured rabbit RPE cells. Scale bar equals 10  $\mu\text{m}$  for both (A) and (B).

culture. Two typical cells from which recordings were made are shown in figure 3-2B and C. These cells were chosen for recording because they were compact and spherical in shape, thereby allowing good voltage-clamp control with an approximately uniform voltage distribution in the cytoplasm of the cell being tested. No recordings were made from cells which were devoid of pigment or cells which appeared to have contact with neighboring cells. The first criterion was to ensure that electrical recordings were made from RPE cells, and the second was to avoid spatial nonuniformity of imposed voltage changes, as well as to avoid any incorrect cell capacitance and/or macroscopic current measurements which may be contributed by the adjacent cell.

### **3. Whole-cell currents and membrane properties in cultured rabbit**

#### **RPE cells**

Under voltage-clamp, RPE cells exhibited both outward and inward current in response to depolarizing and hyperpolarizing voltage commands. Figure 3-4 shows whole-cell currents recorded from two different RPE cells with 130 mM KCl in the pipette. Cells were held at -60 mV and stepped from -120 mV to +60 mV in 20 mV increments for 500 msec with 1500 msec interval between steps. In figure 3-4A, the cell shows little current in response to hyperpolarizing voltage commands, however, at positive potentials an outward current is apparent. The peak current-voltage (I-V) relationship for this cell, measured at 50 ms after the start of the voltage command, is shown in figure 3-4B with outwardly rectifying current activating at -20 mV. Figure 3-4C shows whole-cell currents recorded from a cell which exhibited steady inward current

## RESULTS

**Fig. 3-4.** Voltage-dependent currents in rabbit RPE cells. Whole-cell currents recorded from RPE cells in standard NaCl external Ringer with 130 mM KCl in the pipette. The voltage-clamp protocol is shown at the top center. (A) Currents elicited in an RPE cell by a group of voltage commands from -120 mV to +60 mV, from a holding potential ( $V_h$ ) of -60 mV. Outward current is activated at potentials of -40 mV and more positive, with little current apparent at more negative potentials. A linear leak of 1.7 G $\Omega$  was subtracted from the current traces shown. (B) Peak current-voltage (I-V) plots for the cell shown in panel (A), measured 50 ms after the start of the voltage command. (C) Currents recorded in another RPE cell using the same voltage-clamp protocol. At hyperpolarized potentials a steady inward current is observed with the outward current activating at more positive potentials. Currents were subtracted for a linear leak of 2 G $\Omega$ . (D) The I-V plot for the cell in panel (C) shows inwardly rectifying current between -50 to -120 mV and outwardly rectifying current activating at -40 mV. Capacitance of the cells shown in panels (A) and (C) was 24 pF and 57 pF, respectively. Dashed lines indicate the zero current potential in this and subsequent whole-cell recording figures.

RESULTS

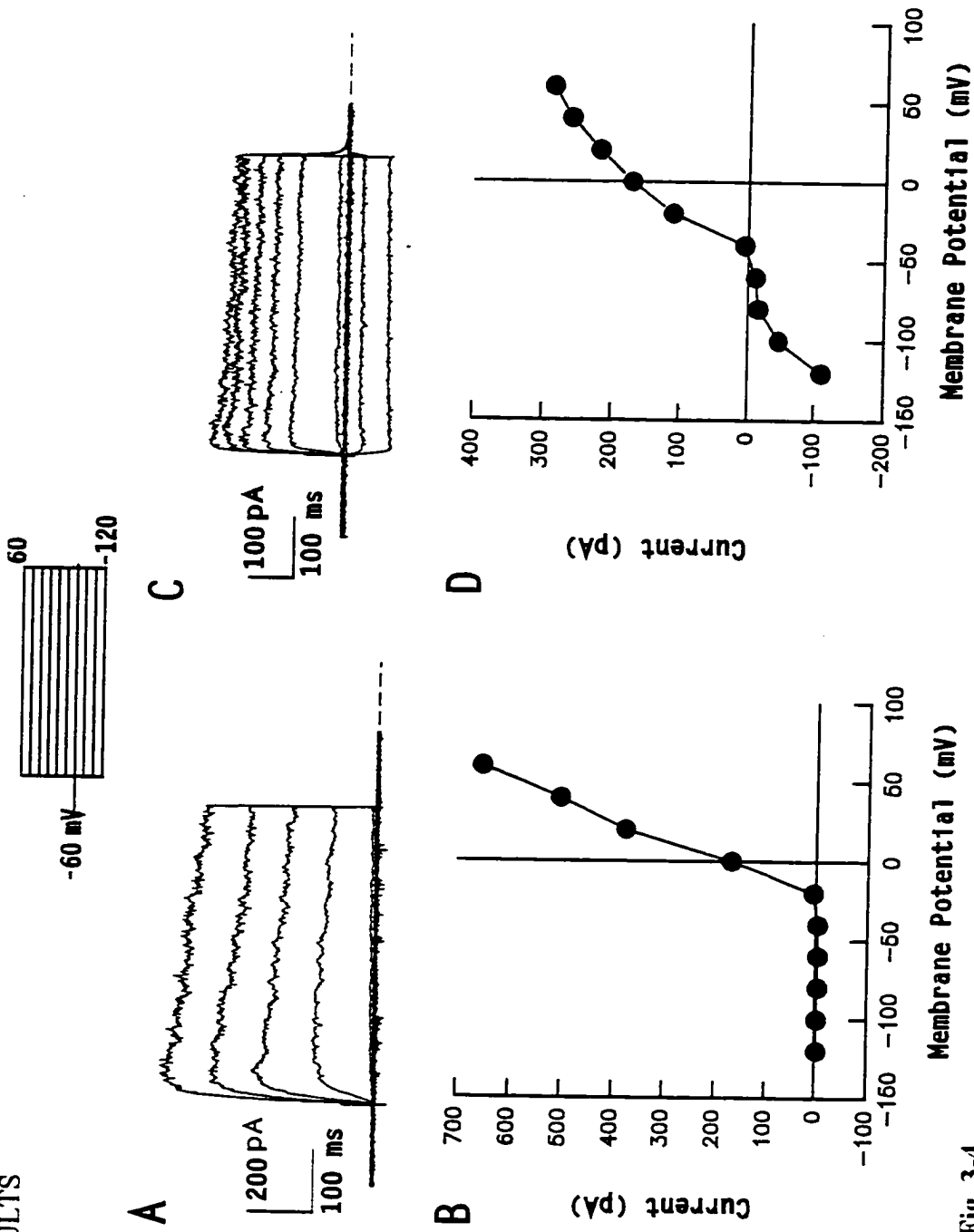


Fig. 3-4.



at hyperpolarized potentials as well as outward current at depolarized potentials. The I-V relation in figure 3-4D shows that inwardly rectifying current is apparent between -120 to -70 mV, with outwardly rectifying current activating around -40 mV.

The two voltage-dependent currents described above were the predominant currents observed in cultured rabbit RPE cells. Of a total of 294 RPE cells recorded using standard whole-cell recording conditions (130 mM KCl in the pipette, 130 mM NaCl external solution), 79-80% of RPE cells exhibited outwardly rectifying current and 40% exhibited inwardly rectifying current. Only 36% of cells recorded from exhibited both inward and outward current. A small number of cells (7%) also exhibited a fast-inactivating outward current. Table 3-1 summarizes the membrane properties and the different currents which were recorded from cultured rabbit RPE cells.

**Table 3-1. Summary of Membrane Properties and Currents Recorded from Rabbit RPE Cells in primary culture**

| Cap. (pF)<br>(mean±SE) | RMP* (mV)<br>(mean±SE) | whole-cell currents in RPE cells<br>(n=294) |                   |                   |                                 |
|------------------------|------------------------|---|-------------------|-------------------|---------------------------------|
|                        |                        | I <sub>o</sub> **                           | I <sub>t</sub> ** | I <sub>i</sub> ** | I <sub>o</sub> + I <sub>i</sub> |
| 27.0 ± 0.8<br>(n=294)  | -31.0 ± 1.4<br>(n=110) | 127(43%)                                    | 20(7%)            | 11(4%)            | 107(36%)                        |

\* RMP: resting membrane potential; \*\* I<sub>o</sub>: delayed outward current; I<sub>t</sub>: fast-inactivating outward current; I<sub>i</sub>: inward rectifying current.

To determine whether the observed currents result from the activity of a single class of ion channels or from several different channel types, ion selectivity, kinetics and pharmacology of both outward and inward currents recorded from rabbit RPE cells were

examined.

#### 4. Characterization of outward current in cultured rabbit RPE cells

##### 4.1 Outward current is $K^+$ selective

The most basic criterion for the identification of a current is the identity of the ion(s) which pass through the channel. This is best established by varying the concentrations of various ions, and observing subsequent shifts in the reversal potential ( $E_{rev}$ ) of the macroscopic current. The advantage of  $E_{rev}$  is that it is a null point measurement. Neither blockage nor simple saturation has any effect on it, while these phenomena do reduce the effective number of active channels (Hille, 1992). Currents which occur during channel deactivation (the reversal of the activation process) are called tail currents. The initial amplitude of the tail current following steps to different voltages is a measure of the amount of  $K^+$  conductance activated during the step. In this study, the ionic selectivity of the outward current was investigated in external solutions with different  $K^+$  concentrations by examining the  $E_{rev}$  of the tail current elicited by -90 to 0 mV steps in 10 mV increments, following activation of the outward current by a test voltage step to +10 mV (see Fig. 3-5A). The  $E_{rev}$  of tail currents was extrapolated mathematically from the amplitude of the two current traces which reversed direction. Tail currents recorded in standard 5 mM  $[K^+]_o$ , 25 mM  $[K^+]_o$  and 50 mM  $[K^+]_o$  are shown in figure 3-5B. In 5 mM  $[K^+]_o$  tail currents reversed direction at  $-71 \pm 3$  mV ( $n=5$ ), which approaches the value of -82 mV calculated for the  $K^+$  equilibrium potential ( $E_K$ ) under the recording conditions used. When  $[K^+]_o$  was increased to 25 and 50 mM, the  $E_K$  of the

## RESULTS

**Fig. 3-5.** Outward currents in rabbit RPE cells are carried by K<sup>+</sup> ions. (A) Representative tail currents recorded at various potentials in standard 5 mM K<sup>+</sup> Ringers following a step pulse to +20 mV to activate outward current. The voltage-clamp protocol is shown above the traces. (B) Expanded view of tail currents recorded from the same cell following sequential superfusion of 5, 25 and 50 mM [K<sup>+</sup>]<sub>o</sub>. Tail currents reversed near -75, -40 and -28 mV respectively. (C) Plot of the reversal potential of the tail currents versus extracellular [K<sup>+</sup>] for 3-5 cells. The number of cells studied at each [K<sup>+</sup>]<sub>o</sub> is indicated in parentheses beside each data point. The slope of the line fitted by least squares is 50 mV per 10-fold change in extracellular [K<sup>+</sup>]. Error bars indicate SE for this and subsequent figures unless indicated otherwise. Capacitance of the cell shown in panels (A) and (B) was 27 pF.

RESULTS

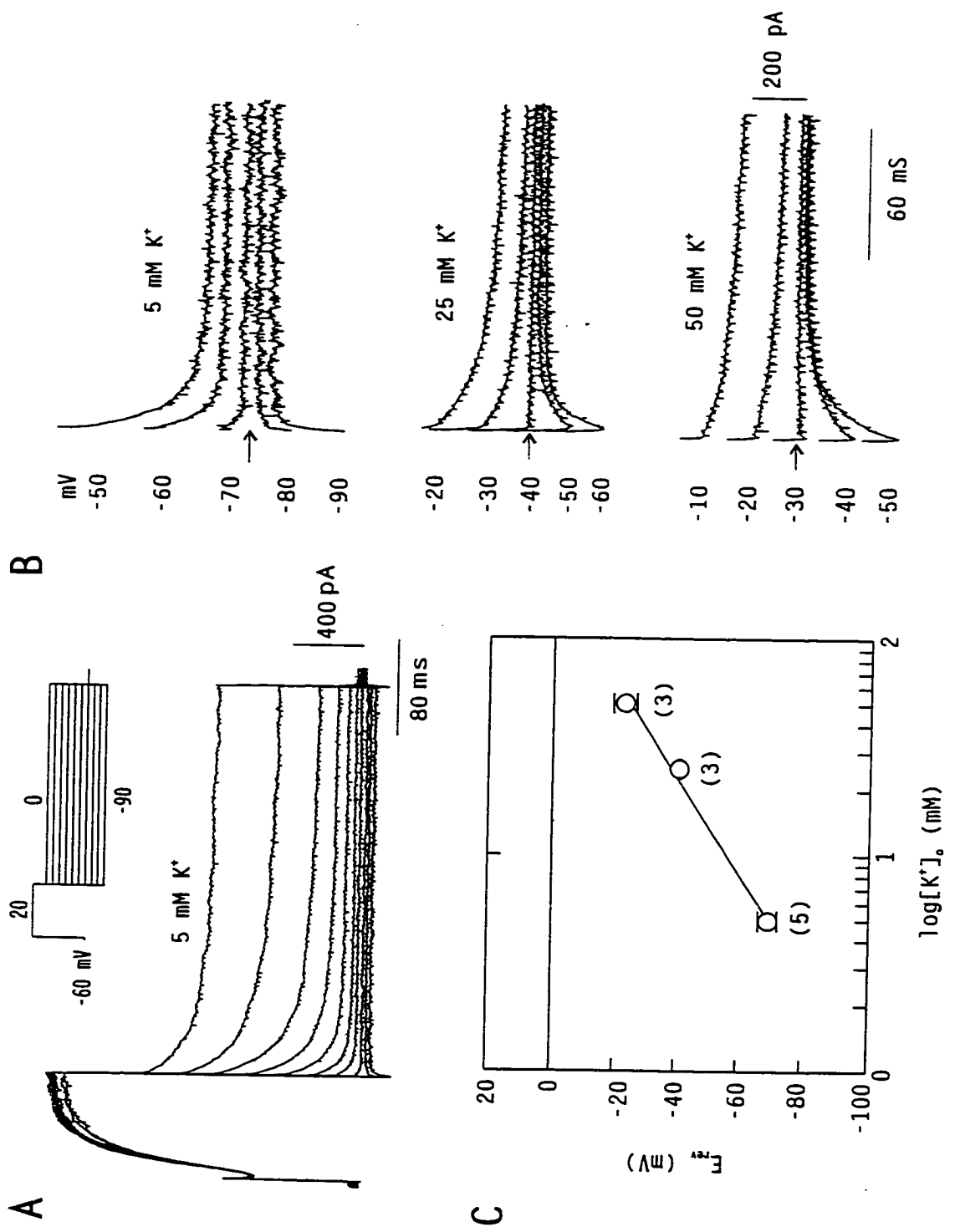


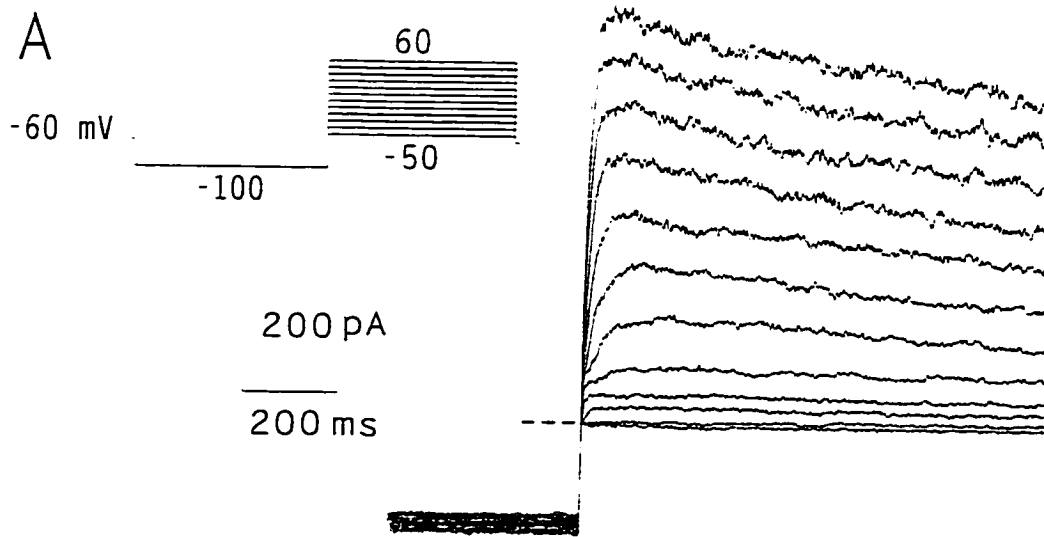
Fig. 3-5.

tails shifted to more positive values. In 25 mM  $[K^+]_o$  tail currents reversed at  $-41 \pm 0.5$  mV ( $n=3$ ) and in 50 mM  $[K^+]_o$  tail currents reversed at  $-24 \pm 2$  mV ( $n=3$ ). A least-squares fit to the data is shown in figure 3-5C. The fitted line has a slope of 50 mV per 10-fold change of  $[K^+]_o$ , which is approaching to the predicted value of 58 mV per 10 fold change in  $[K^+]_o$ , and suggests that the outward current is largely selective for  $K^+$  ions. Further analysis of the tail currents revealed that they were best approximated by single exponentials. The time constants for the decay of the tail currents were voltage-dependent and this dependence was similar in 5, 25 and 50 mM  $[K^+]_o$  (not shown), suggesting that one population of  $K^+$  channels was predominantly giving rise to the outward current.

#### 4.2. Voltage-dependence and kinetics of the outward $K^+$ current

Outwardly rectifying  $K^+$  current ( $I_K$ ) was the predominant current recorded in rabbit RPE cells under standard whole-cell recording conditions with KCl in the recording pipette (234/294 cells). Examination of the activation of the  $I_K$  was carried out using small voltage increments from a prepulse potential of -100 mV. The negative prepulse was used in order to eliminate any possible channel inactivation between each step, thereby avoiding the repetitive accumulation of inactivation between steps which would otherwise distort the slope factor. Figure 3-6A illustrates a typical family of outward currents evoked by 1 sec voltage pulses, ranging from -50 to +60 mV in 10 mV increments.  $I_K$  in the cell shown begins to activate at around -40 mV, with the activation rate increasing at more positive potentials. Since tail current analysis demonstrated that

**Fig. 3-6.** Activation of outward  $K^+$  current in rabbit RPE cells. (A) Outward current was evoked by voltage steps from -50 mV to +60 mV in 10 mV increments, from a prepulse voltage of -100 mV. The voltage protocol is shown at the top of panel (A). Outward current activates around -40 mV and activation becomes more rapid with increasing depolarization. Current traces were leak subtracted for a linear leak of 1.6 G $\Omega$ . (B) Outward  $K^+$  conductance (expressed as a fraction of the maximum conductance at +60 mV) plotted as a function of the membrane potentials from 3 individual RPE cells. Conductance values were calculated from the peak current values using equation (4) given in the text. The smooth line was fitted to the mean value of the conductance of the 3 cells using the Boltzmann equation (5). Capacitance for the cell in (A) was 41 pF.



B

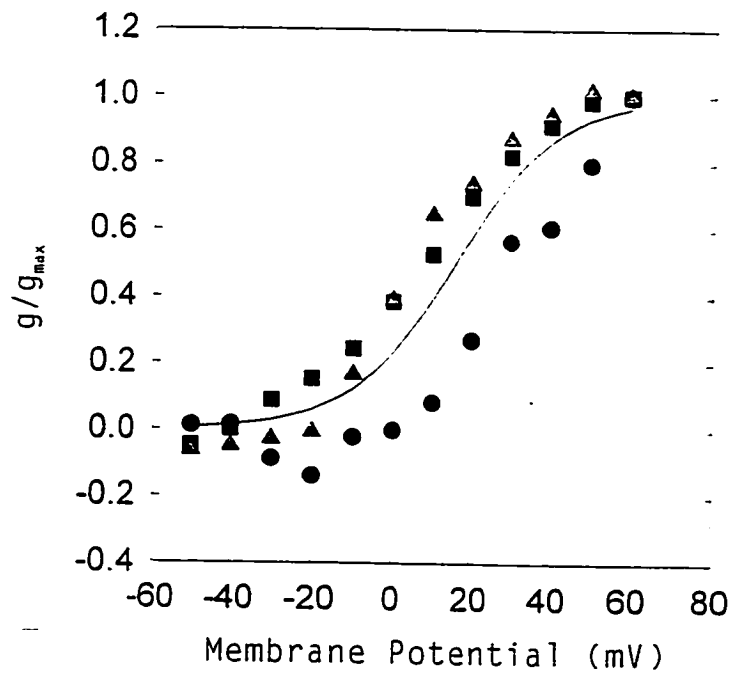


Fig. 3-6.

the outward current is carried by  $K^+$ , chord conductance can be calculated using the following relationship:

$$I_p = g(V - E_K) \quad (4)$$

where  $I_p$  is the peak outward current at membrane potential  $V$ ,  $g$  is the corresponding conductance and  $E_K$  is -82 mV, calculated under the recording conditions used. The calculated peak conductance for each test pulse was then normalized with respect to the peak conductance evoked by a depolarizing step to +60 mV. Figure 3-6B shows the conductances for 3 individual cells plotted versus the command potentials. The voltage dependence of activation is well described by the Boltzmann equation:

$$g/g_{max} = \{1 + \exp[(V_n - V)/k_n]\}^{-1} \quad (5)$$

where  $g/g_{max}$  is the normalized conductance,  $V$  is the membrane potential during the test pulse,  $V_n$  is the voltage at which the conductance  $g$  is half-maximal and  $k_n$  gives the steepness of the voltage dependence. The conductance increased sigmoidally with a threshold for activation at -40 mV and saturated at approximately +60 mV. The Boltzmann distribution of channel open steady-state probability (sigmoidal activation curve) suggests that both the channel opening and closing rates were dependent exponentially on voltage; with depolarization, the opening rate increases, and the closing rate decreases. The maximal conductance ( $g_{max}$ ) averaged  $5.4 \pm 0.89$  nS ( $n=3$ ),  $V_n$  was +15 mV and  $k_n$  was +13 mV.

The amplitude of the  $I_K$  exhibited a slow decline during maintained depolarizing pulses. Figure 3-7A shows outward currents elicited by 1 sec voltage pulses from a prepulse potential of -100 mV to various potentials ranging from 0 mV to +60 mV. The



time course of the decay of the  $I_K$  was well described as a single exponential process, as shown by the smooth curve overlying the traces, which displayed little voltage-dependence between 0 to +60 mV (Fig. 3-7B). The time constant for decay of the  $I_K$  at positive potentials ranged from 1.0 - 2.2 sec, with a mean value of  $1.74 \pm 0.34$  sec ( $n=4$ ) at +60 mV. The  $I_K$  inactivated during depolarizing voltage pulses. To study the extent of the steady-state, voltage-dependent inactivation of the  $I_K$ , the following protocol was used: outward current was activated by a depolarizing voltage pulse of +10 mV for 200 ms and was preceded by a prolonged conditioning pulse during which the membrane potential was stepped for 10 sec from -100 to +10 mV in 10 mV increments. A representative example of  $I_K$  evoked by this protocol is shown in figure 3-7C. Because a steady-state level of inactivation is reached at the end of the conditioning pulse, the peak current evoked by the test pulse is a direct measurement of the number of channels still available for activation. A measurement of the voltage dependency of steady-state inactivation can therefore be obtained by correlating the peak current evoked during the test pulse with the membrane potential during the conditioning pulse. Figure 3-7D shows the peak outward currents from the cell in figure 3-7C and one other representative cell plotted as a function of the prepulse potentials. Peak current values were normalized with respect to the peak current evoked from the most hyperpolarizing prepulse. The smooth curve is the non-linear least-squares fit of the data to a Boltzmann function:

$$I/I_{max} = \{1 + \exp[(V - V_n)/k_n]\}^{-1} \quad (6)$$

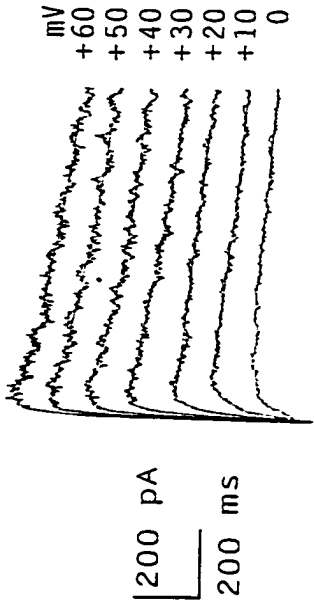
where  $I/I_{max}$  is the normalized peak current,  $V$  is the membrane potential during the test pulse,  $V_n$  is the voltage at which  $I$  is half-maximal and  $k_n$  is the slope factor. In the two

## RESULTS

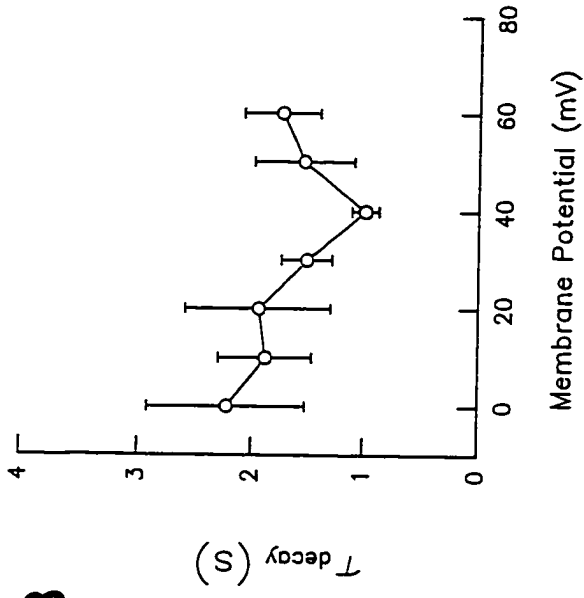
**Fig. 3-7.** Inactivation of outward K<sup>+</sup> currents. (A) Outward currents recorded from an RPE cell superfused with 130 mM NaCl Ringers with 130 mM KCl in the pipette. The cell was held at -100 mV for 1 sec and then the membrane potential was stepped to potentials ranging from 0 to +60 mV in 10 mV increments. The outward current shows a slow time-dependent decline during the voltage-clamp step. The smooth curves overlying the traces indicate single exponential fits to the data. (B) Voltage-dependence of the decay time constant. Each point represents the mean measurement from 4 cells. (C) Steady-state inactivation of the outward K<sup>+</sup> current. The cell was held at -60 mV and then stepped from -100 mV to +10 mV in 10 mV increments for 10 sec prior to a test pulse to +10 mV. The outward current decreased with prepulse potentials positive to -50 mV. Currents were subtracted for a linear leak of 1.95 GΩ. (D) Plot of the peak outward current (I), expressed as a fraction of the maximal current ( $I_{max}$ ) at +10 mV, as a function of the prepulse potentials for the cell in (C) (O) and one other representative cell (●). The smooth curve through the data points is the best fit to a Boltzmann function, given by equation (6) in the text.

RESULTS

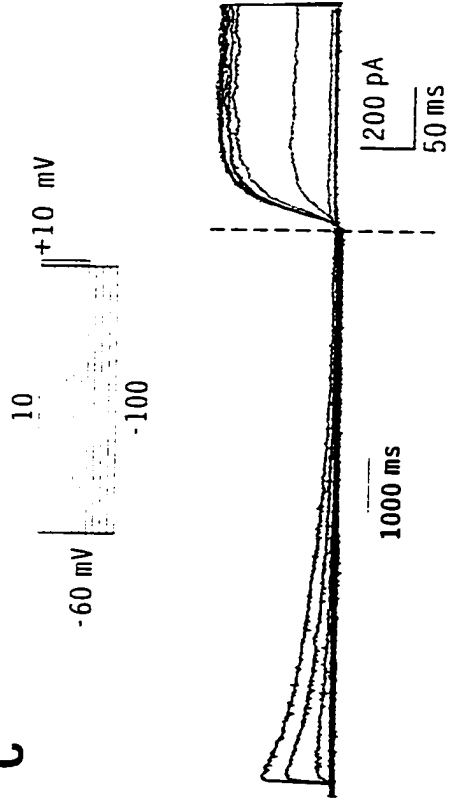
**A**



**B**



**C**



**D**

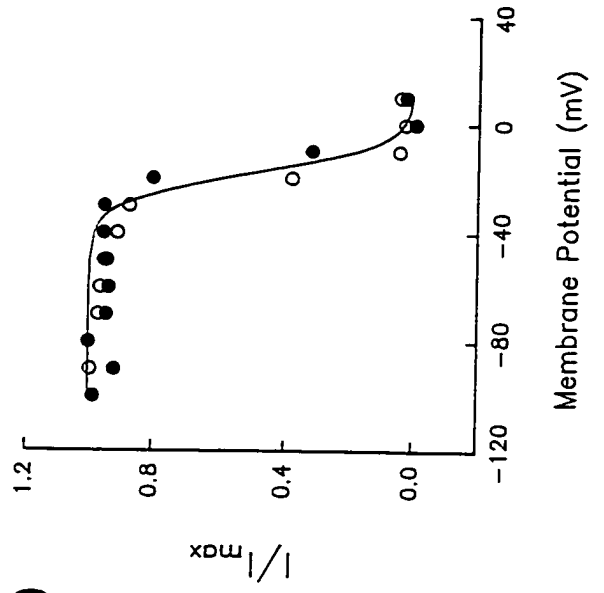


Fig. 3-7.

cells shown in figure 3-7D, steady-state inactivation of the  $I_K$  was half-maximal at -18 mV, with a slope factor of -5.4 mV.

In the cell shown in figure 3-7C and others, the amplitudes of  $I_K$  during the test pulse to +10 mV was greater than that observed during the prepulse to a similar potential. This observation may be due to accumulation of slow inactivation at the  $V_h$  of -60 mV which persists during positive prepulses (Hoshi, Zagotta and Aldrich, 1991).

#### 4.3 Effects of $K^+$ channel blockers on the outward $K^+$ current

The sensitivity of the outwardly rectifying  $K^+$  current to  $K^+$  channel blockers was examined. Tetraethylammonium ions ( $TEA^+$ ) block different  $K^+$  conductances with a one-to-one stoichiometric binding interaction (one  $TEA^+$  blocking one  $K^+$ -channel), in a wide variety of cell types (Stanfield, 1983). Among the different  $K^+$  conductances, outwardly rectifying  $K^+$  channels are most sensitive to external  $TEA^+$ , whereas blockage of inward rectification needs higher concentrations of external  $TEA^+$  (Stanfield, 1983).  $TEA^+$  is membrane impermeant (Rudy, 1988) and its blocking effects differ when applied internally or externally, suggesting that its effects are mediated through different binding sites (Armstrong and Hille, 1972). The binding site for internal  $TEA^+$  resides within the membrane field. Therefore, internal  $TEA^+$  can only block open channels and produces a voltage-dependent block, which can be overcome by increasing the external  $K^+$  concentration ("knock-off") (Armstrong and Hille, 1972; Latorre and Miller, 1983). An external  $TEA^+$  binding site near the outer mouth of the outwardly rectifying  $K^+$  channel has also been demonstrated (Heginbotham and MacKinnon, 1992; Hurst et al., 1992;

## RESULTS

**Fig. 3-8.** Effect of external TEA on the outward K<sup>+</sup> current in rabbit RPE cells. (A) Currents evoked from a representative cell by the voltage protocol shown on the top of the panel measured before and during superfusion of 10 mM TEA and 2 min after TEA washout. Currents were subtracted for linear leaks of 2.3 G $\Omega$  for both control and 10 mM TEA conditions, and 3.0 G $\Omega$  for washout. (B) I-V plots for currents measured at the end of the voltage pulse from the cell shown in panel A, before (O), and during superfusion with TEA (□). The TEA difference current (∇) is also shown. (C) Outward currents recorded at +60 mV from a V<sub>h</sub> of -60 mV before and during application of 1 mM TEA are superimposed for comparison. A linear leak of 0.55 G $\Omega$  and 0.70 G $\Omega$  was subtracted for traces in control and in 1 mM TEA, respectively. Capacitance of the cells shown was 20 pF for the cell in panel (A) and (B), and 41 pF for the cell in panel (C), respectively.

RESULTS

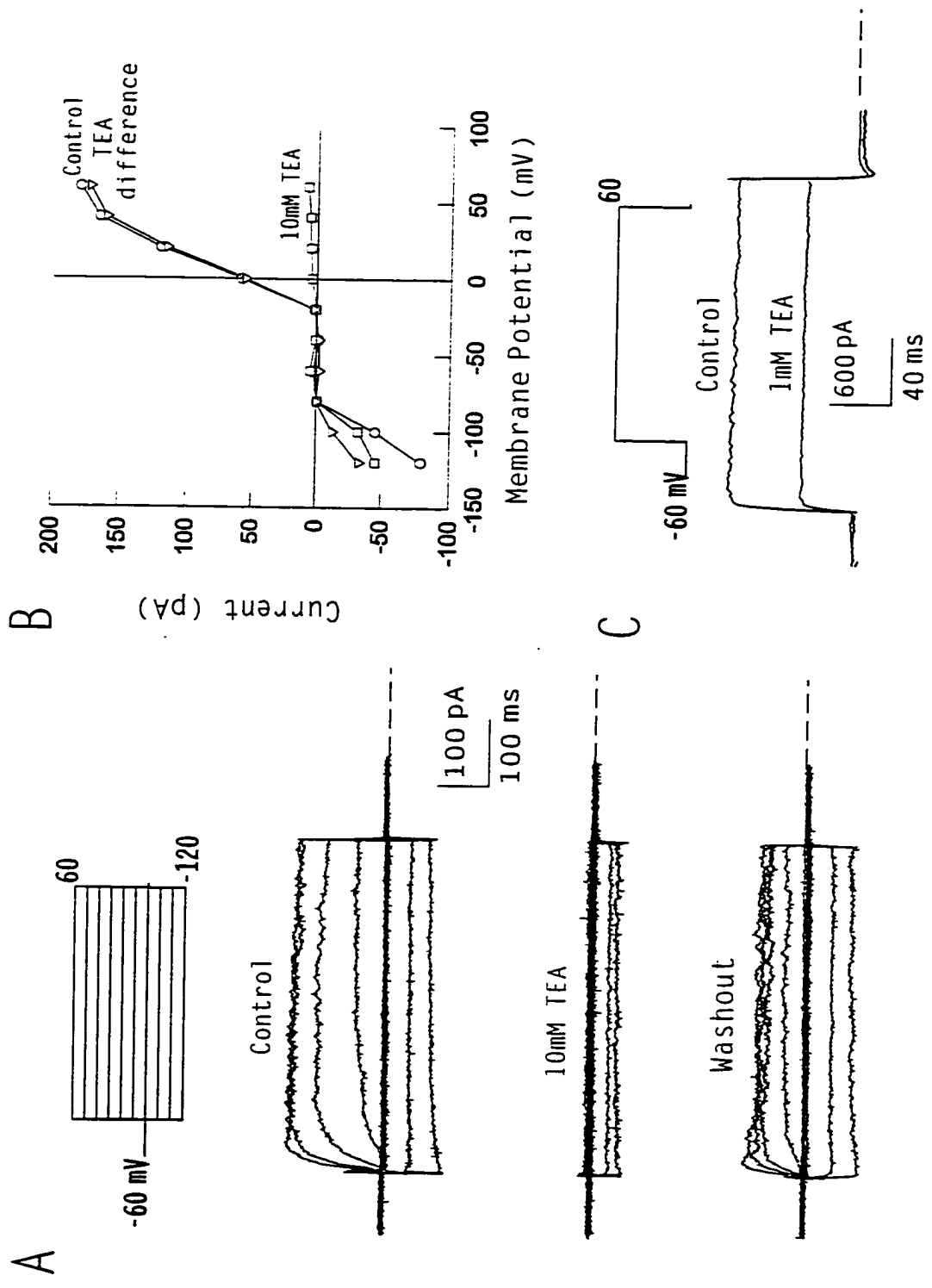


Fig. 3-8

Kavanaugh et al., 1992), with external TEA<sup>+</sup> producing a voltage- and time-independent block (Armstrong and Hille, 1972; Latorre and Miller, 1983).

In this study, external TEA<sup>+</sup> blocked the  $I_K$  in rabbit RPE cells. In six cells tested, superfusion of 1 mM TEA reduced the outward current measured at 0 mV by  $60 \pm 17\%$  and by  $64 \pm 14\%$  at +60 mV with little effect on inward current. Figure 3-8C shows superimposed outward current traces at +60 mV before and during superfusion with 1 mM TEA<sup>+</sup>. The cell was held at a  $V_h$  of -60 mV. The blocking effect of TEA<sup>+</sup> on  $I_K$  in rabbit RPE cells is dose-dependent. Increasing the TEA<sup>+</sup> concentration to 10 mM further reduced the  $I_K$ . As shown in figure 3-8A, 10 mM TEA<sup>+</sup> abolished the  $I_K$ . At this concentration of TEA<sup>+</sup>, the inward current was also reduced. The effects of TEA<sup>+</sup> on both  $I_K$  and inward current were partially reversible. Figure 3-8B shows the current, measured at the end of the voltage command, and the voltage (I-V) curves for the cell shown in panel A, in control Ringers and during superfusion with 10 mM TEA<sup>+</sup>. The TEA<sup>+</sup> difference current, obtained by digital subtraction of currents measured in control Ringers and following superfusion of TEA<sup>+</sup>, is also shown. The TEA<sup>+</sup> difference current is the portion of the total current sensitive to TEA<sup>+</sup>. Thus, TEA<sup>+</sup> reduced the  $I_K$  and inward current at all potentials where they were activated. The inhibition of inward current by TEA<sup>+</sup> (10 mM) is voltage-dependent; for the cell shown, inward current was reduced at -100 and -120 mV by 27% and 42%, respectively. In three other cells, 10 mM TEA<sup>+</sup> reduced the  $I_K$  at 0 and +60 mV by  $85 \pm 5.5\%$  and  $88 \pm 4.1\%$  (n=4), respectively. Similar sensitivity to TEA<sup>+</sup> has been reported for K<sup>+</sup> currents in other tissues (Ishikawa and Cook, 1993).

## RESULTS

**Fig. 3-9.** Effect of external 4-AP on outward K<sup>+</sup> current. (A) Outward currents elicited by depolarizing voltage pulses before and during 100  $\mu\text{M}$  4-AP superfusion. Currents are subtracted for linear leaks of 2.0 G $\Omega$  and 0.7 G $\Omega$  for control and 100  $\mu\text{M}$  4-AP conditions, respectively. (B) Corresponding I-V curves measured at the end of the voltage pulses from the cell shown in (A) before (O) and after 100  $\mu\text{M}$  4-AP ( $\bullet$ ). The difference current for 100  $\mu\text{M}$  4-AP ( $\nabla$ ) is also shown. (C) Outward currents recorded from another cell before and during 1 mM 4-AP superfusion. The initial 8 ms of the capacitance transient has been blanked for clarity. (D) Corresponding I-V curves before (O), after 1 mM 4-AP ( $\bullet$ ), and for 4-AP (1 mM) difference current ( $\nabla$ ). Capacitance of the cells was 22 pF and 29.5 pF in panel (A) and (C), respectively.



RESULTS

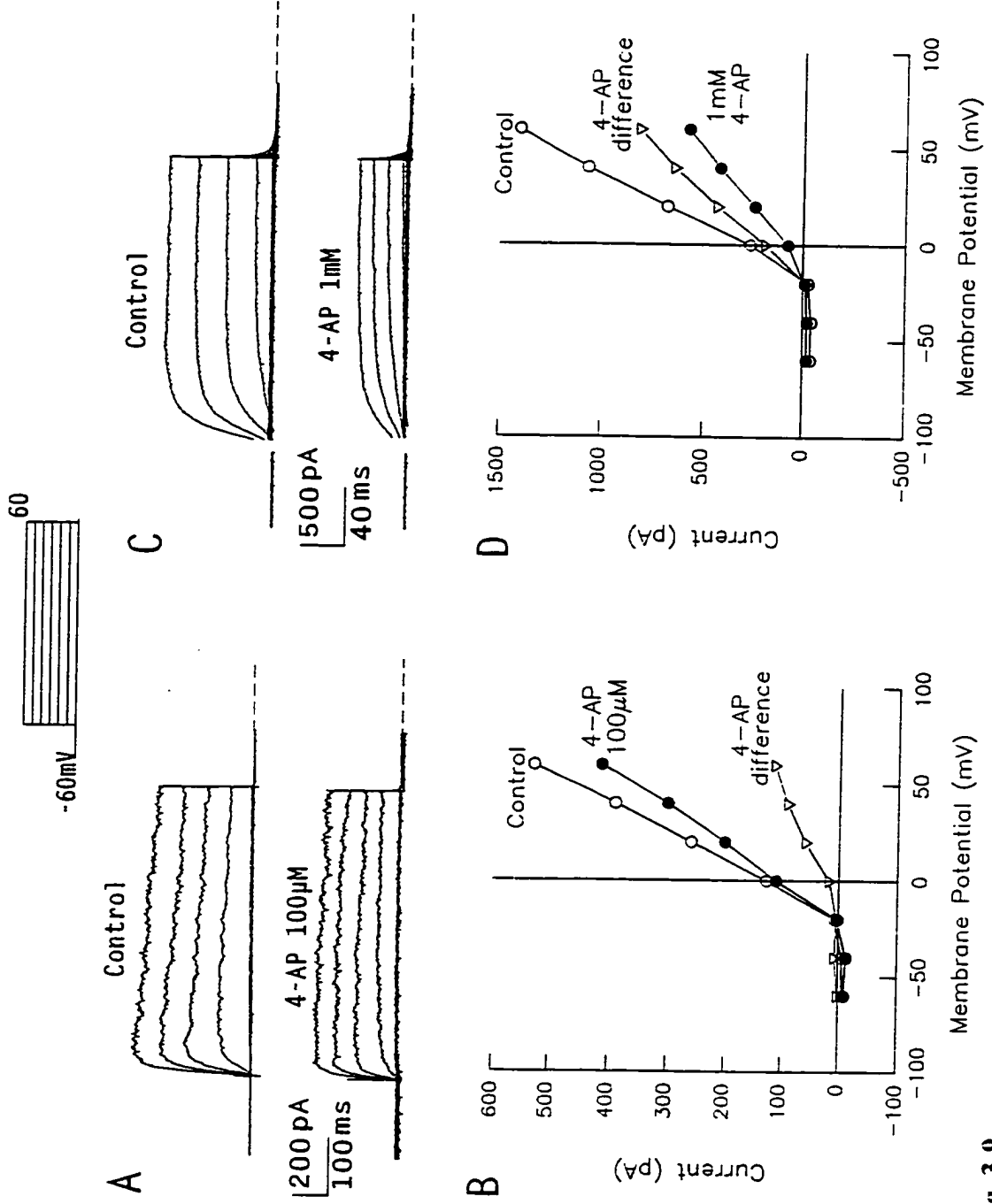


Fig. 3-9.

4-aminopyridine (4-AP) is another  $K^+$  channel blocker which shows a high specificity for a variety of  $K^+$  channels. It is believed that 4-AP preferentially affects transient, fast-inactivating  $K^+$  currents although the specificity is not always clear cut (Dreyer, 1990). The mechanisms of block by 4-AP for different  $K^+$  channels are complex and depend on both the cell type and the specific type of  $K^+$  channel. In general, the membrane permeable uncharged form of the organic base, 4-AP ( $pK_a \sim 9.2$ ) enters the cell when applied externally, there, its charged cationic form (the predominant form at pH 7.4) interacts with an intracellular site within the channel pore, thereby producing the potential- and use-dependent blocking effects (Hirsh and Quandt, 1993; Rasmusson et al., 1995). The blocking potency of 4-AP on outwardly rectifying  $K^+$  currents is increased at more negative potentials suggesting a low affinity of the open channel for 4-AP and trapping of 4-AP in the closed state of this channel type (Kirsch et al., 1993).

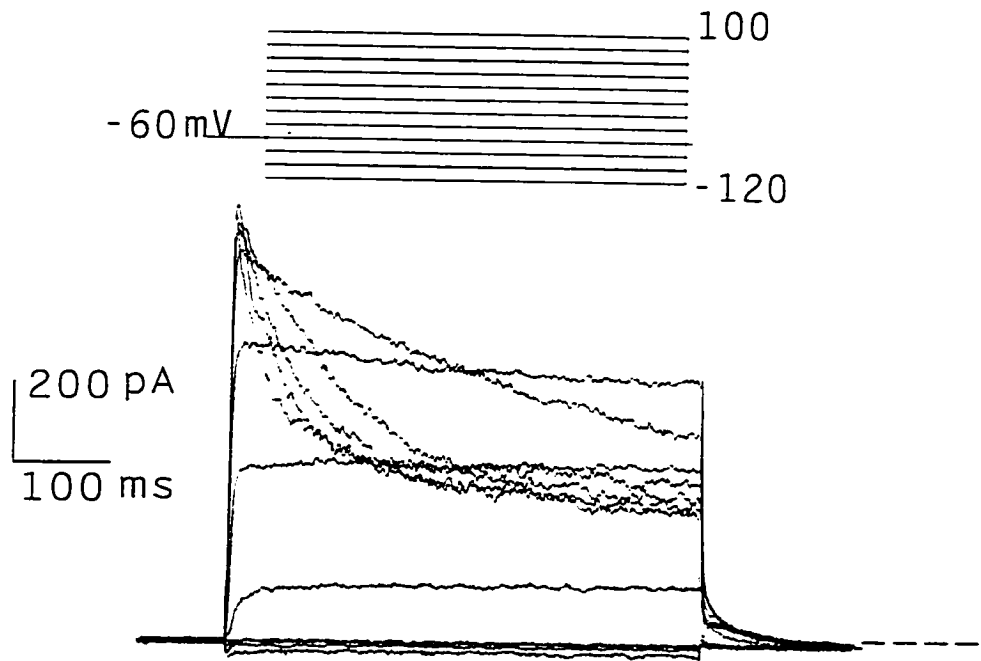
In rabbit RPE cells, the outwardly rectifying  $K^+$  current was blocked by external 4-AP in a dose-dependent manner. Superfusion of low concentrations of 4-AP partially blocked  $I_K$  (Fig. 3-9). At a concentration of 100  $\mu$ M, 4-AP reduced  $I_K$  at 0 mV and +60 mV by approximately  $48 \pm 22\%$  and  $37 \pm 8\%$  ( $n=3$ ) (Fig. 3-9A & B). Increasing the concentration of 4-AP to 1 mM, resulted in a further reduction of the outward current by  $70 \pm 6\%$  at 0 mV and  $40 \pm 9\%$  ( $n=4$ ) at +60 mV (Fig. 3-9C & D).

#### 4.4 Fast-inactivating outward $K^+$ current

Although the majority of RPE cells recorded exhibited a slowly inactivating outward current, in 20 of the 294 rabbit RPE cells investigated the outward  $K^+$  current

**Fig. 3-10.** Activation of the fast-inactivating outward  $K^+$  currents. (A) Current recorded from a cell held at -60 mV and stepped from -120 mV to +100 mV in 20 mV increments for 500 ms. A pronounced time-dependent outward current is apparent. (B) Chord conductance, calculated from the peak current using equation (2) from the text, is expressed as a fraction of the maximum conductance at +40 mV and plotted as a function of the membrane potential during the test pulse. The activation curve was sigmoidally shaped and well described by the Boltzmann equation (3) reported in the text (continuous smooth line), with  $V_n = -33.5$  mV and a slope factor of +9.5 mV. Capacitance of the cell was 44 pF.

A



B

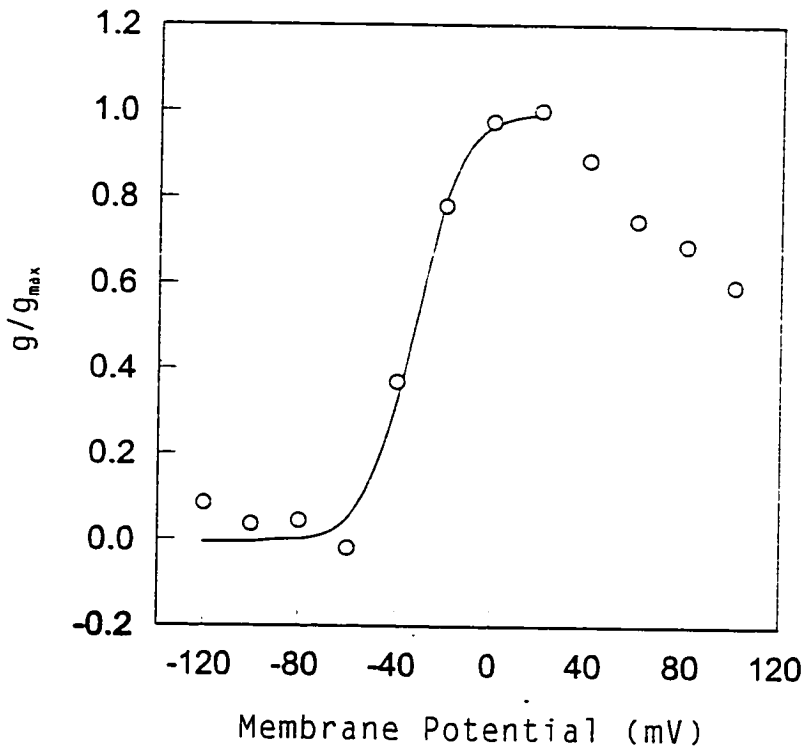


Fig. 3-10.

**Fig. 3-11.** Inactivation of the fast-inactivating outward  $K^+$  currents. (A) I-V relationship for the currents shown in figure 3-11A. Outward current was measured at 2 msec (○) and also at 485 msec (●) after the start of the voltage step. (B) Currents evoked by depolarizing pulses ranging from 0 to +100 mV, taken from figure 3-11A. The current traces were separated for clarity. The currents showed a rapid time-dependent decline during the voltage clamp steps. The smooth curves overlying the traces are single exponential fits to the data. (C) Voltage-dependence of the decay time constant measured from the cell in (B).

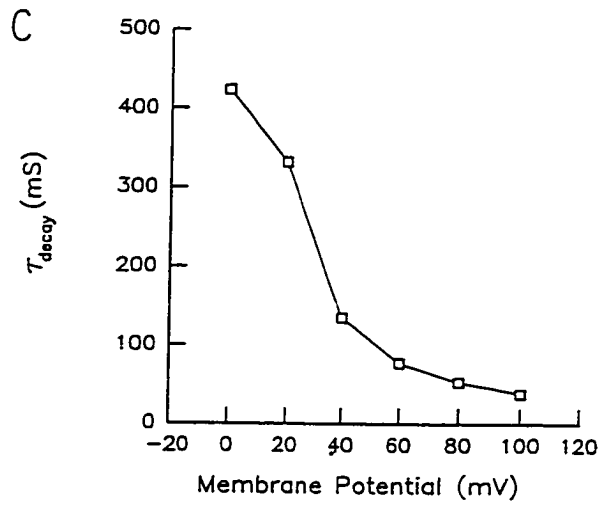
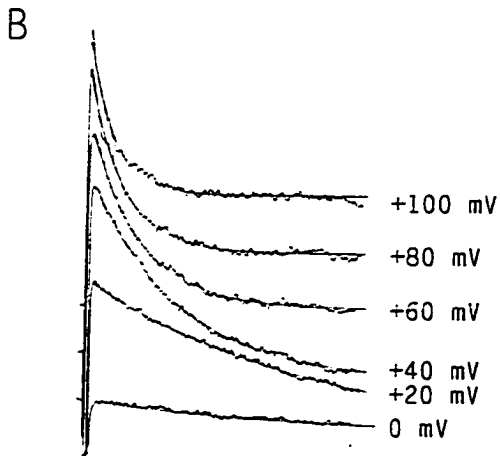
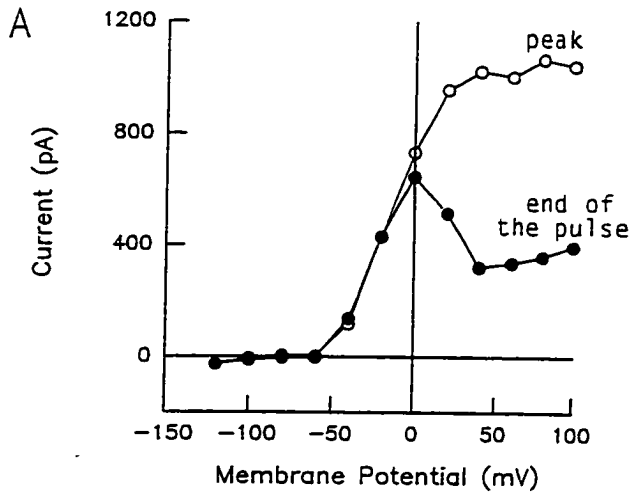


Fig. 3-11.

had an initial fast inactivation followed by a slower inactivation phase at depolarized potentials. Figure 3-10A shows current traces recorded from a cell with fast inactivating outward current. The cell was held at -60 mV and stepped from -120 mV to +100 mV in 20 mV increments. Outward current activated around -60 mV and reached a maximum between +40 and +80 mV (figure 3-11A). Figure 3-10B shows the chord conductance plotted as a function of membrane potential for the cell shown in figure 3-10A. Since the outward conductance peaked at +40 mV and then declined at more positive potentials, chord conductances measured at all potentials tested were normalized to the peak conductance at +40 mV. The voltage dependence of the outward  $K^+$  conductance was well described by the Boltzmann equation given previously (3) (continuous smooth line). The maximal peak conductance was 9.97 nS,  $V_n$  was -33.5 mV and  $k_n$  was +9.5 mV.

The amplitude of the outward  $K^+$  current exhibited a rapid decline during maintained depolarization. Figure 3-11A shows the I-V plot for the peak and steady-state currents displayed in figure 3-10A. Time-dependent inactivation of the outward current was apparent at potentials positive to 0 mV and increased with depolarization, as evident by the difference between the peak and steady-state current at depolarized potentials. Figure 3-11B shows current traces from the same cell shown in figure 3-10A, the traces have been separated for clarity. The time course of decay of current was well fitted by a single exponential, as shown by the smooth curves superimposed on the data points. Inactivation of the outward  $K^+$  current showed strong voltage dependence (Fig. 3-11C), with a time constant of  $122 \pm 10$  ms at +40 mV ( $n=3$ ).

Quinine and its D-stereoisomer quinidine are known to decrease several different

## RESULTS

Fig. 3-12. Quinine blocks the fast inactivating outward current. (A) Current recorded from the same cell as shown in figure 3-

11. The cell was held at -60 mV and stepped to +60 mV for 500 ms. The trace labeled "Quinine 1 mM" was obtained 30 sec after application of quinine from a pipette located  $\approx 100 \mu\text{m}$  from the cell. The quinine difference current, obtained by subtracting current recorded after quinine application from control current is also shown. Currents were leak subtracted by 2.3 G $\Omega$  and 3.2 G $\Omega$  for control and during quinine application, respectively. (B) Corresponding peak I-V curves for currents recorded before quinine application (O) and during quinine application (●) from the cell shown in panel A. Peak I-V relationships for recovery current and (∇) quinine difference current (▼) are also plotted. Capacitance of the cell was 44 pF.



RESULTS

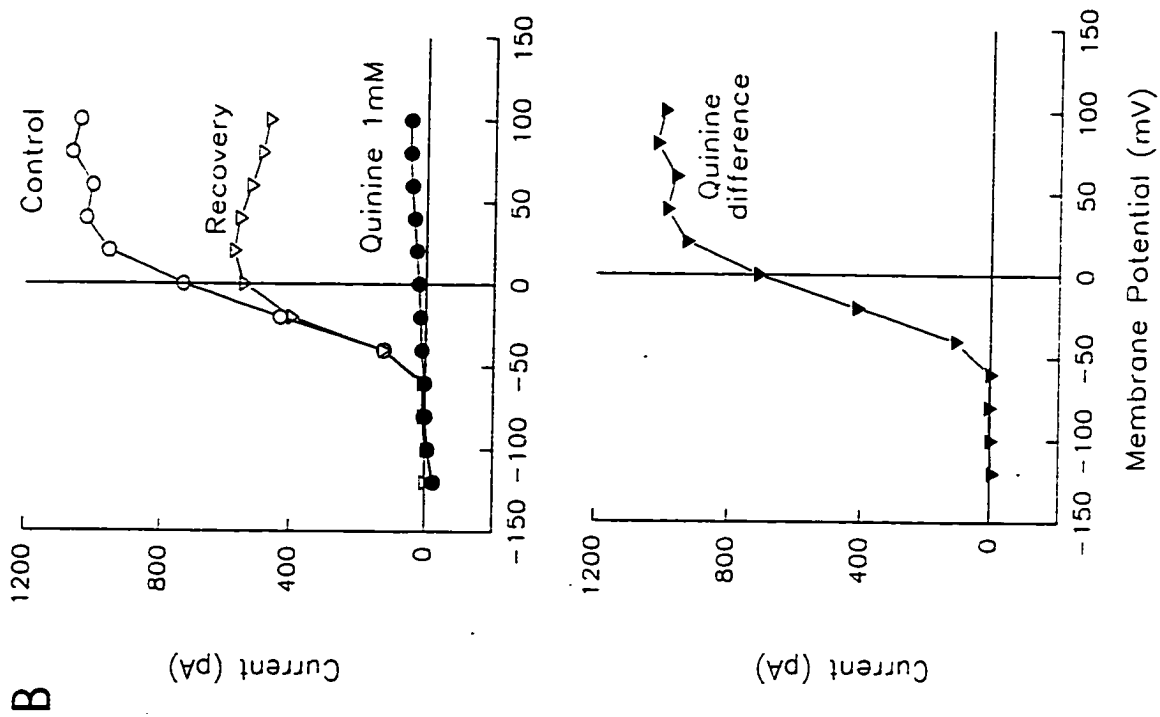
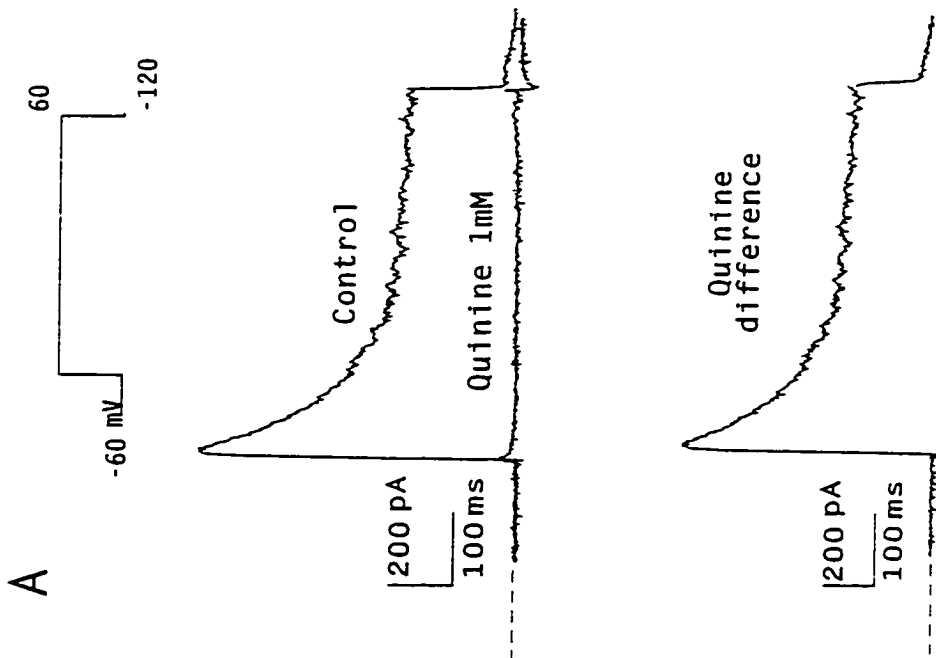


Fig. 3-12

$K^+$  currents in other cells (Iwatsuki and Petersen, 1985; Lu et al., 1990; Amigorena et al., 1990), although there is evidence suggesting that they may not be specific for  $K^+$  channels in some cell types (Gögelein and Capek, 1990). Since only 7% of rabbit RPE cells at 3-5 days in culture exhibited fast-inactivating outward  $K^+$  current, extensive pharmacological characterization was not carried out. However, in two cells with fast-inactivating outward current, quinine reversibly blocked the fast-inactivating outward current. Figure 3-12A shows current traces recorded from a  $V_h$  of -60 mV to a potential of +60 mV from the same cell shown in figure 3-10 with fast-inactivating outward current. Current traces before and during quinine application are superimposed for comparison. Application of 1 mM quinine via a puffer pipette blocked the outward current at 0 and +60 mV by 97 and 96%, respectively. The quinine difference current, obtained by subtracting current in the presence of quinine from control current at +60 mV, is also shown (Fig. 3-12A bottom trace). Figure 3-12B shows the corresponding peak I-V relation for currents recorded from the cell shown in figure 3-12A. The outward current activated at around -60 mV. The quinine effect on the fast-inactivating outward current was readily reversible, as evident by recovery of the peak I-V relation towards control values as shown. The recovery current was recorded immediately after taking the application pipette out of the bath.

#### **4.5 The inwardly rectifying current in rabbit RPE cells is selective for $K^+$**

Under voltage-clamp, 40% (118/294) of RPE cells exhibited inward current in response to hyperpolarizing voltage commands (Fig. 3-13). The selectivity of the

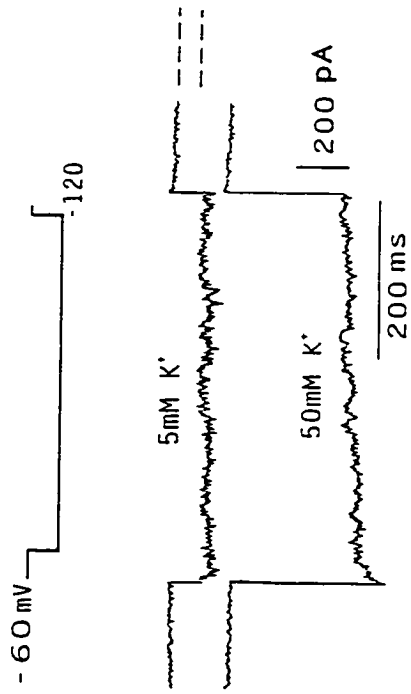
## RESULTS

**Fig. 3-13.** The inwardly rectifying current in rabbit RPE cells is dependent on  $[K^+]_o$ .

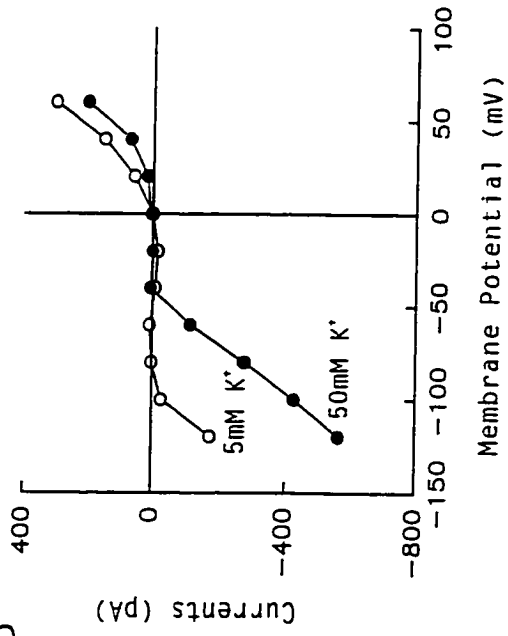
(A)  $I_{K_i}$  was activated by stepping the membrane potential from a  $V_h$  of -60 mV to -120 mV for 500 msec. The cell was superfused with standard 5 mM  $K^+$  Ringers and then subsequently with 50 mM  $K^+$  Ringers. (B) Corresponding peak I-V relationship for the cell shown in panel (A). Increasing external  $K^+$  from 5 mM  $K^+$  (○) to 50 mM  $K^+$  (●), increased the  $I_{K_i}$  and shifted the  $V_{rev}$  and the voltage at which the rectification occurred, positive along the voltage axis. (C) Reversal potentials for 7-12 cells are plotted as a function of  $[K^+]_o$ . The straight line is the least-squares best fit of the data, with a slope of 50 mV per 10-fold change of  $[K^+]_o$ . The numbers of cells studied at each  $[K^+]_o$  are indicated in parentheses beside each data point. (D) Voltage-dependent decay of  $I_{K_i}$  for another cell, bathed in 5 mM  $[K^+]_o$ . From a  $V_h$  of -60 mV, the membrane potential was stepped to -140 mV to activate  $I_{K_i}$  and then to various potentials, as indicated by the voltage command protocol. Tail currents reversed direction at  $\approx$  -82 mV (see arrow), which is close to the predicted equilibrium potential for  $K^+$ . Cell capacitance was 22 pF for the cell in panel (A) and (B) and 32 pF for the cell in panel (D).

RESULTS

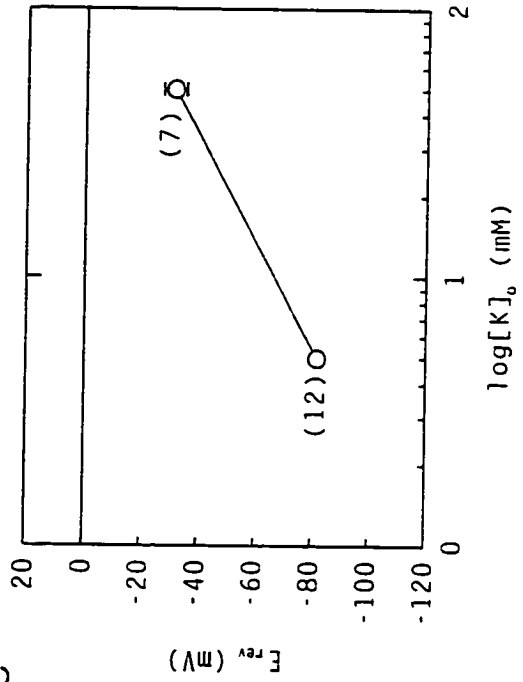
A



B



C



D

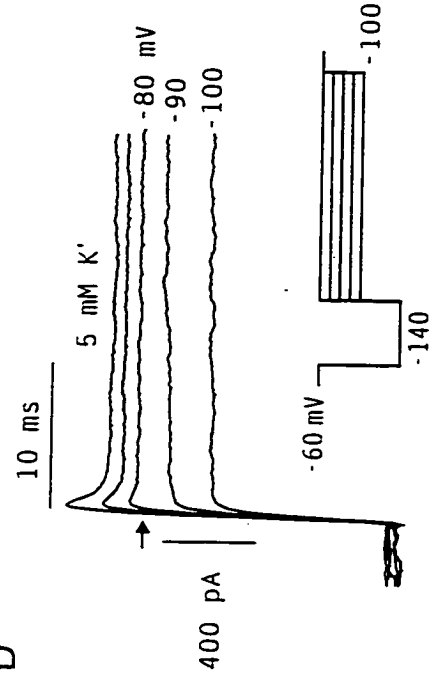


Fig. 3-13.

inwardly rectifying current for  $K^+$  was investigated by varying the concentration of  $K^+$  in the bath solution. Figure 3-13A shows inward current recorded in a rabbit RPE cell superfused with 5 mM and subsequently with 50 mM  $[K^+]_o$ . In 5 mM  $[K^+]_o$ , inward current is apparent on hyperpolarization of the cell from the  $V_h$  of -60 mV to -120 mV. When the bath solution was switched to one containing 50 mM  $[K^+]_o$ , inward current at -120 mV increased. Figure 3-13B shows the peak I-V relationships for the cell shown in figure 3-13A, recorded in standard external solution (5 mM  $K^+$ ), and then during superfusion with 50 mM  $[K^+]_o$ . Voltage values for current reversal ( $V_{rev}$ ) were determined as the potential at which the I-V relation intersected the zero current level. Increasing  $[K^+]_o$  shifted the reversal potential, and the voltage around which the rectification occurred, positive along the voltage axis. The slope conductance of the I-V relationship at negative potentials also increased as  $[K^+]_o$  was increased, which is the characteristic for the inward rectifier that the channel has multiple binding sites, and repulsion between  $K^+$  within the channel increases the channel conductance. For the cell shown in figure 3-13A, the slope conductance, calculated from the I-V relationship in figure 3-13B, increased from 5.25 nS in 5 mM external  $K^+$  solution to 19.8 nS in 50 mM external  $K^+$  solution.  $V_{rev}$  was dependent on  $[K^+]_o$ . The straight line in figure 3-13C is the least-squares best fit of the data measured in 7-12 cells and has a slope of 50 mV per 10-fold change of  $[K^+]_o$ , suggesting that the inward rectifier in rabbit RPE cells is largely selective for  $K^+$ . Further verification that the hyperpolarization-activated inward current is a  $K^+$  current was obtained by examination of time- and voltage-dependent current relaxations following a step to -140 mV to activate inward current and then to more

depolarized potentials to observe current relaxations (Fig. 3-13D). The reversal potential for "tail" currents was calculated by interpolation between the two nearest points where the current reversed direction. In standard solution, the reversal potential was  $-82 \pm 1.4$  mV ( $n=12$ ) which is very close to the  $K^+$  equilibrium potential ( $-82$  mV) calculated under the recording conditions.

#### 4.6. Barium ( $Ba^{2+}$ ) and cesium ( $Cs^+$ ) block the inward rectifier

The divalent cation,  $Ba^{2+}$  is a commonly used  $K^+$  channel blocker. It has been shown to block various  $K^+$  channels including the inward rectifier and outward rectifier, and the maxi- $K_{Ca}$  channel (Ishikawa and Cook, 1993; Kelly, Dixon and Sim, 1992; Iwatsuki and Petersen, 1985; Lindau and Fernandez, 1986). It has been reported that the inward rectifying  $K^+$  current ( $I_{K_i}$ ) has much higher sensitivity to  $Ba^{2+}$  than the outwardly rectifying  $K^+$  current ( $I_{K_o}$ ) (Ishikawa and Cook, 1993; Lindau and Fernandez, 1986). Figure 3-14 shows the effects of externally applied  $Ba^{2+}$  on whole-cell  $K^+$  currents recorded from a rabbit RPE cell. The currents shown were recorded from a cell bathed in standard 5 mM  $K^+$  solution with 130 mM KCl in the recording pipette. At hyperpolarizing potentials,  $I_{K_i}$  is apparent with a relatively small outward current activated at more positive potentials (left panel). Following a 30 sec exposure of the cell to external  $Ba^{2+}$  (1 mM from an application pipette), the inward current is abolished (95% block) (right panel). The I-V relation measured 10 msec after the onset of the voltage pulses for the cell before and after  $Ba^{2+}$  is shown in figure 3-14B.  $Ba^{2+}$  also reduced depolarization-activated  $I_{K_o}$  by 40% at +60 mV in this cell. Similar results were observed

## RESULTS

**Fig. 3-14.** Effect of external  $Ba^{2+}$  on inwardly rectifying  $K^+$  current. (A) Currents recorded in 5 mM  $K^+$  Ringer with 130 mM KCl in the electrode. The cell is held at -60 mV and stepped from -120 mV to +60 mV in 20 mV increments (left panel). Following a 30 sec application of 1 mM external  $Ba^{2+}$  via a puffer pipette, the inward current is abolished and the outward current is reduced (right panel). A linear leak of  $1\text{ G}\Omega$  was subtracted for the current recorded following  $Ba^{2+}$  application. (B) Corresponding peak I-V plots for the cell in panel (A), before (O) and following  $Ba^{2+}$  application (●). Current values were measured 10 msec after the onset of the voltage pulses from -120 mV to +60 mV. (C) peak I-V plot for the  $Ba^{2+}$  difference current (∇) obtained by digitally subtracting the current recorded after  $Ba^{2+}$  application from the control current. Capacitance of the cells was 37 pF.

RESULTS

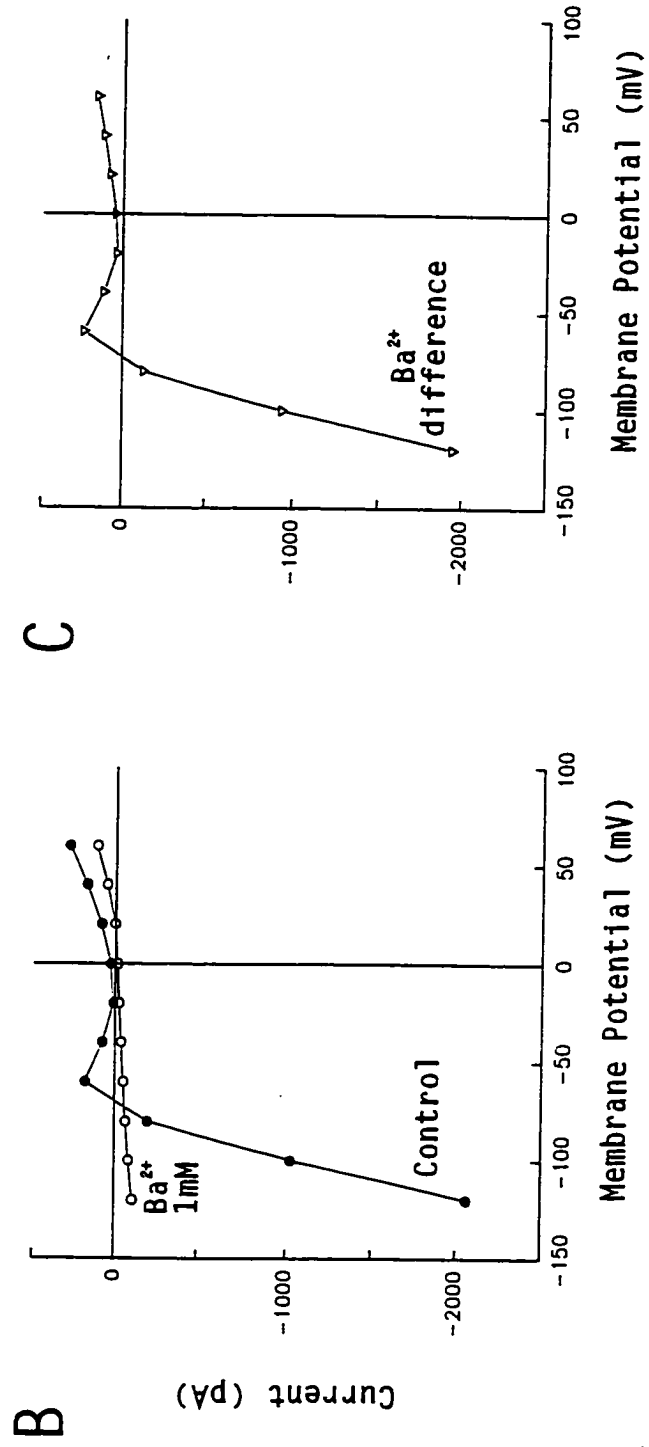
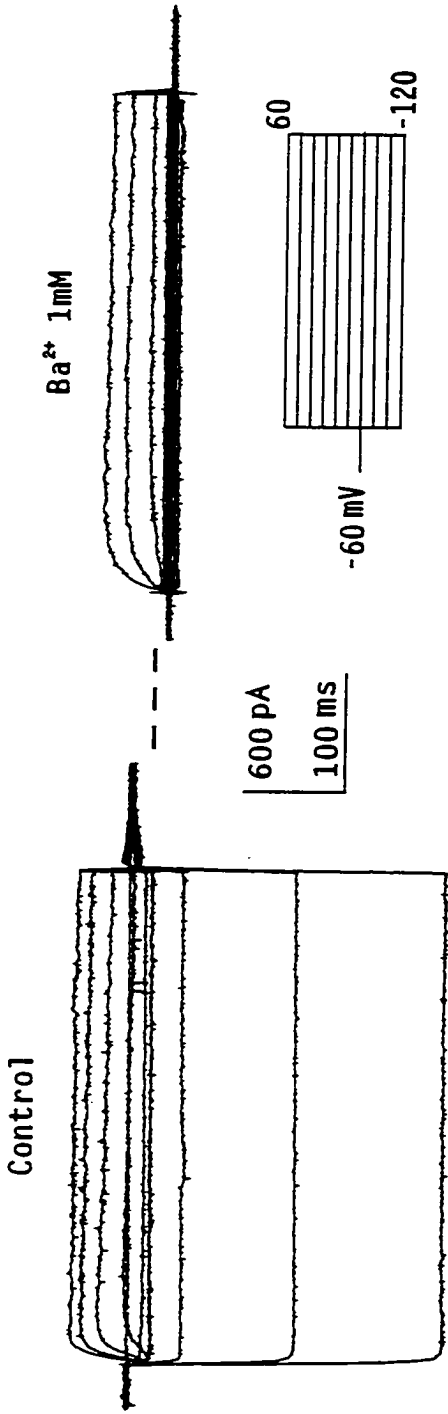


Fig. 3-14

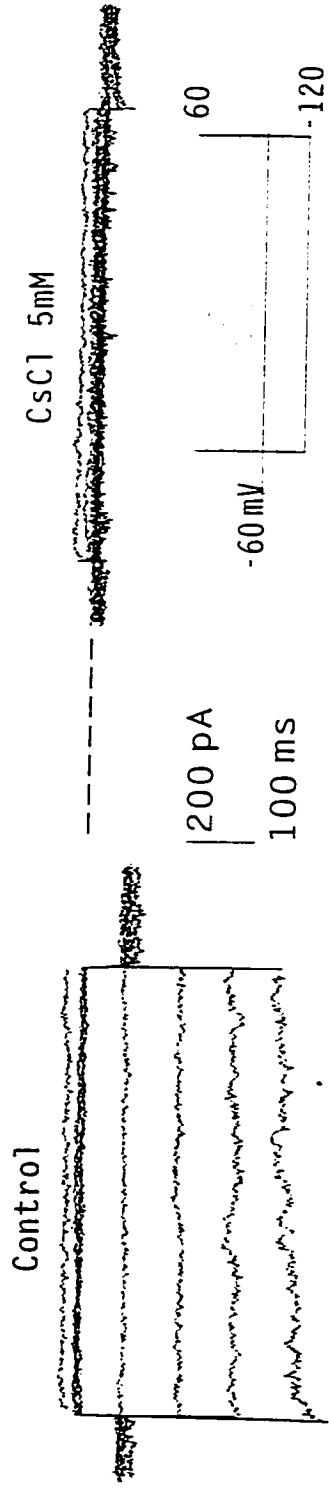


## RESULTS

**Fig. 3-15.** Effect of external Cs<sup>+</sup> on inward rectifier. (A) Currents recorded from the same cell shown in figure 3-15A bathed in 50 mM [K<sup>+</sup>]<sub>o</sub>, before and after the addition of 5 mM Cs<sup>+</sup> via a puffer pipette. (B) Peak I-V plots for the cell shown in panel (A). (O), control; (●), Cs<sup>+</sup>. The cell shows pronounced inward current at negative potentials which was abolished by exposure to Cs<sup>+</sup>. (C) Peak I-V plot for the Cs<sup>+</sup> difference current (▼) obtained by digitally subtracting the current recorded after Cs<sup>+</sup> application from the control current. Capacitance of the cells was 22pF.

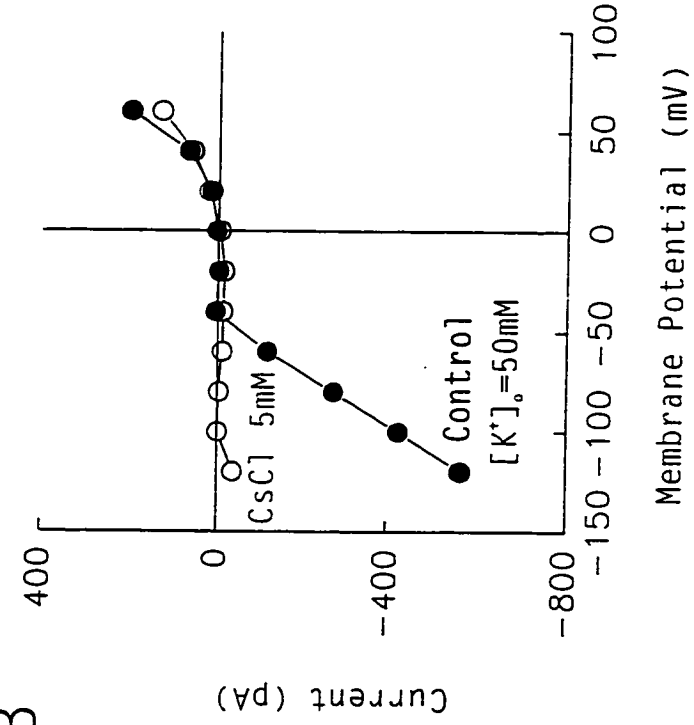
RESULTS

A



$[K^+]_o = 50mM$

B



C

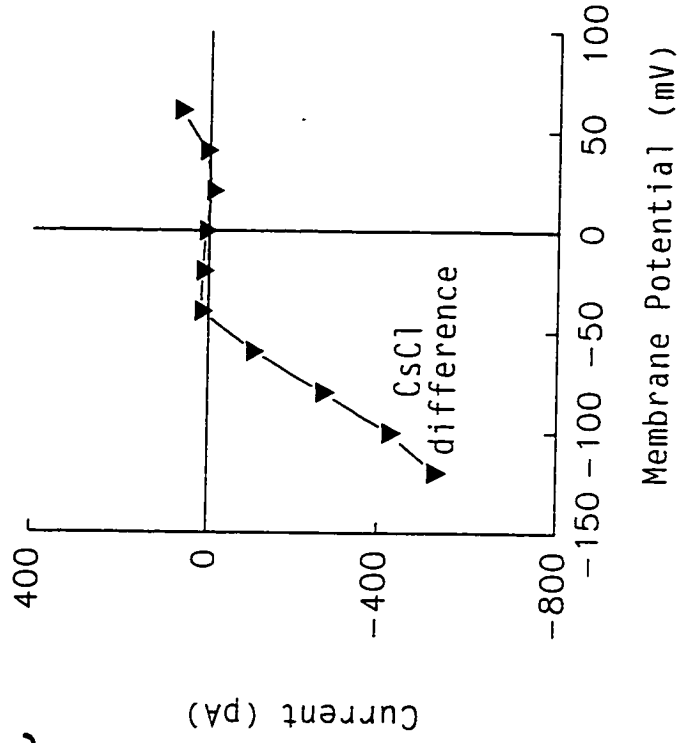


Fig. 3-15

in other cells tested, with a mean reduction of  $75 \pm 12\%$  ( $n=3$ ) of  $I_{K_i}$  measured at  $-120$  mV and a reduction in  $I_K$  of  $57 \pm 3\%$  ( $n=6$ ) at  $+60$  mV. The  $Ba^{2+}$  effects on both  $I_{K_i}$  and  $I_K$  were reversible.

The effect of external  $Cs^-$  on the inward rectifier was also tested. External  $Cs^-$  is known to block  $I_{K_i}$  (Ishikawa and Cook, 1993; Kelly et al., 1992; Lindau and Fernandez, 1986; Latorre and Miller, 1983). When  $Cs^-$  is added to the internal medium, it can also block  $I_K$  (Latorre and Miller, 1983). This monovalent cation enters the channel but cannot pass through the selective filter of the channel, thereby occluding the conductive pathway (Latorre and Miller, 1983). Figure 3-15A shows current traces recorded from the same cell shown in figure 3-13 bathed in 50 mM  $K^-$  Ringer. Inward current is blocked by 5 mM  $Cs^-$  applied from a puffer pipette. Figure 3-15B shows the I-V relation recorded for the cell in figure 3-15A. This cell exhibited little outward current at depolarized potentials. Inward current activated at hyperpolarized potentials was abolished (92% block) by 5 mM externally applied  $Cs^-$ , leaving only a linear "leak" current (2.5 G $\Omega$ ) at negative potentials. In four other cells tested, puffer application of 5 mM  $Cs^-$  also reduced the  $I_{K_i}$  significantly. The mean reduction in  $I_{K_i}$  by external  $Cs^-$  at  $-120$  mV was  $67 \pm 9\%$  ( $n=5$ ).

#### **4.7. Time-dependent decay of the inward rectifier at negative potentials**

Time-dependent decay of the inward current at hyperpolarized potentials is a characteristic of the inward rectifier in several different cell types (Ohmori, 1978; Standen and Stanfield, 1979; Harvey and Ten Eick, 1988; Cooper et al., 1991). This

## RESULTS

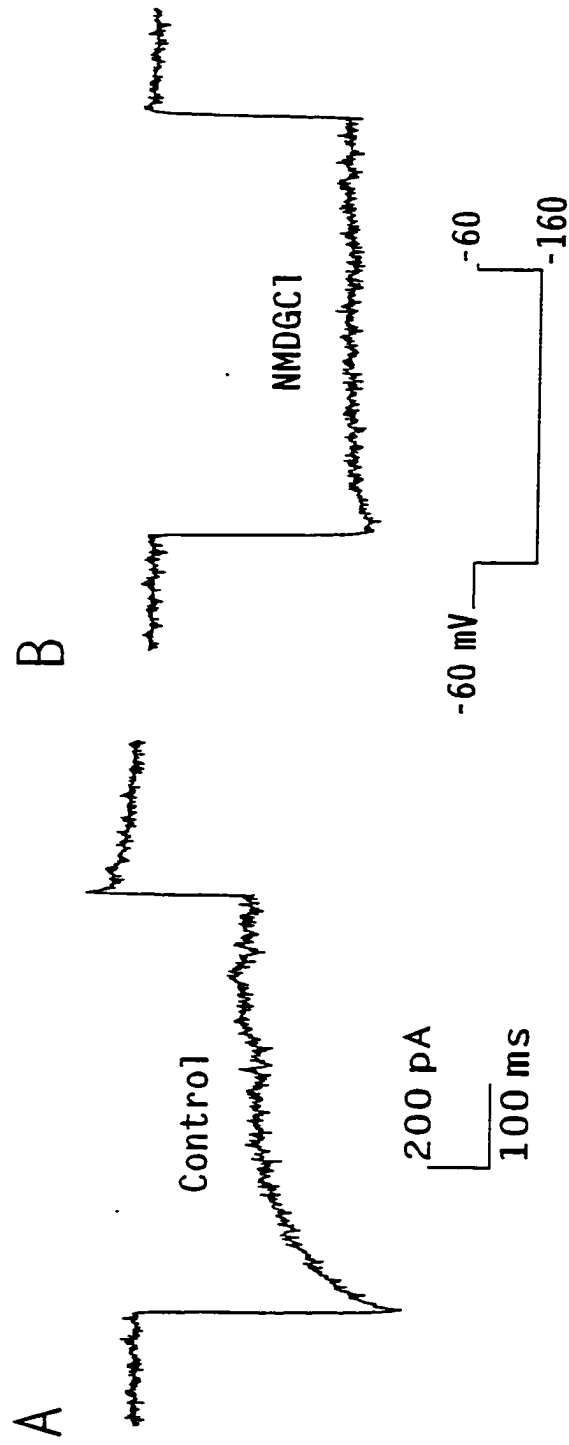


**Fig. 3-16.**  $[Na^+]_o$ -dependent reduction of the inward current at negative potentials. (A) Whole-cell current recorded from a cell bathed in standard 5 mM K<sup>+</sup> Ringers (Na<sup>+</sup>-containing). The cell was held at -60 mV and stepped to -160 mV. (B) Inward current recorded from the same cell in Na<sup>+</sup>-free (NMDG<sup>+</sup>) external solution. Time-dependent decay of the inward current has been largely removed in nominally Na<sup>+</sup>-free bathing solution. Capacitance of the cell was 41.5 pF.

reduction of the  $I_{K_i}$  at negative potentials has been attributed to a combination of blockage by external  $\text{Na}^+$ ,  $\text{K}^+$  depletion from the extracellular space, and inherent voltage dependent gating (Ohmori, 1978; Standen and Stanfield, 1979; Harvey and Ten Eick, 1988). Extracellular  $\text{K}^+$  depletion is unlikely to give rise to  $I_{K_i}$  decay in isolated cells. In rabbit RPE cells,  $I_{K_i}$  also exhibits a time-dependent decay at potentials hyperpolarized to -100 mV. To test whether the decay of the  $I_{K_i}$  could arise from a blockage by external  $\text{Na}^+$ ,  $I_{K_i}$  was recorded in standard external Ringer solution and then in  $\text{Na}^+$ -free solution (substituting NMDG<sup>+</sup> for  $\text{Na}^+$ ) (Fig. 3-16). In standard external Ringer solution, time-dependent decay of the  $I_{K_i}$  was readily observed at -160 mV (Fig. 3-16A). When external  $\text{Na}^+$  was replaced by NMDG<sup>+</sup>, the decay of steady-state  $I_{K_i}$  at negative potentials was largely removed (Fig. 3-16B). Similar results were found in three other cells suggesting that external  $\text{Na}^+$  is mainly responsible for  $I_{K_i}$  decay at negative potentials in rabbit RPE cells.

## **5. Evidence for the presence of large conductance $\text{Ca}^{2+}$ -activated $\text{K}^+$ (maxi- $\text{K}_{Ca}$ ) channels in rabbit RPE cells**

### **5.1 Whole-cell recording**

#### *5.1.1 Increases in $[\text{Ca}^{2+}]_i$ enhance voltage-dependent outward $\text{K}^+$ current ( $I_K$ )*

In approximately 25% of the cells recorded from,  $I_K$  recorded under standard conditions (2.5 mM  $\text{Ca}^{2+}$  in the bath/100 nM  $\text{Ca}^{2+}$  in the pipette) appeared "noisy" at depolarized potentials, suggesting activation of large conductance channels. Removal of  $[\text{Ca}^{2+}]_o$  was found to decrease both  $I_K$  and current noise. In order to investigate if a

## RESULTS

**Fig. 3-17.** Ionomycin enhances and quinine blocks the outward currents. (A) Whole-cell currents from a cell in response to a series of voltage-clamp steps before and during pressure application of 1  $\mu$ M ionomycin. A linear leak of 1.7 G $\Omega$  was subtracted from both the current traces shown. (B) Corresponding I-V curves measured at the end of the pulse in control Ringer (O), during application of ionomycin (●), and in the presence of quinine (0.5 mM) (∇). (C) I-V relationship for the ionomycin-sensitive K<sup>+</sup> current (▼), obtained by digitally subtracting the control outward current from current recorded in the presence of ionomycin. Capacitance of the cell was 20 pF.

RESULTS

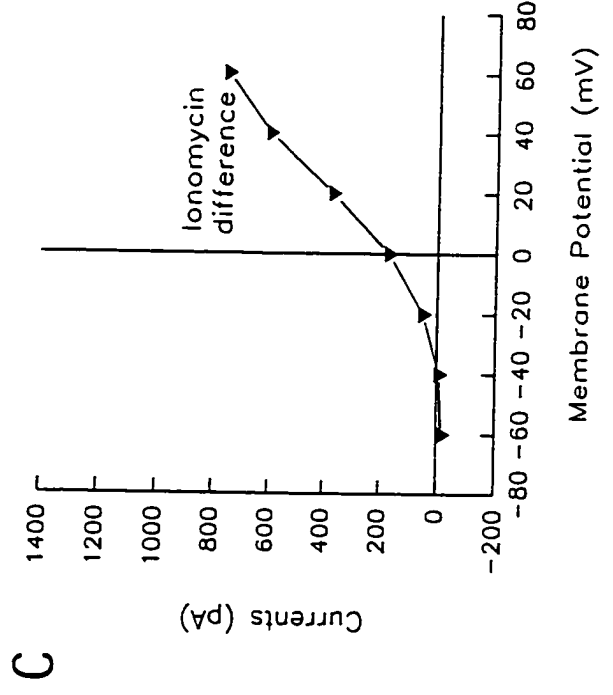
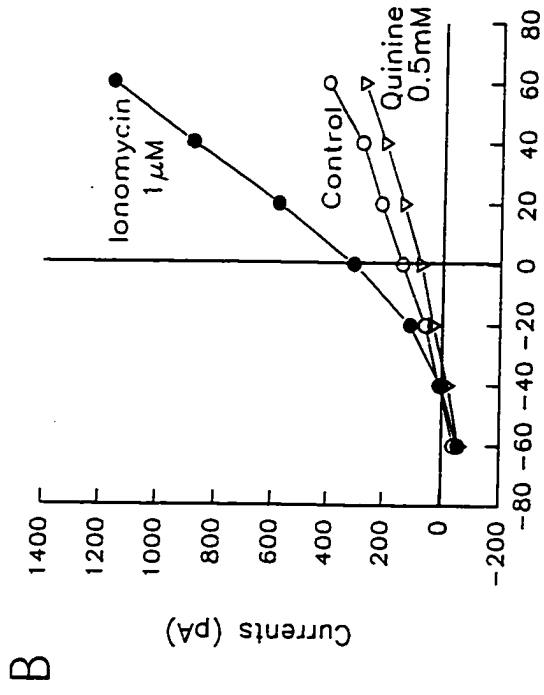
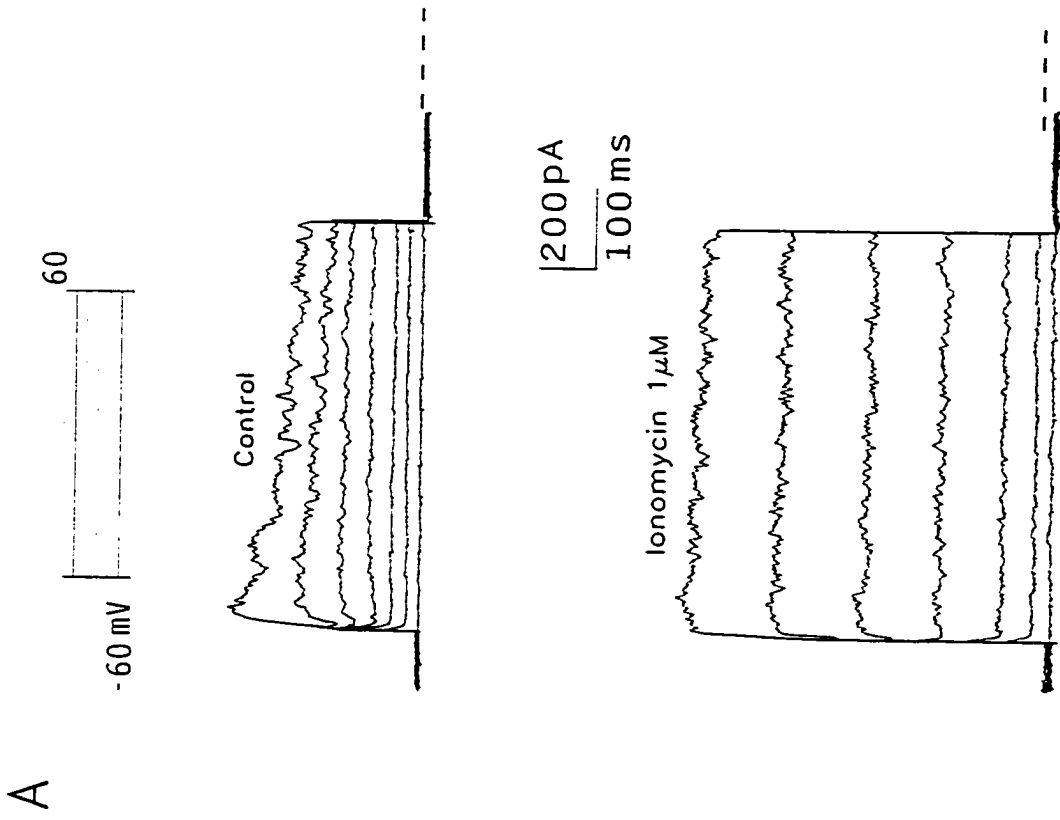


Fig. 3-17

component of the  $I_K$  in rabbit RPE cells was attributable to the activation of  $Ca^{2+}$ -activated  $K^+$  channels, the effect of the  $Ca^{2+}$  ionophore, ionomycin, on the  $I_K$  was examined. Ionomycin, an antibiotic agent produced by *Streptomyces conglobatus* ATCC 31005, binds  $Ca^{2+}$  preferentially over other divalent cations in a one to one stoichiometry and acts as a mobile ion carrier to move  $Ca^{2+}$  from the extracellular space into the cell cytosol (Liu and Hermann, 1978).

The addition of ionomycin (1  $\mu$ M) to the bath medium from a puffer pipette caused a large increase in the outward current compared to the current evoked by the same voltage protocol in control external solution (2.5 mM  $[Ca^{2+}]_o$ , Fig. 3-17). Figure 3-17B shows the I-V relationship measured at the end of the pulse for the same cell shown in figure 3-17A. In control external solution, depolarization-evoked current activates around -40 mV and is outwardly rectifying. The addition of ionomycin increased the outward current at all potentials depolarized to -40 mV. Subsequent superfusion of quinine (0.5 mM) in the presence of ionomycin blocked the outward current by 83% at +60 mV (trace not shown), consistent with the outward current being  $K^+$  selective. Subtraction of the control current from that obtained during ionomycin application was carried out digitally and gives the ionomycin difference current (Fig. 3-17C). The ionomycin difference current represents the  $Ca^{2+}$ -dependent component of the outward current. In 67% (12/18) of the cells tested, 1  $\mu$ M ionomycin increased  $I_K$  by  $125 \pm 54\%$  ( $n=12$ ;  $P < 0.05$ , paired t test).

In another cell shown in figure 3-18, puffer application of 10  $\mu$ M ionomycin ionomycin effect is readily reversible. Removal of the ionomycin application pipette



**Fig. 3-18.** The effect of ionomycin on  $I_K$ . Whole cell currents recorded from an RPE cell in control Ringer, during ionomycin application (10  $\mu$ M), and during subsequent superfusion with control Ringer. Control currents were subtracted for a linear leak of 2.8 G $\Omega$ . Cell capacitance was 31 pF.

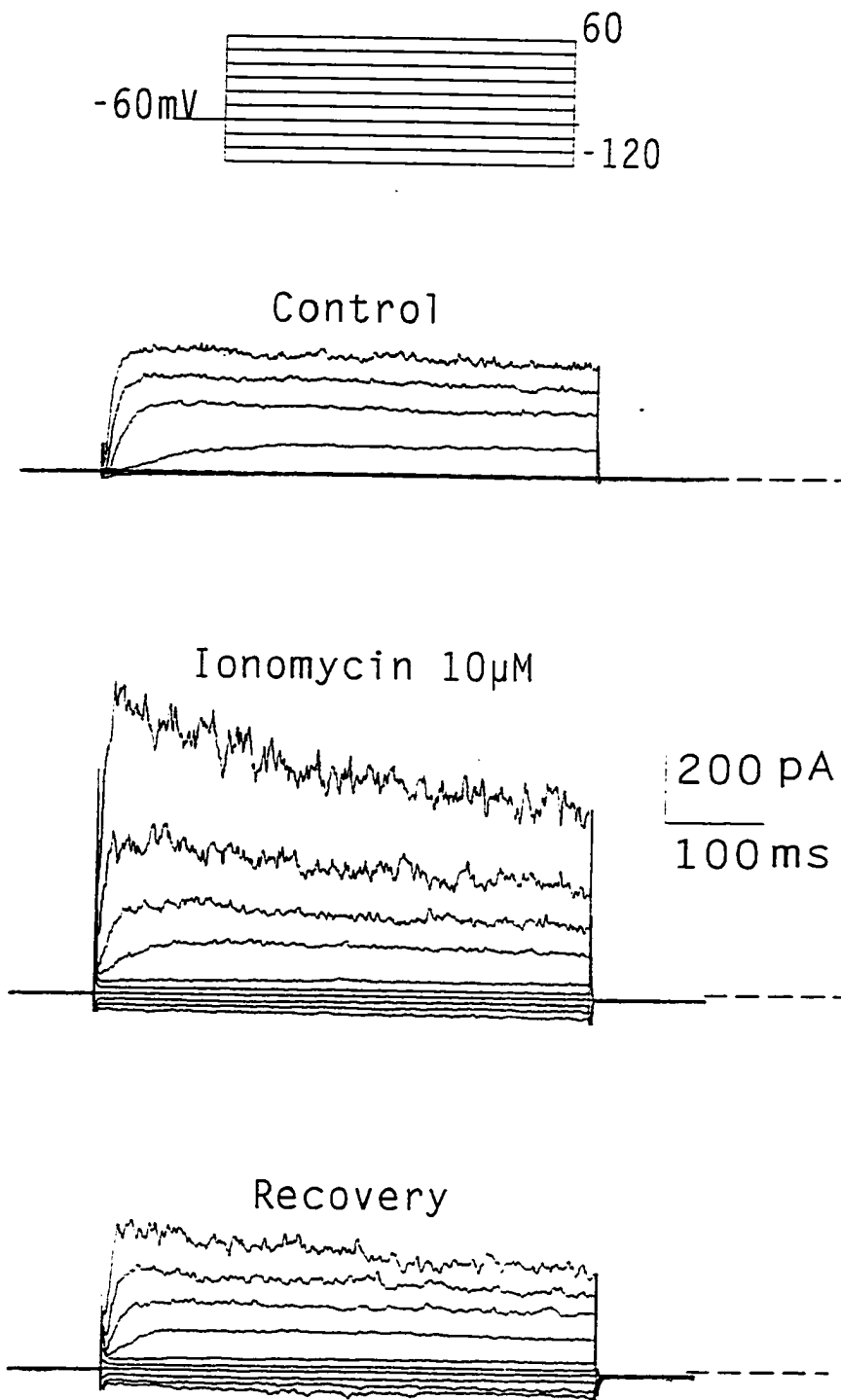


Fig. 3-18.

**Fig. 3-19.** Ionomycin has no effect on the  $I_{K_i}$ . (A) Whole-cell currents recorded from another RPE cell. In the absence of ionomycin, hyperpolarizing voltage steps activated  $I_{K_i}$  while depolarizing voltage steps evoked only a small outward current (top panel). Inclusion of ionomycin ( $1 \mu\text{M}$ ) in the superfusate increased the depolarization-activated  $I_K$ , leaving the  $I_{K_i}$  unchanged (lower panel). Linear leaks of  $2.2$  and  $1 \text{ G}\Omega$  were subtracted from the traces shown in the top and lower panels, respectively. (B) I-V plots for the cell shown in (A), measured at the end of the voltage pulse, for the control current ( $\circ$ ), the current recorded in the presence of ionomycin ( $\bullet$ ) and the ionomycin difference current ( $\nabla$ ). Capacitance of the cell shown was  $37 \text{ pF}$ .

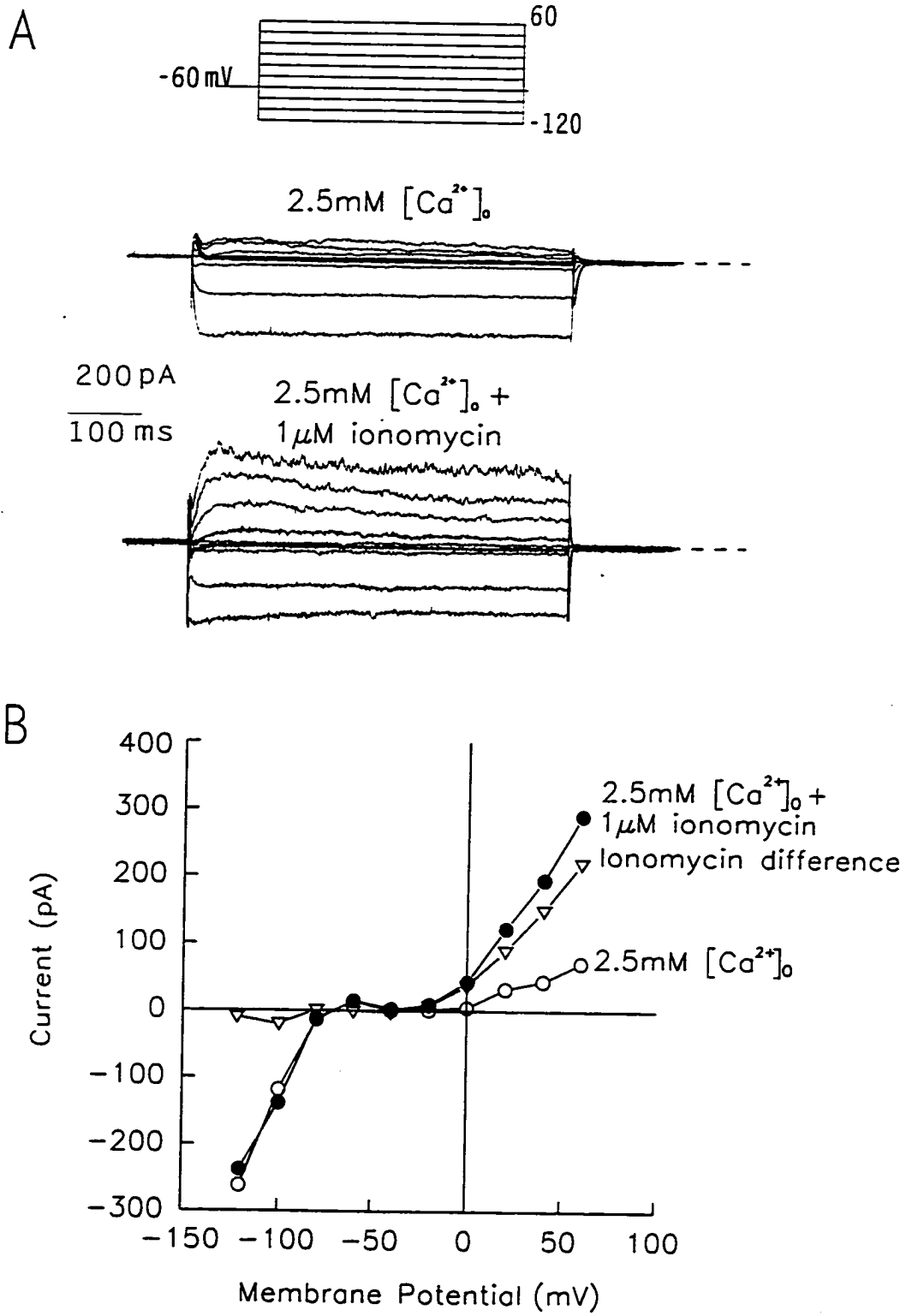


Fig. 3-19

from the bath solution resulted in recovery of the amplitude of the  $I_K$  (within 1 min) to approximately the same level as found in control.

In contrast to the effect on the outward  $K^+$  current, ionomycin had no effect on  $I_{K1}$  in cultured rabbit RPE cells. Figure 3-19A shows whole-cell currents recorded from another rabbit RPE cell. In control Ringer solution, hyperpolarizing voltage steps between -120 and -75 mV activated  $I_{K1}$  while depolarizing voltage steps positive to -25 mV evoked only a small outward current (upper panel). In the presence of 1  $\mu$ M ionomycin,  $I_{K1}$  remained unchanged, however the depolarization-activated outward  $K^+$  current was increased markedly. The I-V curves measured at the end of the pulse for the cell in figure 3-19A show that in the presence of ionomycin, the activation potential for the outward  $K^+$  current was shifted to approximately -40 mV from -25 mV, and the  $I_K$  was increased at all potentials positive to the activation potential, as compared to the control current which was measured in the absence of ionomycin. Only 10% (6/57) of the cells tested were found to co-express both  $Ca^{2+}$ -activated  $K^+$  current and  $I_{K1}$ .

### 5.1.2 Dependence of the outward $K^+$ current upon $[Ca^{2+}]_i$

The  $Ca^{2+}$  sensitivity of the  $I_K$  was examined by altering the extracellular  $Ca^{2+}$  concentration ( $[Ca^{2+}]_o$ ) both in the absence and presence of ionomycin (1  $\mu$ M). In the absence of ionomycin, reducing the  $[Ca^{2+}]_o$  from 2.5 to 1 and 0 mM decreased the outward  $K^+$  current giving mean values of  $13.4 \pm 2.3$ ,  $8.6 \pm 1.1$  and  $5.4 \pm 1.3$  (P < 0.05, paired t test, compared to 2.5 mM  $[Ca^{2+}]_o$  group) pA/pF at +60 mV for 2.5, 1 and 0 mM  $[Ca^{2+}]_o$ , respectively (n=3). In figure 3-20, the amplitude of the outward  $K^+$  current

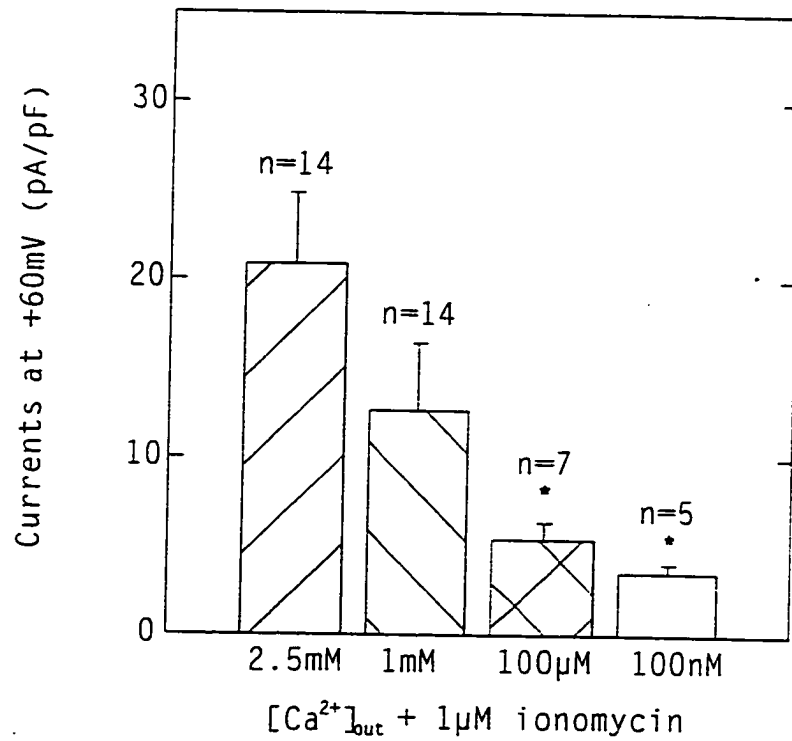


**Fig. 3-20.** Outward K<sup>+</sup> currents in rabbit RPE cells are Ca<sup>2+</sup>-sensitive. Peak outward currents measured at +60 mV, normalized for cell capacitance for cells superfused with 2.5 mM, 1 mM, 100 µM and 100 nM Ca<sup>2+</sup> solutions in the presence of 1 µM ionomycin. Numbers of cells studied are indicated for each [Ca<sup>2+</sup>]<sub>o</sub>. \*P < 0.05 as compared to 2.5 mM [Ca<sup>2+</sup>]<sub>o</sub> group.

measured at +60 mV and normalized for cell capacitance, is shown for 5-14 cells sequentially superfused with 4 different  $[Ca^{2+}]_o$  (100 nM, 100  $\mu$ M, 1, and 2.5 mM) in the presence of 1  $\mu$ M ionomycin. The amplitude of outward  $K^+$  current was diminished after decreasing the external  $[Ca^{2+}]_o$  in a concentration-dependent manner giving mean values of  $20.8 \pm 4.0$  (n=14),  $12.6 \pm 3.8$  (n=14),  $5.4 \pm 0.97$  (n=7) and  $3.8 \pm 0.5$  (n=5) pA/pF for 2.5, 1 mM, 100  $\mu$ M and 100 nM  $[Ca^{2+}]_o$ , respectively.

### 5.1.3 Sensitivity of $I_K$ to selective maxi- $K^+$ channel blockers

Further verification of the presence of a  $Ca^{2+}$ - and voltage-dependent outward  $K^+$  current in rabbit RPE cells was obtained by using potent blockers of maxi- $K_{Ca}$  channels: iberiotoxin (IbTX) and charybdotoxin (CTX). Both IbTX and CTX are 37-amino acid polypeptide toxins isolated from the venom of *Buthus tamulus* and *Leiurus quinquestriatus var. Hebraeus* scorpion, respectively. These two peptide toxins share 68% identical sequence and have similar 3-dimensional structures, and both block the maxi- $K_{Ca}$  channels within the nanomolar dose range in smooth muscle, skeletal muscle and other cell types (Candida, Garcia and Latorre, 1992; Giangiacomo, Garcia and McManus, 1992; Miller et al., 1985). IbTX and CTX also exhibit similar blocking mechanisms of the maxi- $K_{Ca}$  channels -- simple, reversible, bimolecular and pore-directed binding events: a single toxin molecule binds to the extracellular mouth of the pore and physically occludes its conduction pathway (Giangiacomo et al., 1992; MacKinnon and Miller, 1988). However, they differ in their selectivity; CTX blocks both maxi- $K_{Ca}$  and outwardly rectifying  $K^+$  channels with slightly different affinities, whereas IbTX blocks

only the maxi- $K_{Ca}$  channel with a higher potency than CTX (Schneider et al., 1989; Giangiacomo et al., 1993; Goldstein and Miller, 1993).

Figure 3-21A and B show an example of IbTX blocking experiments. The control current was recorded in the presence of 1  $\mu$ M ionomycin with 2.5 mM  $Ca^{2+}$  in the bath. Outward currents were diminished following puffer application of 1 nM IbTX (62 - 66% at +60 mV, n=2) (Fig. 3-21A). The IbTX blocking effect was partially reversed after 15 minutes of washing with the control perfusate (Fig. 3-21A, lower panel). This incomplete recovery could be due to the fact that the washout time was not long enough, for it has been reported that complete recovery from an IbTX block exhibits a slow time-course (Gribkoff et al., 1996). Figure 3-21B shows the I-V relationship for the currents displayed in figure 3-21A, measured at the end of the pulse. The IbTX difference current gives the portion of the total current sensitive to IbTX, and reflects the activation of maxi- $K_{Ca}$  channels. Both the control and IbTX sensitive outward currents were activated at -40 mV. Blocking the IbTX-sensitive component shifted the activation potential for the outward current towards more positive potentials. The sensitivity of the ionomycin-induced outward  $K^+$  current to IbTX is consistent with activation of maxi- $K_{Ca}$  channels in rabbit RPE cells.

For CTX blocking experiments, CTX was applied by superfusion in the control external Ringer (2.5 mM  $Ca^{2+}$ ) in the absence of ionomycin using the same protocol as described before. Application of 50 nM CTX reduced the outward  $K^+$  currents in 5/7 cells tested. At +60 mV CTX inhibited  $I_K$  by  $43 \pm 19\%$  (n=5) (Fig. 3-21C). However the CTX concentration used in this study (50 nM) may also block both maxi- $K_{Ca}$  and

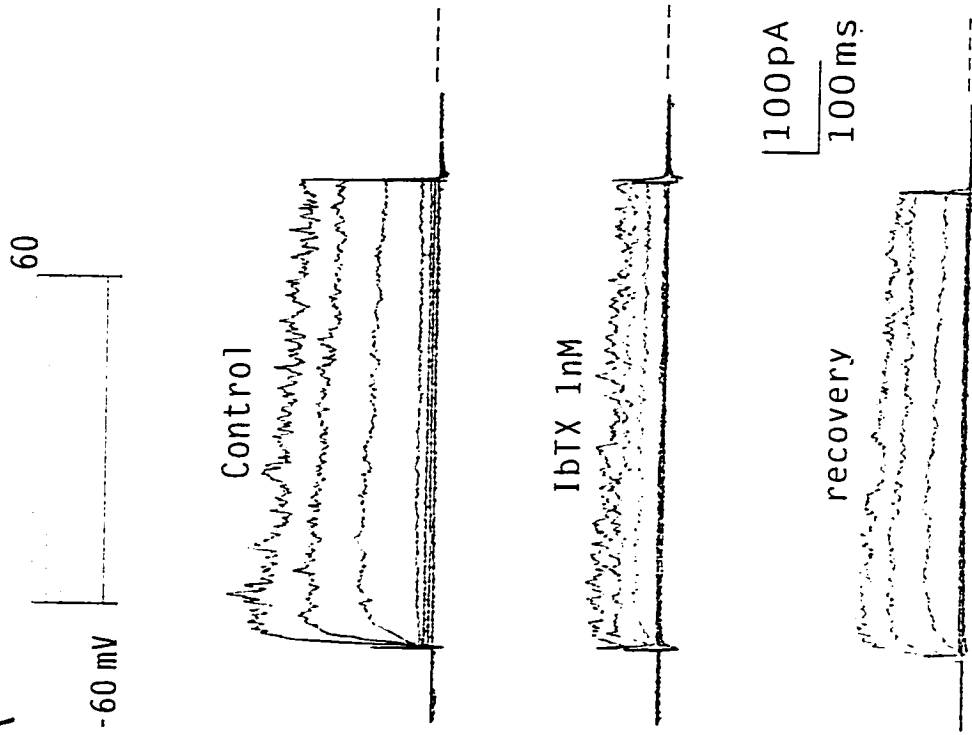


## RESULTS

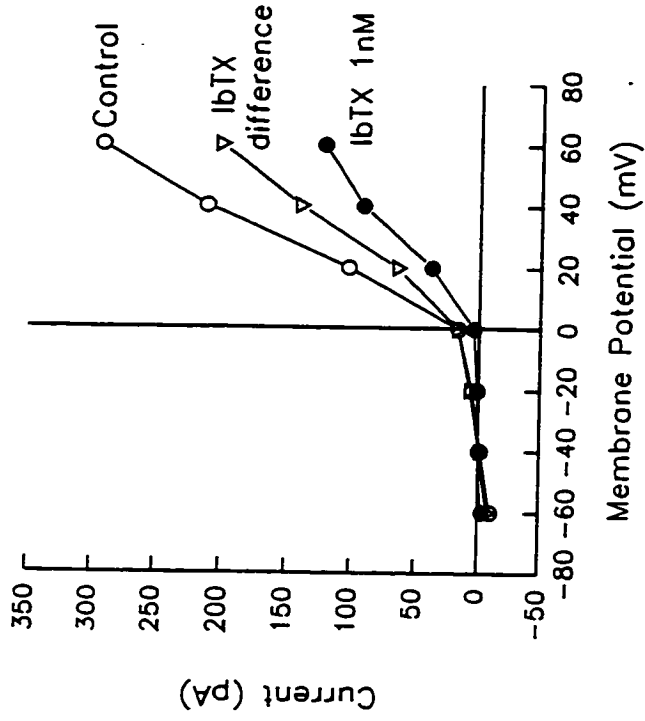
**Fig. 3-21.** IbTX and CTX block the outward K<sup>+</sup> current. (A) Whole cell current recorded from a cell in standard external Ringer (2.5 mM [Ca<sup>2+</sup>]<sub>o</sub>) in the presence of 1 μM ionomycin before (top panel), during application of 1 nM IbTX (middle panel), and 15 min after removal of the IbTX application pipette out of the bath (bottom panel). Currents were subtracted for linear leaks of 2.0, 1.3 and 1.6 GΩ for traces shown in the top, middle and bottom panels, respectively. (B) Corresponding I-V relationship measured at the end of the voltage pulse before (○) and during (●) IbTX application. The IbTX difference current (∇), obtained by subtracting the current recorded during IbTX application from the control current, is also shown. (C) Whole-cell currents measured at +60 mV (V<sub>h</sub> = -60 mV), from a different cell before and during CTX (50 nM) superfusion. Current traces are superimposed for comparison. Capacitance of the cell shown was 67 pF in panel (A), and 46 pF in panel (C).

RESULTS

A



B



C

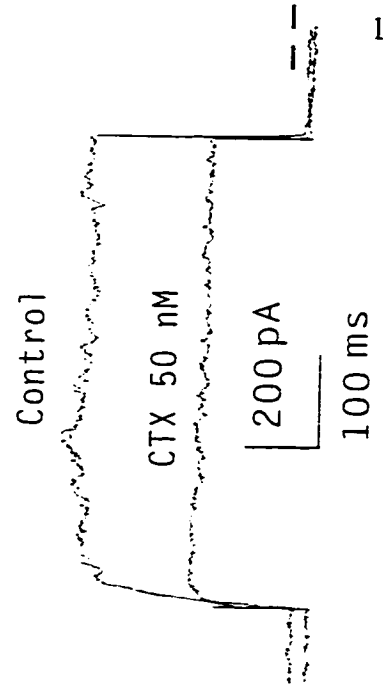


Fig. 3-21

outwardly rectifying  $K^+$  channels (Schneider et al., 1989).

## 5.2 Single-channel recording

Single channel recordings were made from rabbit RPE cells in the cell-attached mode and in the excised inside-out configuration. In the cell-attached configuration, 130 mM external KCl with 130 mM KCl in the recording pipette, the most obvious single-channels which could be recorded in rabbit RPE cells were large-conductance channels, which had slope conductances close to or greater than 200 pS and reversed around 0 mV. This channel was present in 50% (10/20) of patches recorded from in early cultures (less than 3 days), however by 14 days in culture this incidence increased to between 70-80% of membrane patches. Figure 3-22A shows examples of single channel records recorded in the cell-attached configuration at different estimated clamped potentials of the membrane patch (negative of the electrode potential). Single channel activity was not apparent in this patch until +40 mV, whereupon channel activity increased with increasing patch depolarization. The I-V plot (Fig. 3-22B) for the unitary currents shown in figure 3-22A, indicates that the channel has a conductance of 198 pS. Figure 3-22C shows a plot of the channel activity ( $NP_o$ ) versus the clamped membrane potential for unitary currents from the same patch. In the cell-attached configuration, channel openings were seldom found at potentials hyperpolarized to +40 mV. This phenomenon may be explained by two reasons: 1) low  $[Ca^{2+}]_i$  which results in low channel open probability at negative membrane potentials, and 2) the cell resting membrane potential was not clamped to a value close to 0 mV (i.e.  $[K^+]_i \gg 130$  mM as estimated) so that the

## RESULTS

**Figure 3-22.** Identification of a large-conductance voltage-dependent K<sup>+</sup> channel. (A) Single-channel currents recorded in cell-attached configuration in 130 mM KCl in both bath and electrode solutions. Estimated clamped potential of the membrane patch (negative of electrode potential) is indicated at the left of each trace. Dashed lines indicate the channel closed state in this and subsequent unitary current recordings. (B) The corresponding I-V plot for the unitary currents recorded from the patch shown in (A). The channel has a slope conductance of 198 pS. (C) Plot of channel open probability ( $NP_o$ ) versus clamped potential of the membrane patch.

RESULTS

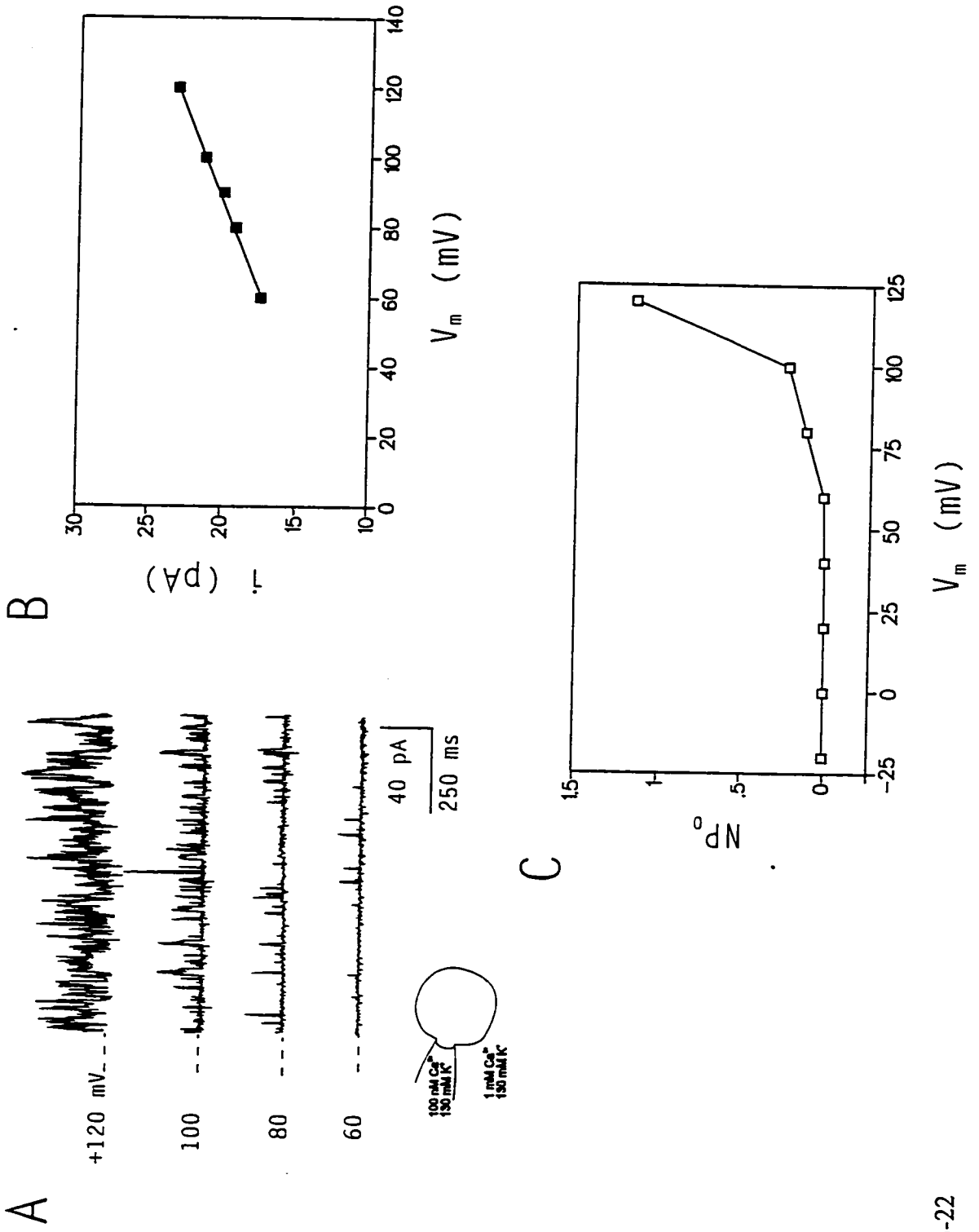


Fig. 3-22

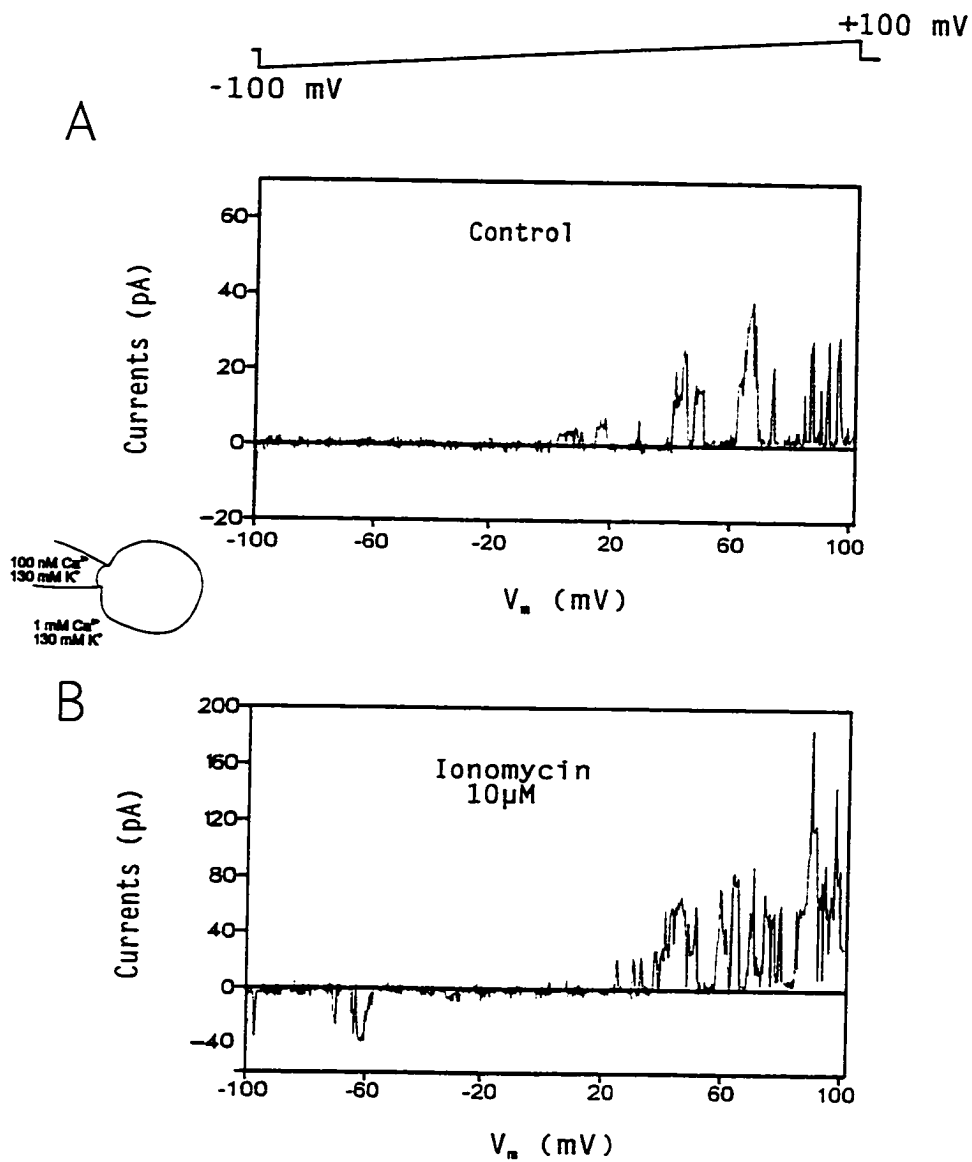


Fig. 3-23. The effect of ionomycin on the activity of the large conductance channel . Unitary currents recorded from a cell-attached patch using a voltage ramp (shown at the top). (A) A representative trace under control conditions (symmetrical 130 mM  $K^+$  with 1 mM  $Ca^{2+}$  in the bath). (B) A representative trace during puffer application of 10  $\mu$ M ionomycin. The unitary currents shown have a slope conductance of 232 pS.

actual potential that the membrane patch under the recording pipette saw was less depolarized than  $-V_p$  ( $V_m = \text{RMP} - V_p$ ).

Ionomycin was used to further explore the  $[\text{Ca}^{2+}]_i$  sensitivity of the large conductance channel activity. Puffer application of 10  $\mu\text{M}$  ionomycin substantially increased unitary current at depolarized potentials and shifted the channel opening to more hyperpolarized potentials. Figure 3-23 shows the unitary current-voltage relation recorded from a cell-attached patch using voltage ramps (130 mM  $\text{K}^+$  in both bath and recording pipette Ringers with 1 mM  $\text{Ca}^{2+}$  in the bath) before and during ionomycin application. The channel in this patch had a slope conductance of 232 pS and the unitary currents increased 7.5-fold upon ionomycin application over the same voltage range indicating increased channel openings.

In order to further determine slope conductance and reversal potential as well as the  $\text{Ca}^{2+}$  sensitivity of the channel, the channel activity was examined in excised inside-out patches. Figure 3-24 A and B show average currents recorded from a patch using voltage ramps in the cell-attached and subsequently in the inside-out excised patch configurations (130 mM  $\text{KCl}$  in the pipette and bath, 1 mM  $\text{Ca}^{2+}$  in the bath). The data shown are the average of three current ramps. In the cell-attached patch configuration, channels were not open until the patch potential was very depolarized. However, excision of the patch into 1 mM bath  $\text{Ca}^{2+}$  resulted in increased channel activity. The unitary currents were outward at depolarized potentials, and inward at hyperpolarized potentials due to the reversal of the driving force. The unitary currents were outwardly rectifying and reversed at close to 0 mV, consistent with  $\text{Ca}^{2+}$ -activated  $\text{K}^+$  selective

## RESULTS

**Figure 3-24.** The large-conductance channel is  $\text{Ca}^{2+}$ -activated and  $\text{K}^+$  selective. (A) Single channel currents recorded in a patch with symmetrical KCl. Current shown is the average current measured from 3 voltage ramps (-100 to +100 mV in a 2 sec duration) in the cell-attached and inside-out excised patch configuration. In the cell-attached patch configuration (CAP), channels were not open near the reversal potential, however excision of the patch into 1 mM bath  $\text{Ca}^{2+}$  resulted in channel activity at both hyperpolarized and depolarized potentials. (B) A plot of  $P_o$  versus holding potential for channel activity recorded from the excised patch shown in (A). (C) Single-channel currents recorded in symmetrical  $\text{K}^+$  in another inside-out patch using a voltage-ramp command (-100 to +100 mV). Currents were inward at negative potentials, outward at positive potentials and reversed around 0 mV. The slope conductance of the channel was 236 pS. (D) Single channel currents recorded from the same patch with asymmetric KCl (5 mM KCl inside/ 130 mM KCl outside). The reversal potential for the single channel currents shifted to around +60 mV and the slope conductance for the channel was 166 pS, consistent with the channel being selective for  $\text{K}^+$  ions.



RESULTS

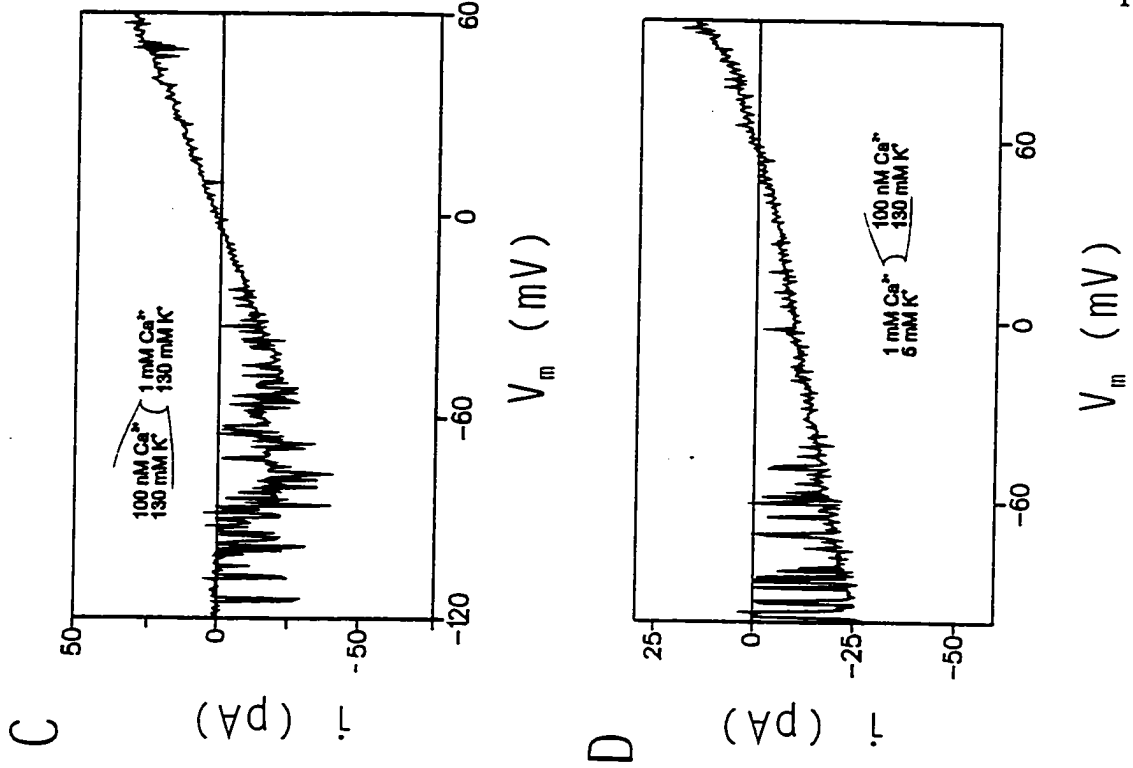
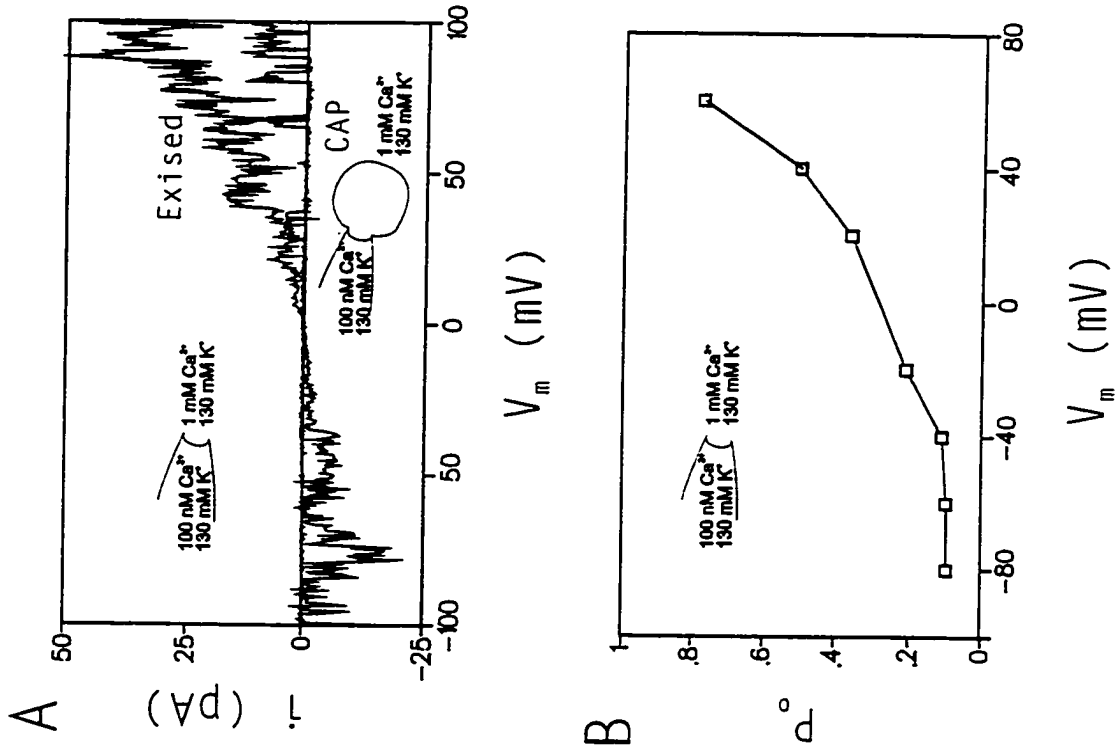


Fig. 3-24

channels. Figure 3-24B shows a plot of the  $P_o$  versus patch potential for the channel activity from the excised patch shown in figure 3-24A.  $P_o$  was calculated from the averaged current above baseline as described in METHODS (see chapter 2, section 2.7, page 50) and is affected by the patch potentials. That is,  $P_o$  is lowest at more negative potentials and increases with membrane depolarization.

Figure 3-24C and D show the current-voltage relationship for the large-conductance channel recorded initially in 130 mM symmetrical  $K^+$  and subsequently in asymmetrical  $K^+$  (130/5 mM, outside/inside) bath Ringers containing 1 mM  $Ca^{2+}$ . In the symmetrical [ $K^+$ ] condition, currents were outward at positive potentials, inward at negative potentials and reversed at  $-1.23 \pm 0.87$  mV ( $n=7$ ), close to the calculated  $E_K$  (0 mV). The slope conductance (between -60 mV and +60 mV) for the channel recorded in excised patches with symmetrical 130 mM  $K^+$  was  $223 \pm 5$  pS ( $n=7$ ) (Fig. 3-24C). The reversal potential for unitary currents shifting positive to  $+61 \pm 8$  mV ( $n=3$ ; 43 mV/10 fold change in  $K^+$ ) when the bath solution was changed to standard 5 mM  $K^+$  Ringer containing 1 mM  $Ca^{2+}$  (Fig. 3-24D) consistent with channel being  $K^+$  selective. In asymmetrical  $K^+$  conditions (130 mM/5 mM, outside/inside), the channel conductance at negative potentials was  $158 \pm 6$  pS ( $n=3$ ). Similar decreases in unitary channel conductance has also been observed in other cell types in asymmetrical [ $K^+$ ] conditions (Berweck et al., 1994), suggesting a saturating function of salt activity on channel conductance (Cecchi, Alvarez and Wolf, 1986).

The activity of the maxi- $K_{Ca}$  channels depends on both the transmembrane potential and on  $[Ca^{2+}]_i$ . Figure 3-25A shows typical unitary current records of  $K^+$

## RESULTS

**Fig. 3-25.** The effect of  $[Ca^{2+}]_i$  and cytosolic  $Ba^{2+}$  on the open probability of the  $K_{(Ca)}$  channel. (A) Single channel activity recorded from an inside-out patch ( $V_m = -60$  mV) is reduced when bath  $Ca^{2+}$  is decreased from 2.5 mM ( $P_o > 0.9$ ) to a nominally  $Ca^{2+}$ -free bath solution ( $P_o < 0.05$ ). (B) Single-channel currents at different  $[Ca^{2+}]_i$  recorded from another inside-out patch at +60 mV. The bath  $Ca^{2+}$  concentrations are indicated at the left of each trace. Single channel activity decreased with reduced  $[Ca^{2+}]_i$ . (C) Open probability ( $P_o$ ) for the maxi- $K_{(Ca)}$  channel is plotted as a function of  $[Ca^{2+}]_i$  on semilogarithmic co-ordinates. Data were obtained from the same patch as shown in (B) at +60 mV. (D) The maxi- $K_{(Ca)}$  channel is blocked by  $Ba^{2+}$ . Application of 1 mM  $Ba^{2+}$  to the cytosolic surface of another inside-out patch ( $V_m = -60$  mV) reduced channel activity and results in long periods of channel closure. The  $P_o$  of the channel decreases from  $>0.8$  to  $<0.1$  after 10 min exposed to  $Ba^{2+}$ .

RESULTS

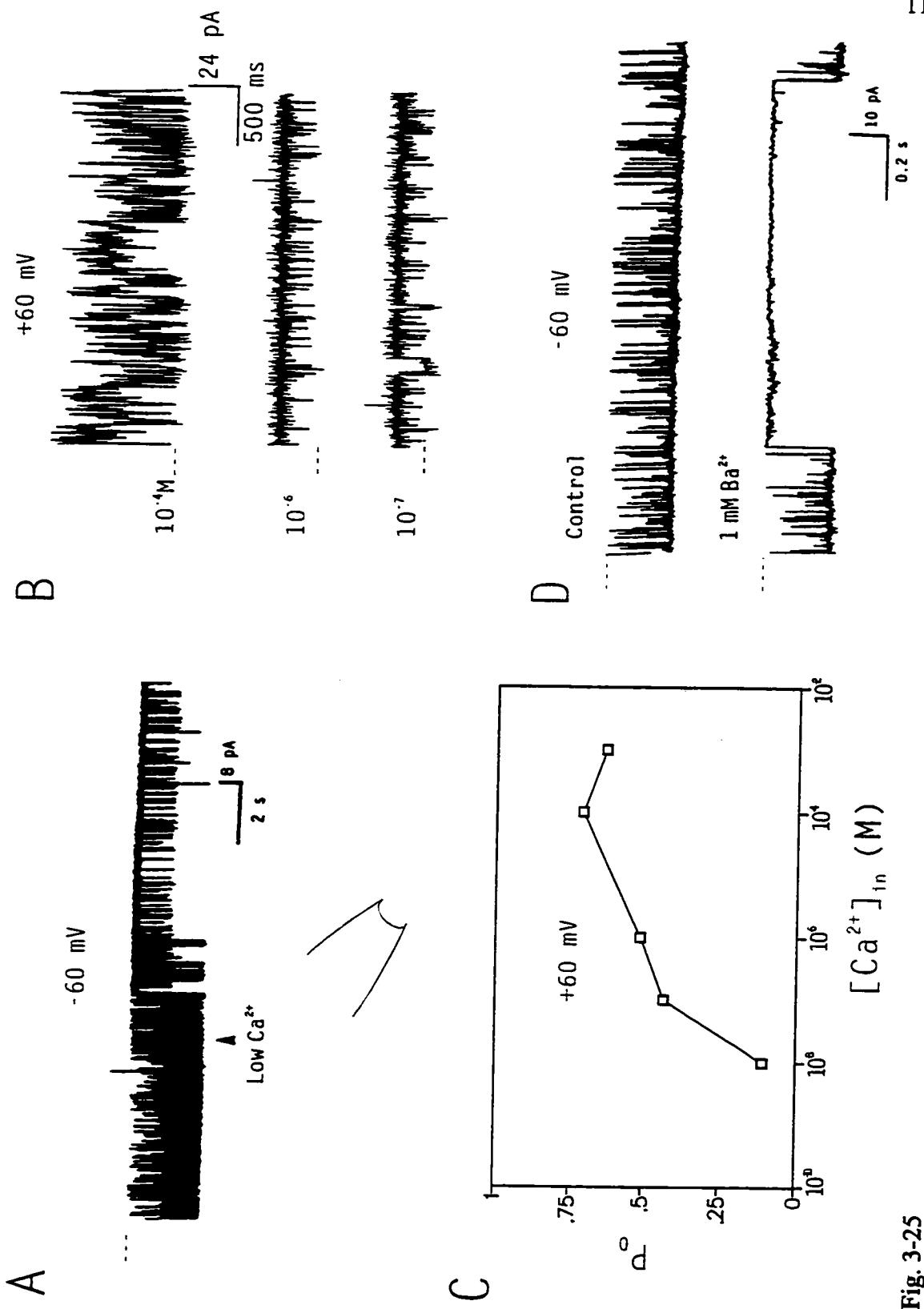


Fig. 3-25

channel activity recorded with symmetrical 130 mM  $K^+$  solutions, in an inside-out patch, at a holding potential of -60 mV. When  $[Ca^{2+}]_i$  is reduced from 1 mM to nominally  $Ca^{2+}$ -free solution ( $< 10^{-8}$  M), channel activity decreased. The  $P_o$  for the channel shown in figure 3-25A was 0.87 in 1 mM  $[Ca^{2+}]_i$  and 0.044 after 10 minutes exposure to nominally  $Ca^{2+}$ -free solution. The dependence of the channel on  $Ca^{2+}$  is shown in more detail in figures 3-25B and C. Figure 3-25B shows unitary  $K^+$  currents recorded from another patch in the inside-out configuration ( $V_m = +60$  mV) at three different internal  $Ca^{2+}$  concentrations. The channel  $P_o$  decreased from 0.77 to 0.48 when  $Ca^{2+}$  was changed from  $10^{-4}$  M to  $10^{-7}$  M, respectively. Figure 3-25C shows the effect of internal  $Ca^{2+}$  on the  $P_o$  of maxi- $K_{Ca}$  channels in the same patch at  $V_m = +60$  mV. The lowest value of  $[Ca^{2+}]_i$  at which single channel openings were detected was  $10^{-9}$  M. In the patch shown and two other patches recorded from in the inside-out configuration, the mean  $[Ca^{2+}]_i$  at which single maxi- $K_{Ca}$  channels were open half of the time was  $4.8 \times 10^{-6}$  M ( $V_m = +60$  mV). Note that at +60 mV and with  $[Ca^{2+}]_i > 10^{-4}$  M the  $P_o$  does not reach 1. This is due to longer lasting closures of the channel which decrease the channel  $P_o$  and may reflect  $Ca^{2+}$ -dependent block of the channel at higher  $[Ca^{2+}]_i$  (Cechi et al., 1986).

Maxi- $K_{Ca}$  channels were blocked by the  $K^+$  channel blocker  $Ba^{2+}$ . As mentioned previously,  $Ba^{2+}$  is an effective blocker for maxi- $K_{Ca}$  channels. It can exert its action either through internal or external application.  $Ba^{2+}$  applied via either route, binds to the same site within the channel pore (Latorre and Miller, 1983). The block shows a simple ion interaction;  $Ba^{2+}$  and  $K^+$  compete for the channel, one  $Ba^{2+}$  molecule binds the channel and occludes its conductive pathway (Eaton and Brodwick, 1980). Figure 3-25D

shows unitary currents recorded at  $-60$  mV from an inside-out patch in symmetrical 130 mM KCl with 1 mM  $\text{Ca}^{2+}$  in the bath (upper trace). Subsequent application of  $\text{Ba}^{2+}$  (1 mM) to the cytosolic membrane surface decreased maxi- $\text{K}_{\text{Ca}}$  channel activity and reduced  $P_o$  from  $>0.8$  to  $<0.035$  (lower trace). Similar results were obtained in two other patches.

## 6. $\alpha_1$ -Adrenergic modulation of maxi- $\text{K}_{\text{Ca}}$ channels in rabbit RPE cells

There are several types of  $\text{K}_{\text{Ca}}$  channels. Two of them are well characterized; maxi- $\text{K}_{\text{Ca}}$  and slow AHP  $\text{K}_{\text{Ca}}$  channels. All types of  $\text{K}_{\text{Ca}}$  channels are targets for modulation by either neurotransmitters or hormones (Rudy, 1988) as they provide a direct link between  $\text{Ca}^{2+}$ , a major intracellular second messenger, and the membrane potential. Among them, maxi- $\text{K}_{\text{Ca}}$  channels are of particular importance for modulation due to their large conductances. Activation of these channels will result in large changes in membrane potential.  $\alpha_1$ -Adrenergic receptors have been identified in rabbit RPE cells (Frambach et al., 1988b), and their activation has been reported to modulate ionic and fluid transport across the RPE in the bovine retina (Edelman and Miller, 1991; Lin and Miller, 1991b; Edelman and Miller, 1992; Joseph and Miller, 1992; Quinn and Miller, 1992).  $\alpha_1$ -Adrenergic receptor coupled pathways lead to an increase of  $[\text{Ca}^{2+}]_i$ , therefore, adrenergic modulation of maxi- $\text{K}_{\text{Ca}}$  channels in rabbit RPE cells was examined using a selective  $\alpha_1$ -adrenergic receptor agonist, phenylephrine (PhE).

### 6.1 Whole-cell recording

#### 6.1.1 Phenylephrine (PhE) increases the macroscopic outwardly rectifying $\text{K}^+$ current

When external and internal Ringer solutions containing low  $\text{Cl}^-$  (~40 mM) and low  $\text{Ca}^{2+}$  (100 nM) were used, puffer application of 10  $\mu\text{M}$  PhE caused a mean increase in  $I_K$  of  $77 \pm 18\%$  ( $n=28$ ) at +60 mV in 70% cells recorded (28/40;  $P < 0.05$ , paired t test). Figure 3-26A shows whole-cell current recorded from a rabbit RPE cell before (upper panel), during application of PhE (middle panel), and after 9 min washout of PhE (bottom panel), using the same whole-cell voltage protocol as before. Figure 3-26B shows the corresponding I-V curves measured at the end of the voltage pulse from the currents shown in figure 3-26A. In the cell shown, depolarizing steps from a  $V_h$  of -60 mV elicited outward  $\text{K}^+$  current which activated positive to -60 mV. In the presence of PhE, the same voltage steps elicited an increased outward current at all voltages positive to the activation potential. The inset in figure 3-26A shows the whole-cell current from the same cell shown in figure 3-26A under control conditions and during PhE application, at -80 and +60 mV ( $V_h = -60$  mV). The current traces recorded at -80 mV in control conditions and in the presence of PhE overlapped indicating that PhE has no effect on leak current. At +60 mV the current recorded during PhE application was significantly increased over the control. The effect of PhE was readily reversible. The outward current recovered to the control level ~10 min after the puffer pipette was moved out of the bath. It was also demonstrated that the PhE effect on the outward current was reproducible. A second application of the same amount of PhE after ~10 min washout evoked a similar mean increase in the outward current amplitude ( $72 \pm 26\%$ ,  $n=3$ , Fig. 3-26C). Figure 3-26C is a bar graph plotting the mean amplitude of outward current measured at +60 mV for three separate cells under different conditions. Both a first and second puffer

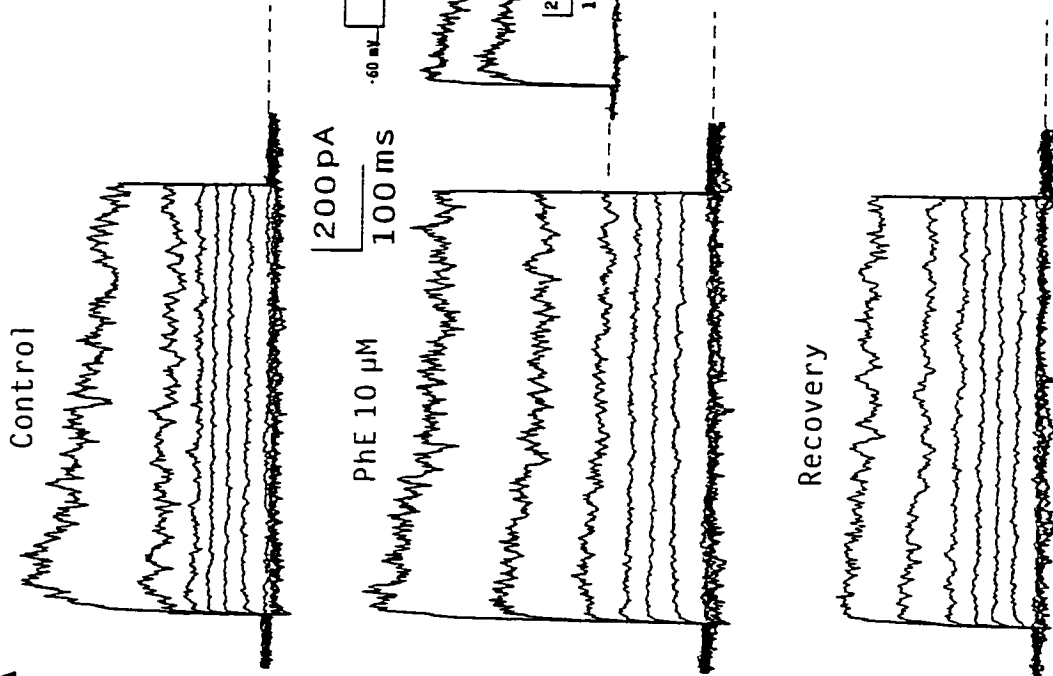
## RESULTS

**Fig. 3-26.** PhE increased macroscopic  $I_K$ . (A) Whole-cell currents recorded from a rabbit RPE cell in 130 mM K<sup>+</sup>, 40 mM Cl<sup>-</sup> and 100 nM Ca<sup>2+</sup> external Ringer (modified standard Ringer) before (top panel), during puffer application of 10  $\mu$ M PhE (middle panel) and 9 min after the puffer electrode was moved out of the bath chamber (bottom panel). A linear leak of 1.0, 2.0 and 1.4 G $\Omega$  was subtracted from the traces for control, PhE and recovery, respectively. Inset: current traces recorded at -80 and +60 mV ( $V_h = -60$  mV) under control conditions and during application of PhE. (B) Corresponding I-V curves at the end of the voltage pulse for the cell shown in (A) under control conditions (O), during exposure to PhE (●) and after washout of PhE (∇). Capacitance of the cell shown was 16 pF. (C) Mean current amplitude measured at +60 mV for three separate cells under different conditions: control; PhE; recovery; and a second PhE application.

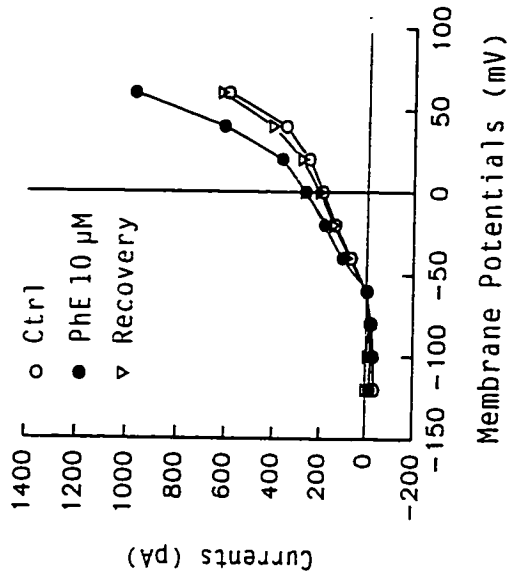


RESULTS

A



B



C

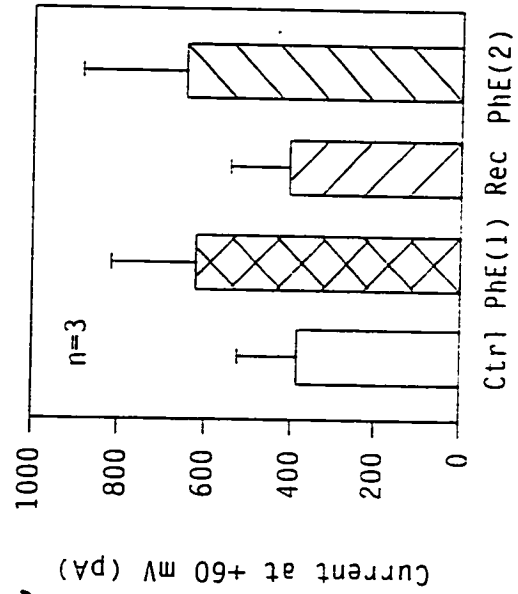


Fig. 3-26

application of PhE caused a similar increase in the outward current as compared to control and recovery following PhE application. Thus, the PhE effect on the outward current is both recoverable and reproducible.

*6.1.2 The outward  $K^+$  current induced by PhE was sensitive to the specific maxi- $K_{Ca}$  channel blocker, IbTX*

In order to determine whether the actions of PhE involved activation of the maxi- $K_{Ca}$  channels, the ability of the potent maxi- $K_{Ca}$  channel blocker, IbTX in blocking the PhE induced outward  $K^+$  current was examined. The following approach was used: The cell was first exposed to 10  $\mu$ M PhE, to determine whether there was any PhE-inducible  $I_K$ . Following PhE application, the agonist was washed out for 10 min in the presence of IbTX, and the cell was exposed to a second application of PhE (10  $\mu$ M). In four cells tested, IbTX (1 nM) blocked the subsequent PhE-induced increases in the  $I_K$ . Figure 3-27A shows macroscopic current recorded from an RPE cell under various conditions, as labeled at the top of each family of current traces. Depolarizing steps positive to -20 mV elicited a slowly inactivating outward current. The I-V curves for the current shown in figure 3-27A was outwardly rectifying (Fig. 3-27B). External application of 10  $\mu$ M PhE increased the  $I_K$  at all voltages positive to -20 mV. The PhE effect was abolished by 1 nM externally applied IbTX. It was shown that IbTX (1 nM) by itself has little effect on the  $I_K$  in the absence of the agonist, for superfusion with IbTX during PhE washout did not significantly inhibit the  $I_K$ . Figure 3-27C summarizes the results obtained from four cells tested with IbTX. The mean amplitudes of  $I_K$  at +60 mV for four cells under different

## RESULTS

**Fig. 3-27.** IbTX blocked PhE's effect on the  $I_K$ . (A) Whole-cell current recorded from an RPE cell in modified standard Ringer before (top left panel), during puff application of 10  $\mu$ M PhE (top right panel), after 10 min washout of PhE with 1 nM IbTX in the superfusate (lower left panel), and during a second puff application of PhE in the presence of IbTX (lower right panel). Currents were corrected for linear leaks of 1.7, 1.8, 1.25 and 0.78 G $\Omega$ , respectively. (B) Corresponding I-V curves for the cell shown in (A) measured at the end of the voltage pulse under control conditions (O), during exposure to PhE (●), after washout of PhE (∇), and during a second PhE application in the presence of IbTX (▼). Capacitance of the cell shown was 34 pF. (C) Mean current amplitudes at +60 mV for four cells tested under different recording conditions.

RESULTS

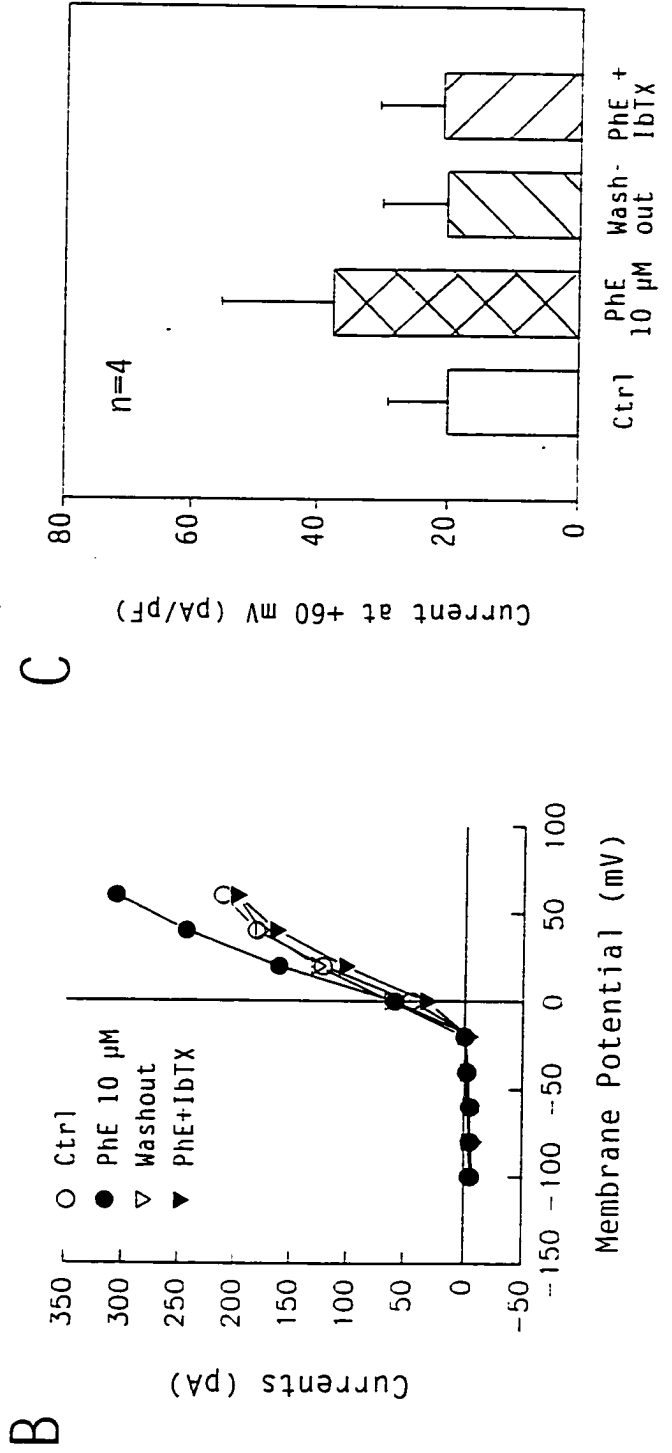
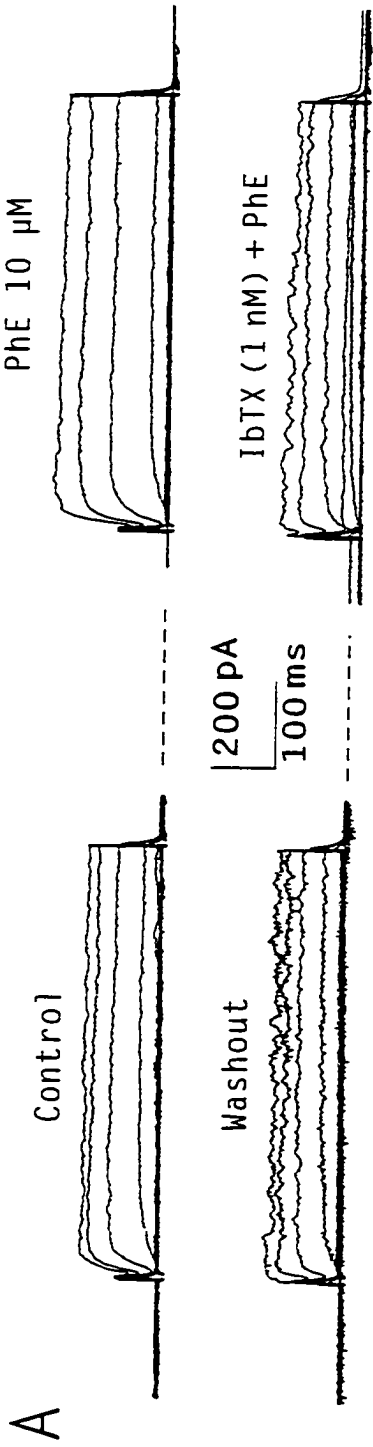
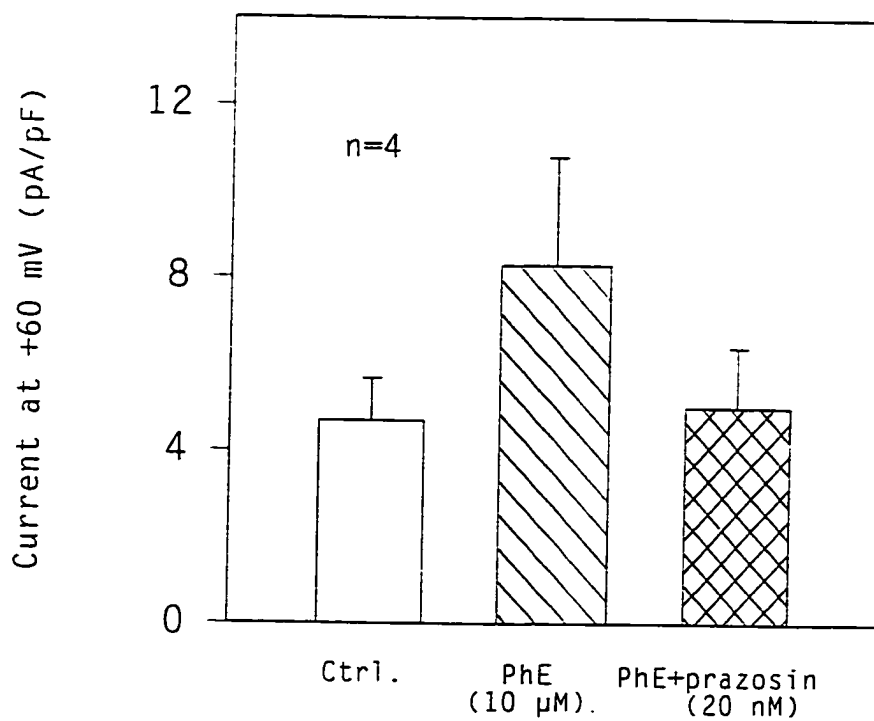


Fig. 3-27

recording conditions was plotted. In all four cells, the amplitude of  $I_K$  under control conditions, after washout of PhE from the bath chamber and during PhE application in the presence of IbTX, was virtually the same. However application of PhE in the absence of IbTX caused an increase in  $I_K$  with a mean value of  $69 \pm 16\%$  ( $n=4$ ). The sensitivity of PhE-induced currents to IbTX suggests that  $\alpha_1$ -receptor activation activates maxi- $K_{Ca}$  channels in rabbit RPE cells.

### *6.1.3 PhE-induced increases in maxi- $K_{Ca}$ current ( $I_{K(Ca)}$ ) involve $\alpha_1$ -adrenergic receptors*

To further confirm that PhE-induced  $I_{K(Ca)}$  is mediated by stimulation of  $\alpha_1$ -adrenergic receptors, the effect of the selective  $\alpha_1$ -adrenergic receptor antagonist, prazosin, on the PhE-induced increase in  $I_{K(Ca)}$  was examined. Addition of prazosin (20 nM) to the perfusate blocked the PhE-induced increase in the  $I_{K(Ca)}$ . The prazosin experiments were carried out using the same approach as described previously for the IbTX protocol. The cells were superfused with prazosin for 10 min during the washout period between first and second puffer application of PhE. Figure 3-28 plotted the mean amplitude of  $I_K$  at +60 mV obtained from four cells tested using 20 nM prazosin to block the effect of 10  $\mu$ M PhE on  $I_{K(Ca)}$ . The whole-cell currents were normalized with cell capacitance before being averaged. As shown, the mean current amplitude during PhE (10  $\mu$ M) application was increased by 73.22% ( $n=4$ ). However, another application of the same amount of PhE after subsequent superfusion with 20 nM prazosin for 10 min failed to induce any increase in  $I_K$ . Prazosin has been reported to have a nonselective effect on  $\alpha_2$ -adrenergic receptor at higher concentrations, therefore a low concentration (nM) of



**Fig. 3-28.** Prazosin inhibited the effect of PhE on  $I_{K(Ca)}$ . Mean  $I_K$  (pA/pF) measured at +60 mV for 4 cells during 10  $\mu$ M PhE application and a second PhE application in the presence of 20 nM prazosin.

prazosin was used in this study to ensure its selective effect on  $\alpha_1$ -adrenergic receptors. In contrast to the blocking effect of prazosin demonstrated here, bath application of yohimbine (10 nM), an  $\alpha_2$ -adrenergic receptor blocker, did not inhibit PhE activation of maxi- $K_{Ca}$  channels ( $n=2$ , data not shown). These results suggest that PhE enhances  $I_{K(Ca)}$  by a mechanism which selectively involves  $\alpha_1$ -adrenergic receptors in rabbit RPE cells..

#### 6.1.4 Effect of internal application of $IP_3$

In many systems,  $\alpha_1$ -adrenergic receptors control intracellular free  $Ca^{2+}$  by increasing cytosolic inositol(1,4,5)-trisphosphate ( $IP_3$ ) production.  $IP_3$  is produced from the phosphodiesterase-mediated hydrolysis of inositol phospholipids, phosphatidylinositol-4,5-bisphosphate ( $PIP_2$ ). To determine whether PhE induced increases in  $I_{K(Ca)}$  are mediated via activation of  $IP_3$ -sensitive  $Ca^{2+}$  stores in rabbit RPE cells, the effect of internally dialyzed  $IP_3$  on  $I_{K(Ca)}$  was investigated.  $I_{K(Ca)}$  was recorded immediately after assuming the whole-cell recording configuration and subsequently 10 min after initiation of whole-cell recording, at which time the cytosol of the cell would have been well dialyzed with  $IP_3$ . Figure 3-29 shows current traces recorded from a cell at +60 mV ( $V_h = -60$  mV). Currents recorded at two different times were superimposed for comparison (Fig. 3-29A). The I-V curves, measured at the end of the voltage pulse from the same cell (Fig. 3-29B), demonstrate that outward  $K^+$  current activated at -20 mV and  $I_{K_i}$  at voltages more negative than -80 mV.  $IP_3$  profoundly increased  $I_K$  little affection. The mean  $I_K$  amplitude at +60 mV after cytosolic  $IP_3$  dialysis was increased by  $80 \pm 56\%$  ( $n=5$ ) as compared to that in control conditions, whereas the mean leak current ( $I_{leak}$ ) after  $IP_3$

## RESULTS

**Fig. 3-29.** The effect of internal application of  $IP_3$  on the  $I_{K(Ca)}$ . (A)  $I_K$  evoked by a voltage step from a  $V_h$  of  $-60$  mV to a test potential of  $+60$  mV for 500 msec. Current trace labeled "break-in" was recorded immediately after the whole-cell configuration was assumed, and trace labeled "10 min" was obtained 10 min after gaining intracellular access to allow  $IP_3$  to diffuse into the cell. Current traces were subtracted for linear leaks of  $0.56$  and  $0.5$  G $\Omega$  respectively. (B) Corresponding I-V curves for the currents recorded from the cell shown in (A) measured at the end of the voltage pulse under control condition (O) and after cytosolic dialysis of  $IP_3$  (●). Capacitance of the cell shown was 47 pF. (C) Mean current amplitude at  $+60$  mV 10 min after assuming the whole-cell recording configuration as compared to that recorded immediately after break-in. The results were obtained from 5 cells tested. The mean leak current ( $I_{leak}$ ) amplitude at  $+60$  mV was not increased by  $IP_3$ .



RESULTS

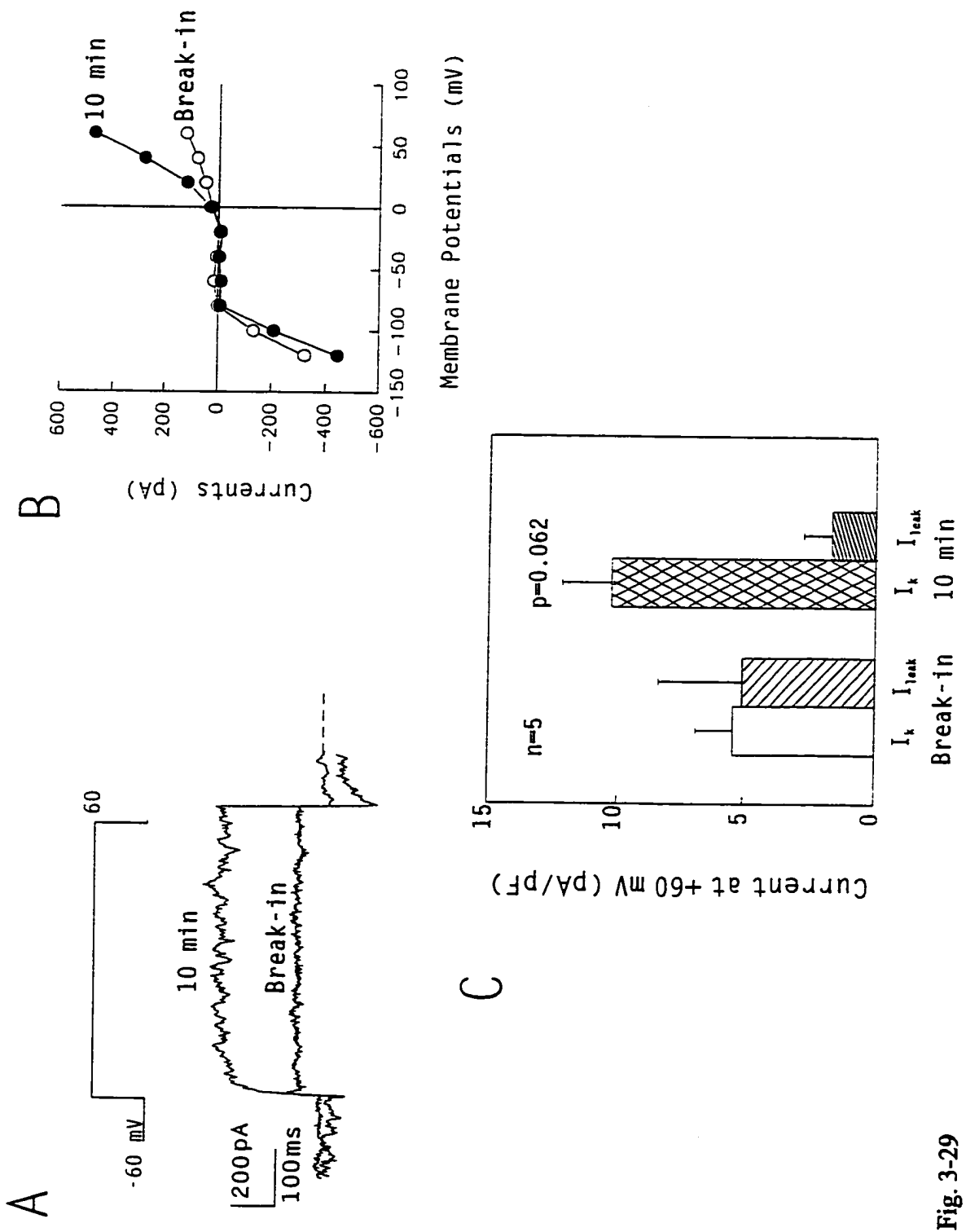


Fig. 3-29

dialysis was not increased (Fig. 3-29C). Therefore, like PhE,  $IP_3$  activates maxi- $K_{Ca}$  channel in rabbit RPE cells in a selective manner. Leak currents shown were normalized mean current amplitude at +60 mV extrapolated from the linear regression obtained from negative potential range.

## 6.2 Single-channel recording

Further confirmation that PhE induces maxi- $K_{Ca}$  channel activity was obtained from single-channel recordings from cell-attached membrane patches. In the cell-attached configuration, the cell remains intact, therefore the intracellular components necessary for signal transduction are preserved. With symmetrical 130 mM  $K^+$  Ringers and 100 nM  $Ca^{2+}$  in both the bath and electrode pipette, puffer application of 10  $\mu$ M PhE activated a large conductance channel among 71% patches recorded (24/34). The channels activated by PhE had a unitary conductance of  $229 \pm 5$  pS ( $n=5$ ). Consistent with the effects of PhE on macroscopic whole-cell current,  $\alpha_1$ -adrenergic receptor agonist activation of the large conductance  $K^+$  channels was reversible (Fig. 3-30). As shown in figure 3-30, single channel activity was not observed in this patch until +20 mV, and was apparent at +100 mV. The channel activity was substantially increased upon puffer application of 10  $\mu$ M PhE, and returned to control levels 18 min after the puffer electrode was moved from the bath chamber. Figure 3-31 shows single-channel recordings from the same cell-attached patch in figure 3-30 using voltage ramp protocol. Under control conditions channel activity was seldom seen at  $V_p < -40$  mV (Fig. 3-31A). However, application of 10  $\mu$ M PhE caused an increased activation of a large conductance channel

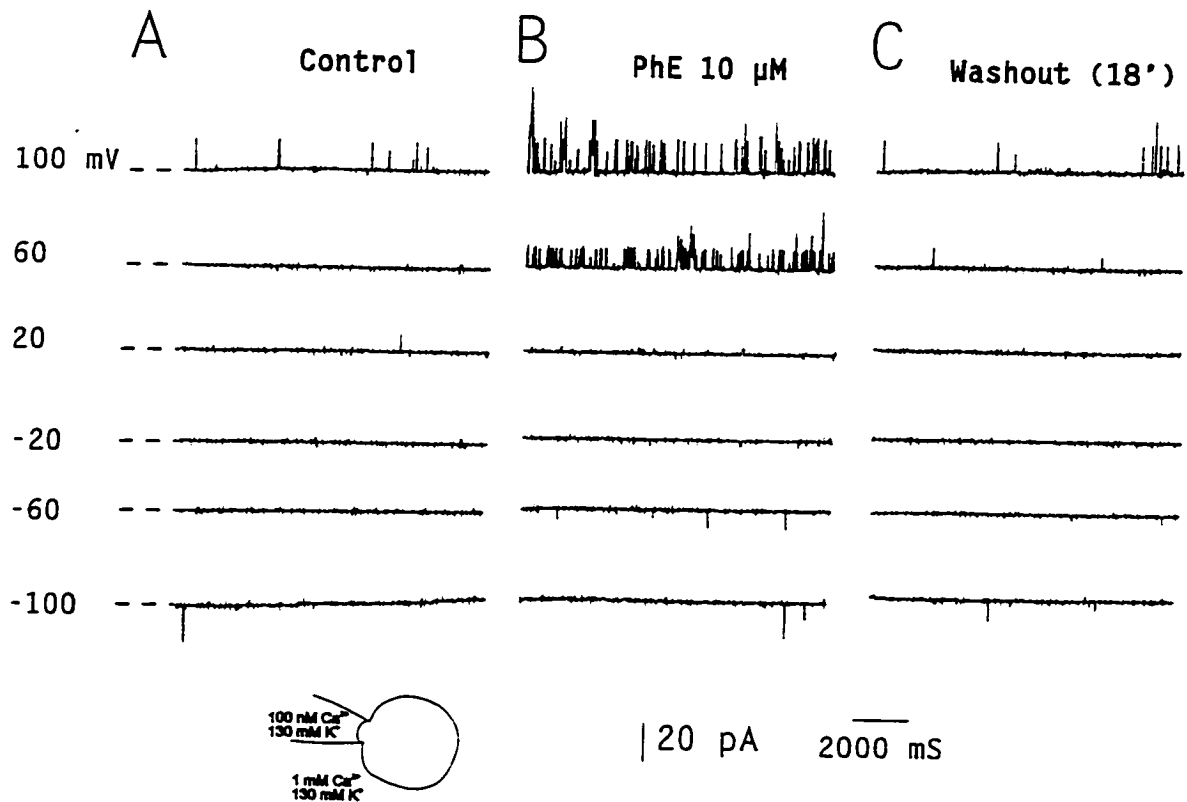


Fig. 3-30. The PhE-induced current is due to the activation of a large conductance channel. Single-channel currents recorded in symmetrical 130 mM  $\text{K}^+$ /100 nM  $\text{Ca}^{2+}$  Ringers from a cell-attached patch under control condition (A), during puffer application of 10  $\mu$ M PhE (B) and 18 min after washing PhE out (C). Holding potential is indicated at the left of each trace. The channel has a slope conductance of 220 pS.

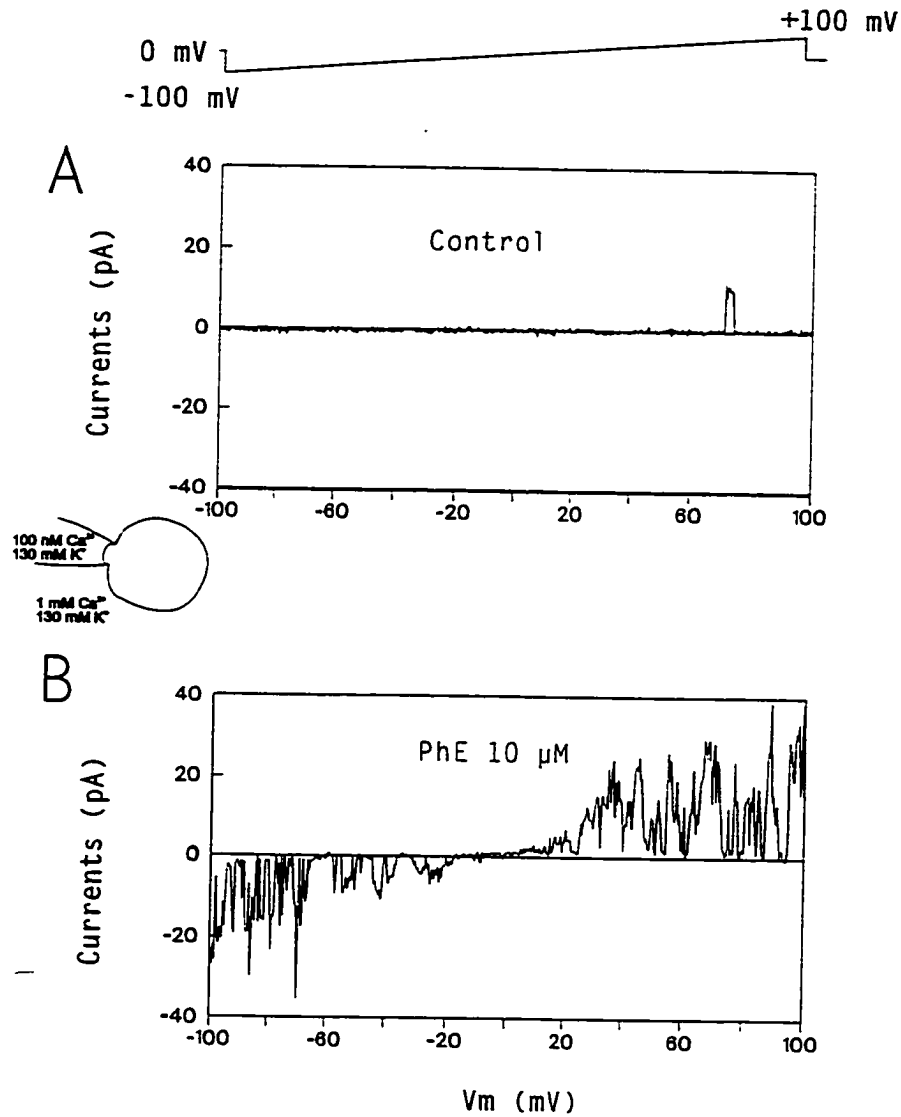


Fig. 3-31. The large-conductance channel activated by PhE is K<sup>+</sup> selective. Single-channel currents recorded from the same patch shown in figure 3-30 using the voltage ramp protocol shown on the top (-100 to +100 mV) under control conditions (A), during puffer application of 10 μM PhE (B). Currents were inward at negative potentials, outward at positive potentials and reversed around 0 mV, consistent with the channel being selective for K<sup>+</sup> under symmetrical [K<sup>+</sup>] recording condition.

at both hyperpolarized and depolarized potentials with unitary currents reversing at  $\sim 0$  mV. The slope conductance of the channel was 220 pS (Fig. 3-31B), which is consistent with PhE activation of maxi- $K_{Ca}$  channels. PhE shifted the threshold for the channel opening to less positive potentials, similar to what was observed when  $[Ca^{2+}]_i$  was increased (see section 5.2 of this chapter, Fig. 3-24A).

In summary, external application of PhE to cell-attached membrane patches caused the activation of large conductance, voltage-dependent, and  $K^+$  selective channels. It also shifted the channel opening threshold to less positive potentials in a manner similar to that found with increased  $[Ca^{2+}]_i$ . The involvement of intracellular signalling pathway(s) was evident as in the cell-attached configuration, the channels under investigation were isolated from the externally applied PhE. These results support the whole-cell findings and indicate that  $\alpha_1$ -adrenergic receptor activation increases maxi- $K_{Ca}$  channel activity in cultured rabbit RPE cells via an intracellular second messenger system which results in an elevation of  $[Ca^{2+}]_i$ .

# 4

## Discussion

---

In the present study, patch-clamp recording techniques have been used to examine membrane properties as well as whole-cell currents and single-channel activity in rabbit RPE cells in primary culture. Cultured rabbit RPE cells express at least four voltage-dependent  $K^+$  currents; three outwardly rectifying  $K^+$  currents including a delayed rectifier, a fast-inactivating  $K^+$  current, a  $Ca^{2+}$ -activated  $K^+$  (maxi- $K_{Ca}$ ) current, and an inwardly rectifying  $K^+$  current. Details of these currents are discussed below and compared to  $K^+$  currents described for RPE cells from other species, as well as  $K^+$  currents reported in other cell types. This study extends previous ion transport studies in the rabbit RPE (Frambach et al., 1988a) by providing the first account of ionic currents and  $\alpha_1$ -adrenergic modulation of maxi- $K_{Ca}$  current at the whole-cell and single-channel levels.

### 1. Membrane properties of rabbit RPE cells in primary culture

The membrane capacitance of cultured rabbit RPE cells averaged  $27 \pm 0.8$  pF ( $n=294$ ). Due to the substantial contribution of both the apical processes and the basal infoldings to the membrane surface area, the estimation of the surface area per cell or the specific membrane capacitance was not attempted. The average resting membrane potential of cultured rabbit RPE cells was  $-31 \pm 1.4$  mV ( $n=110$ ). Similar low average

values have also been recorded in whole-cell recordings of freshly dissociated frog and turtle RPE cells (Hughes, Botchkin and Steinberg, 1990; Fox and Steinberg, 1992), and for human RPE cells in culture (Fox et al., 1988). The exact reasons underlying the relatively low resting membrane potentials found in isolated RPE cells remain unclear, however the breakdown of paracellular junctional complexes during cell isolation may contribute to this. Several cells measured in this study exhibited resting membrane potentials as high as -60 mV, which resemble the values obtained from intact epitheliums [Joseph and Miller, 1991 (bovine); Quinn, R.H. and Miller, S.S., 1992 (human)].

## **2. Voltage-dependent $K^+$ currents in rabbit RPE cells: Comparison with other cell types**

### **2.1. Delayed rectifier**

The predominant macroscopic current expressed in 79-80% of rabbit RPE cells is an outwardly rectifying  $K^+$  current,  $I_K$ . This current activated with a slight delay at potentials positive to -40 mV and decayed slowly after reaching a peak while the depolarization was still maintained. The outward current described in rabbit RPE cells is highly selective for  $K^+$  in 5/130 mM  $[K^+]$  (outside/inside), tail currents reversed direction at -71 mV and the reversal potential shifted 50 mV per 10-fold change in  $[K^+]_o$ , as expected for a  $K^+$ -selective current. The tail currents were well described by a single exponential, and had similar time constants in different  $[K^+]_o$ , therefore this further suggests that the outwardly rectifying  $K^+$  current is the dominant outward current expressed in rabbit RPE cells.

The outward current in rabbit RPE cells was further characterized using pharmacological blockers of voltage-dependent  $K^+$  currents. Extracellular  $TEA^+$  and  $Ba^{2+}$ , which have been shown to block the delayed rectifier  $K^+$  currents in a variety of cell types including human (Strauß et al., 1993; Wen et al., 1993), monkey (Wen et al., 1993), frog (Hughes and Steinberg, 1990) and turtle (Fox and Steinberg, 1992) RPE cells, reversibly decreased outward  $K^+$  current in rabbit RPE cells. Low concentrations of 4-AP (0.1-1 mM) also reduced the outward current, however, the block obtained with 1 mM 4-AP was only partially reversible. The outward  $K^+$  current described here in rabbit RPE cells shows a similar pharmacological specificity to the outward  $K^+$  current described in frog RPE cells, where outward  $K^+$  current was also sensitive to block by low concentrations of 4-AP as well as by  $TEA^+$  and  $Ba^{2+}$  (Hughes and Steinberg, 1990).

The voltage-dependence and kinetics of the outwardly rectifying  $K^+$  current,  $I_K$ , in rabbit RPE cells, resembles the delayed rectifier  $K^+$  current described in several other non-excitable cells, such as T-lymphocytes (Cahalan et al., 1985; DeCoursey et al. 1987) and macrophages (Ypey and Clapham, 1984) as well as in isolated RPE cells from frog (Hughes and Steinberg, 1990) and turtle (Fox and Steinberg, 1992). The outward  $K^+$  current in rabbit RPE cells was similar in several ways to that found in frog and turtle RPE cells, for example it activated following a brief delay at potentials positive to -40 mV, it exhibited slow time-dependent decay at positive potentials and it was inactivated by depolarizing potentials of -30 mV or more positive. A delayed rectifier  $K^+$  current has also been described in whole-cell measurements of cultured human and monkey RPE cells, however, although the delayed rectifier in primate RPE cells activated over a



similar voltage-range to that found in rabbit RPE cells, it was virtually noninactivating (Wen et al., 1993).

## 2.2. Fast-inactivating outward rectifier

In a very small number of cultured rabbit RPE cells (7%), a fast inactivating outward  $K^+$  current,  $I_{Kt}$  was observed. In rabbit RPE cells,  $I_{Kt}$  activated around -50 mV or more negative and inactivated rapidly at depolarized potentials. Inactivation time constants for  $I_{Kt}$  at depolarized potentials, were 10-fold faster than time constants measured for the delayed rectifier current,  $I_K$ . However, the extremely small number of cells in which the fast inactivating current was found has precluded extensive characterization of the properties and conditions regulating  $I_{Kt}$ . The fast inactivating outward  $K^+$  current in rabbit RPE cells resembles the inactivating delayed rectifier  $K^+$  current,  $I_{nK}$ , described in T-lymphocytes (Cahalan et al., 1985; Lewis and Cahalan, 1988), macrophages (Ypey and Clapham, 1984), mouse Schwann cells (Konishi, 1989), and more recently in porcine granulosa cells (Mattoli, Barboni and DeFelice, 1993). In addition, a similar fast-inactivating outward  $K^+$  current, with a threshold for activation at potentials negative to -40 mV, has also been described in turtle RPE cells (Fox and Steinberg, 1992). Like the  $I_{Kt}$  found in rabbit RPE cells, which was completely blocked by quinine, the time- and voltage-dependent outward current in turtle RPE cells was abolished (>80% block) by quinidine, the D-stereoisomer of quinine. A fast transient outward  $K^+$  current which resembles neural A-type current, was also described as the dominant current in both fresh fetal (100%) and cultured adult (33%) human RPE cells.

This A-type current in human RPE cells was completely inhibited by 5 mM 4-AP and was suggested to be expressed as a result of cell dedifferentiation in culture (Wen et al., 1993).

### 2.3. Inward rectifier

In 40% of rabbit RPE cells an inwardly rectifying current was activated at hyperpolarized potentials. The inwardly rectifying current was shown to be carried by  $K^+$  ions based on its voltage-dependence, ionic selectivity and pharmacological blockage. The inward current was dependent on  $[K^+]_o$ , with the zero current potential shifting positive as  $[K^+]_o$  was increased. Examination of the time- and voltage-dependent decay of the inward current confirmed that current relaxations reversed direction close to  $E_K$ . The inward rectifier in rabbit RPE cells was blocked by both  $Ba^{2+}$  and  $Cs^+$ , which have been shown to block inward rectifiers in a number of different cell types (Standen and Stanfield, 1978; Gallin and McKinney, 1988a; Kelly et al., 1992; Ishikawa and Cook, 1993; Cooper et al., 1990 & 1991), including frog (Hughes and Steinberg, 1990), cultured human (Strauß et al., 1993; Wen et al., 1993) and monkey (Wen et al., 1993) RPE cells.

At hyperpolarized potentials rabbit RPE cells exhibited a time-dependent decay of the steady-state inward current, which was largely removed when external  $Na^+$  was replaced with NMDG<sup>+</sup>.  $Na^+$ -dependent reduction of the inward current at hyperpolarized potentials is also a characteristic of the inward rectifier found in frog skeletal muscle (Standen and Stanfield, 1979), macrophages (Gallin and Mckinney, 1988a), osteoclasts (Kelly et al., 1992) and mammalian lens epithelial cells (Cooper et al., 1991) and has

been attributed to low-affinity block within the conductive pathway of the inward rectifying  $K^+$  channel by  $Na^+$  ions. The inwardly rectifying  $K^+$  current in cultured human and monkey RPE cells also exhibits  $Na^+$ -dependent reduction at potentials negative to -120 mV, although  $Na^+$ -dependent inactivation was not observed in fresh primate cells (Wen et al., 1993).

The macroscopic inwardly rectifying  $K^+$  current in rabbit RPE cells exhibits similarities to the inward rectifier described in cultured primate RPE cells (Wen et al., 1993). For example the rabbit RPE inward rectifier exhibited both pronounced rectification at depolarized potentials, with less than 20% of maximum conductance still active around  $E_K$  ( $\approx 45$  pS/pF), as well as a strong dependence on extracellular  $[K^+]_o$ . In rabbit RPE cells, increases in  $[K^+]_o$  enhanced the inward  $K^+$  conductance and shifted both the zero current potential and the voltage around which the current rectified more positive. In contrast, the inward rectifier in frog RPE cells decreased more gradually at depolarizing voltages and the conductance did not increase with increasing  $[K^+]_o$ , although the reversal potential of the inward current in frog RPE cells was dependent on  $[K^+]_o$ .

### **3. Calcium-activated $K^+$ current in rabbit RPE cells**

The properties and types of  $K^+$  currents have been studied in RPE cells from a number of different species. These studies have provided useful data regarding the ion selectivity and voltage-dependence of inward and outward rectifying  $K^+$  currents, however, little information is available concerning the presence of  $Ca^{2+}$ -activated  $K^+$

currents in RPE cells, despite the fact that they are present in a variety of cell types including epithelial cells (Rudy, 1988). Calcium-activated  $K^-$  channels require both  $Ca^{2+}$  and membrane depolarization for their activation (Magleby and Pallotta, 1983). Calcium affects many ion channels through several different mechanisms including surface charge effects (Hille, 1992, Chapter 13), interactions with the gating machinery (Gilly and Armstrong, 1982), and acting as a second messenger which stimulates protein kinase C and  $Ca^{2+}$ -calmodulin kinases (Rudy, 1988). However, for the maxi- $K_{Ca}$  channels, it has now been clearly demonstrated that  $Ca^{2+}$  acts directly on the cytosolic surface of the channel at micromolar or lower concentrations to activate channel opening (Rudy, 1988). Calcium modulates the response of the channel to depolarizing potential by altering the voltage sensitivity of channel activation without any change in channel conductance. Similarly, changes in membrane potential also shift the  $Ca^{2+}$  sensitivity of the channel (Moczydlowski and Latorre, 1983). Thus increasing  $[Ca^{2+}]_i$  shifts the activation potential of the maxi- $K_{Ca}$  channels, and membrane depolarization can activate the channel in lower  $[Ca^{2+}]_i$ .

In this present study, we noticed that in approximately 25% of the cells recorded from under control conditions, the whole-cell currents appeared "noisy" at depolarized potentials. Subsequent removal of  $Ca^{2+}$  from the extracellular perfusate reduced the outward  $K^-$  current by  $\approx 60\%$  and eliminated the channel noise in the current traces (chapter 3, section 5.1). This suggests that large-conductance  $Ca^{2+}$ -activated  $K^-$  (maxi- $K_{Ca}$ ) channels may be present in rabbit RPE cells. Further investigation showed that the outward current was enhanced by the  $Ca^{2+}$  ionophore ionomycin. In the presence of this

ionophore, the degree of enhancement of the outward  $K^+$  current was dependent on both the membrane potential and extracellular  $Ca^{2+}$  concentration. Furthermore, increasing extracellular  $Ca^{2+}$  in the presence of the ionophore shifted the activation potential of the outward current, confirming that the activation of the outward current varied according to intracellular  $Ca^{2+}$  concentration. The outward current was reduced 64% by IbTX at +60 mV. IbTX, a polypeptide toxin extracted from the venom of *Buthus tamulus* scorpion, is a highly selective channel blocker for the maxi- $K_{Ca}$  channels (Miller et al., 1985; Candida et al., 1992; Giangiacomo et al., 1992).

Single-channel recordings from cell-attached and excised membrane patches conclusively demonstrated the presence of the  $K_{Ca}$  channels in rabbit RPE cells. The properties of these channels closely resemble those of  $K_{Ca}$  channels found in other cell membranes from different species and tissues (Cecchi et al., 1986; Gallin and McKinney 1988b; Perez, Toro, Erulkar and Stefani, 1993; Wade and Sims, 1993). Activation of the  $K_{Ca}$  channel in rabbit RPE cells is sensitive to intracellular free  $[Ca^{2+}]_i$ . The probability of channel opening increased from 0.04 when the cytosolic membrane surface was exposed to  $Ca^{2+}$  concentrations of  $< 10^{-8}$  M, to  $> 0.8$  when  $Ca^{2+}$  was increased to  $10^{-3}$  M. The range of  $Ca^{2+}$  sensitivity for activation of  $K_{Ca}$  channels in rabbit RPE cells, over the voltage range -60 to +60 mV, is similar to that described for maxi- $K_{Ca}$  channels found in secretory cells such as chromaffin, salivary and pancreatic acinar cells (Petersen and Maruyama, 1984; Marty, 1987 & 1989). By contrast, in cultured rat muscle cells and smooth muscle cells from the human myometrium, depolarization over a similar voltage range has been shown not to evoke channel opening at  $[Ca^{2+}]_i$  of  $10^{-8}$  M and to have

virtually no effect at  $10^{-7}$  M.

The slope conductance for the  $K_{Ca}$  channel, estimated from both cell-attached and excised patch recordings in high symmetric  $K^+$ , was  $> 220$  pS therefore, the  $K_{Ca}$  channel observed in rabbit RPE cells could be classified as a maxi- $K_{Ca}$  channel. The channels were selective for  $K^+$ , with alterations in  $K^+$  concentration in the bath resulting in changes in both the current reversal potential and conductance. The change in conductance of  $K_{Ca}$  channels observed with alterations in  $[K^+]$  is consistent with previous studies by Cecchi and co-workers (1986), demonstrating that conductance is a saturating function of salt activity for maxi- $K_{Ca}$  channels. In their study, they reported that the slope conductance of maxi- $K_{Ca}$  channels saturates with increased symmetric  $[K^+]$  and that the current- $[K^+]$  curve markedly deviates from a hyperbolic function. These observations suggest the presence of multiple saturable binding sites within the channel (Cecchi et al., 1986).

The maxi- $K_{Ca}$  channels in rabbit RPE cells are sensitive to  $Ba^{2+}$ , which also blocks macroscopic outward  $K^+$  currents in these cells. Furthermore, in cell-attached recordings where IbTX was included in the pipette,  $K_{Ca}$  channel activity was observed in only 14% of patches (1/7) as compared to being found in 75% (12/16) of patches when 130 mM  $K^+$  standard pipette solution was used (data not shown). The pharmacological profile of the single-channel currents is consistent with the whole-cell data and provides further verification for the presence of maxi- $K_{Ca}$  channels in cultured rabbit RPE cells.

The mechanisms by which increases in  $[Ca^{2+}]_i$  occur in rabbit RPE cells is not clear. The lack of evidence for the presence of voltage-dependent  $Ca^{2+}$  channels under the experimental conditions used (see Section 5) suggests that  $Ca^{2+}$  channels are not the

primary route for  $\text{Ca}^{2+}$  entry into the cell. This is consistent with the observed lack of effect of the  $\text{Ca}^{2+}$  channel blocker cadmium ( $\text{Cd}^{2+}$ , 1 mM) on the outward  $\text{K}^+$  current in rabbit RPE cells (data not shown). Although voltage-dependent  $\text{Ca}^{2+}$  channels have not been observed in rabbit RPE cells, high threshold dihydropyridine-sensitive (L-type)  $\text{Ca}^{2+}$  channels have been described in rat RPE cells (Ueda and Steinberg, 1993). Since the activation potential of dihydropyridine-sensitive  $\text{Ca}^{2+}$  channels is depolarized with respect to the activation potential of  $I_{\text{K}(\text{Ca})}$  and considerably depolarized to the resting membrane potential described for intact epithelium, high-threshold  $\text{Ca}^{2+}$  channels would be unlikely to play a prominent role in the activation of maxi- $\text{K}_{\text{Ca}}$  channels in RPE cells. However, under conditions when high-threshold  $\text{Ca}^{2+}$  channels are activated, they could contribute to the activation of maxi- $\text{K}_{\text{Ca}}$  channels in RPE cells. A G-protein activated non-selective cation current has been observed in rat RPE cells (Poyer, Ryan and Kelly, 1996), it is possible that activation of this non-selective cation current could depolarize the membrane potential closer to the activation potential for maxi- $\text{K}_{\text{Ca}}$  channels. In addition, an increase in  $[\text{Ca}^{2+}]_i$  as a result of transmembrane  $\text{Ca}^{2+}$  influx via this cation channel and  $\text{Ca}^{2+}$  release from intracellular stores, could increase the channel opening probability upon membrane depolarization and thereby, enhance  $\text{K}^+$  exit. The resultant  $\text{K}^+$  export from the cell could repolarize the membrane and control salt exit from the RPE.

Macroscopic maxi- $\text{K}_{\text{Ca}}$  current was recorded in approximately 70% of cultured rabbit RPE cells after ionomycin application in the standard external Ringer containing 2.5 mM  $\text{Ca}^{2+}$ , as well as after  $\alpha$ -adrenergic receptor stimulation in low  $[\text{Ca}^{2+}]$  external Ringer. The estimation of channel density obtained by dividing the amount of

ionomycin-induced macroscopic outward current measured at +60 mV by the measured unitary maxi- $K_{Ca}$  current amplitude and  $P_o$  at the same voltage in 2.5  $[Ca^{2+}]_i$ , gave a value of 12 - 16 channels per cell.

#### 4. Modulation of maxi- $K_{Ca}$ channel activity by $\alpha_1$ -adrenergic receptors

Maxi- $K_{Ca}$  channels are targets for modulation by a number of different neurotransmitters and hormones (Marty, 1987 & 1989; Petersen and Maruyama, 1984). This study demonstrated that  $\alpha_1$ -adrenergic receptor stimulation caused activation of maxi- $K_{Ca}$  channels in cultured rabbit RPE cells. Stimulation of  $\alpha_1$ -adrenergic receptors in many cell types involves G-protein mediated activation of phospholipase C, which in turn leads to the generation of two second messengers, DAG and  $IP_3$  (Alberts et al., 1994).

In this study, the  $\alpha_1$ -adrenergic receptor agonist, PhE, increased the macroscopic outward current and activated a large conductance (220 pS) unitary current in low  $[Ca^{2+}]_o$  (100 nM). The concentration of external  $Ca^{2+}$  (100 nM) was kept low in order to eliminate any possible  $Ca^{2+}$  influx from the extracellular solution. At the whole-cell level, the PhE-induced portion of the depolarization-activated outward current was blocked by IbTX (1 nM), a specific maxi- $K_{Ca}$  channel blocker (Fig. 3-28). Introduction of  $IP_3$  into the cytosol mimicked PhE effects on maxi- $K_{Ca}$  currents indicating a possible involvement of the  $IP_3$  signalling pathway in the mediation of the PhE effect. Furthermore, the PhE effect on maxi- $K_{Ca}$  currents was inhibited by nanomolar concentration of prazosin, a selective  $\alpha_1$ -adrenergic receptor antagonist. In cell-attached single-channel recordings, the unitary currents induced by PhE reversed at approximately



0 mV with 130 mM  $K^+$  in both the bath and recording pipette solutions (Fig. 3-31B). PhE caused channel opening at less positive potentials (Fig. 3-31), exactly what would be expected to occur with an elevation of  $[Ca^{2+}]_i$ . Therefore, both the whole-cell and single-channel findings are consistent with PhE releasing  $Ca^{2+}$  from intracellular stores, and subsequently activating maxi- $K_{Ca}$  channels. The effect may be due, in part, to the activation of the  $IP_3$  pathway via stimulation of  $\alpha_1$ -adrenergic receptors. The number of cells in which maxi- $K_{Ca}$  channel activity was increased upon PhE application was also approximately 70%, which is consistent with the findings observed in the presence of ionomycin.

## 5. Other currents in rabbit RPE cells

The rabbit RPE cell membrane is dominated by  $K^+$  conductances. No evidence for voltage-dependent  $Na^+$  or  $Ca^{2+}$  currents was obtained using either standard whole-cell or perforated-patch recordings, even under conditions which would favour their identification (i.e. blocking  $K^+$  currents or  $K^+$  and  $Na^+$  ion substitution). Although a depolarization-activated  $Ca^{2+}$  current was not observed, it is possible that in cultured rabbit RPE cells  $Ca^{2+}$  channels are expressed at very low densities and may not be observed using standard  $Ca^{2+}$  concentrations. Ueda and Steinberg (1993) observed sustained high-threshold voltage-activated  $Ca^{2+}$  channels which were dihydropyridine sensitive and resembled neuronal L-type  $Ca^{2+}$  channels in fresh and cultured rat RPE cells. Low-threshold voltage-activated  $Ca^{2+}$  channels were not found in their study. L-type  $Ca^{2+}$  channels were also demonstrated in human RPE cells (Strauß and Wienrich,

1994).

## 6. Heterogeneity of $K^+$ channel type expression

The expression of individual  $K^+$  channel types in cultured rabbit RPE cells showed considerable heterogeneity with only 36% of studied cells expressing both inward and outward currents. Heterogeneity in the expression of  $K^+$  conductances has also been reported for cultured human RPE cells, with only 25% of cells recorded from exhibiting both inward and outward  $K^+$  conductances (Strauß et al., 1993). However, even in freshly isolated frog RPE cells only a portion of the cell population was found to express an inward rectifier and in those cells the expression of an inward  $K^+$  current was correlated with resting membrane potentials of -50 mV or greater (Hughes and Steinberg, 1990). In cultured rabbit RPE cells, no clear correlation between resting membrane potential and the expression of either outward or inward  $K^+$  currents was found. Recordings made from cells cultured for 24 hrs or between 2-5 days showed similar heterogenous distributions of  $K^+$  currents. It is known that RPE cells from different regions in the eye cup are anatomically different with cells from central region being taller and become flattened when extending peripherally. Therefore, it is possible that the heterogeneity in  $K^+$  channel type expression may reflect the functional differences of RPE cells from different regions of the eye cup.

With regard to the appearance of rapidly inactivating  $K^+$  current ( $I_{Kv}$ ) in 7% of rabbit RPE cells, it is possible that the infrequent appearance of this current may be the result of cell dedifferentiation in culture since this current was never observed in cells

cultured for less than 3 days. In other non-excitabile cells a direct link has been established between the expression of inactivating delayed rectifier current and cell proliferation including T-lymphocytes (Cahalan et al., 1985; Lewis and Cahalan, 1988), macrophages (Ypey and Clapham, 1984), mouse Schwann cells (Konishi, 1989), and porcine granulosa cells (Mattoli et al., 1993). In addition, a recent study examining whole-cell currents from both freshly isolated and cultured fetal and adult human RPE cells has demonstrated that a transient A-type  $K^+$  current is prominent in fresh human fetal RPE cells and expressed in 33% of the cultured adult human RPE cells (Wen et al., 1993). This A current was never observed in freshly isolated adult human RPE cells. The expression of different channel types in fresh fetal and adult human RPE cells indicates that the electrophysiological phenotype changes during RPE cell maturation. Therefore, it is suggested that ion channels may be developmentally regulated in mammalian RPE cells and that dedifferentiation to a more immature phenotype may occur when adult RPE cells are maintained in culture. The reversal of the maturation process in cultured rabbit RPE cells may be an indication of their potential capability to regenerate neural retina as suggested in other species (Wen et al., 1993) given the fact that these two tissues are embryonically coming from the same source: neural tube. This speculation is supported by a dedifferentiation model suggested by Neill and Barnstable (1990) for rat RPE cells in culture in which they reported that the mature rat RPE cells in culture re-expressed a cell adhesion molecule which is only expressed by embryonic RPE cells.

## 7. Functions of various $K^+$ conductances observed in rabbit RPE cells

Alterations in  $[K^+]$  in the subretinal space of the intact eye are known to occur following light-dark transitions and reflect changes in photoreceptor activity. These alterations in subretinal  $[K^+]$  induce a series of slow potential changes in both the apical and basolateral membranes of RPE cells and are accompanied by corresponding alterations in transepithelial potential (TEP) (Steinberg and Miller, 1979; Steinberg, Oakley and Neimeyer, 1980; Oakley and Steinberg, 1982; Immel and Steinberg, 1986; La Cour et al., 1986). The alterations in TEP generate three distinct components of the DC-ERG, named C-wave, fast oscillation and light peak (see Introduction, section 3.1). Experiments conducted using isolated RPE-choroid preparations and isolated cells derived from several vertebrate species, including rabbit, have now identified several different electrogenic, facilitated, and passive transport mechanisms at the RPE apical and basal membranes which may underlie those membrane potential events (Introduction, section 3.2 & 3.3). Figure 4-1 presents a model summarizing our present understanding of these ion transport mechanisms (Joseph and Miller, 1991; Quinn and Miller, 1992). The dashed-lines and squares represent ion transport mechanisms which have been inferred from this study. In the RPE, there are two pathways, cellular and paracellular, for transepithelial ion and fluid transport. The TEP provides the driving force for ion movement via the paracellular pathways (Edelman and Miller, 1991). The ouabain-sensitive  $Na^+-K^+$  pump is located on the apical membrane of RPE cells, this is in contrast to most of other epithelia in which this pump is located on the basolateral membrane. The apical pump location on the apical membrane of the RPE is functionally important

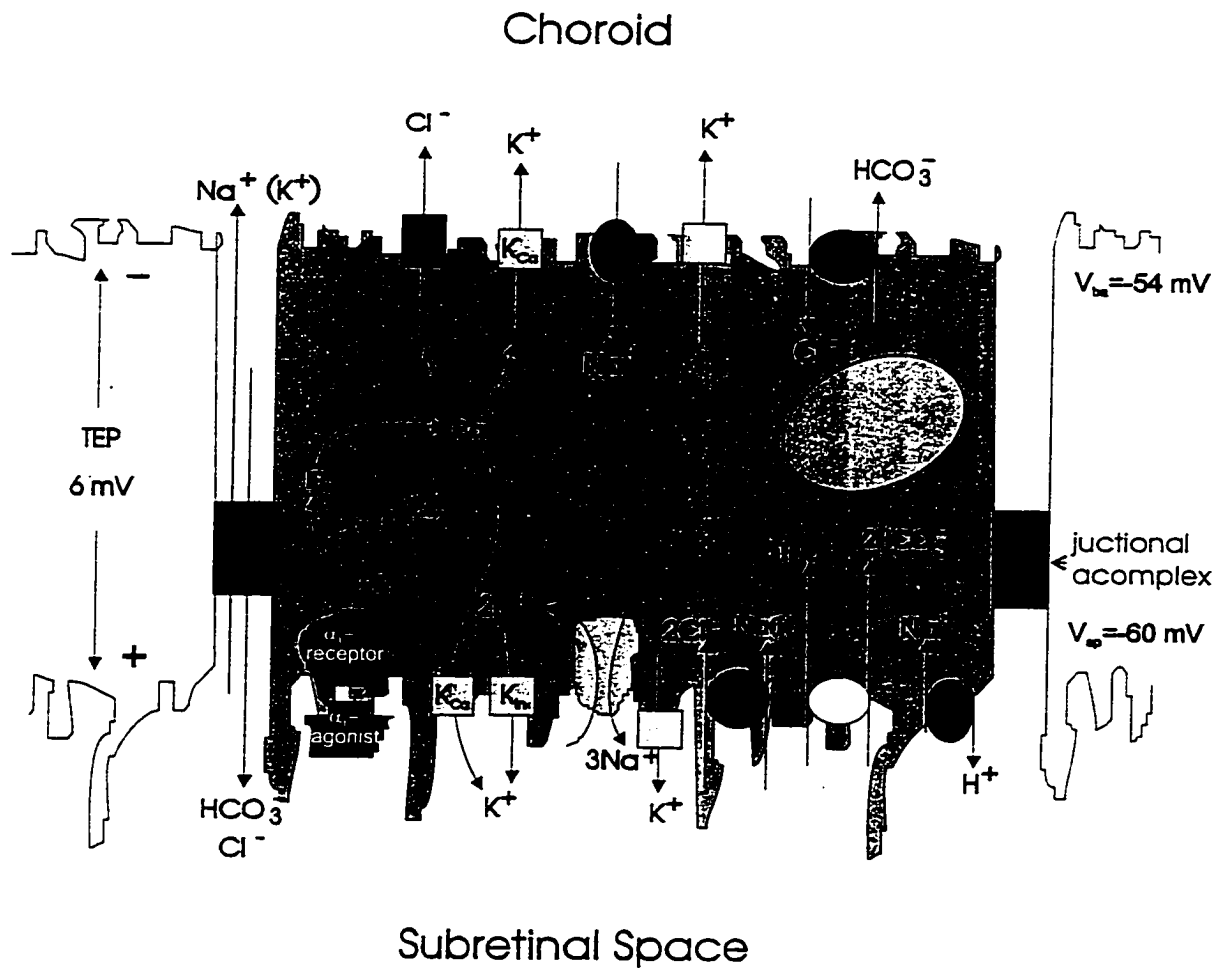


**Fig. 4-1.** Transport model of the RPE. Values of  $V_{\text{ch}}$ ,  $V_{\text{sp}}$  and TEP are taken from bovine RPE. See text for details. (Modified and reproduced from Edelman and Miller, 1991).

due to the fact that it is the only mechanism which returns  $\text{Na}^+$  to the subretinal space. All other transport mechanisms in the RPE which include  $\text{Na}^+$ - $\text{H}^+$  exchanger,  $\text{Na}^+$ - $\text{HCO}_3^-$  and  $\text{Na}^+$ - $\text{K}^+$ - $2\text{Cl}^-$  cotransporters, as well as the paracellular mechanisms move  $\text{Na}^+$  out of the subretinal space. Thus the  $\text{Na}^+$ - $\text{K}^+$  pump helps to maintain a  $\text{Na}^+$  gradient in the subretinal space, which is necessary for proper functioning of  $\text{Na}^+$ -dependent mechanisms located on both the photoreceptors (i.e. light-sensitive  $\text{Na}^+$  conductance and  $\text{Na}^+$ - $\text{Ca}^{2+}$  exchanger) and on the apical and basolateral membranes of RPE cells. As shown in figure 4-1, there are no apparent  $\text{Na}^+$  exit mechanisms at the basolateral membrane,  $\text{Na}^+$  uptake at the apical membrane is recycled into the subretinal space. Therefore, net  $\text{Na}^+$  transport across the RPE is determined by the balance between its secretion by the  $\text{Na}^+$ - $\text{K}^+$  pump and its absorption through the paracellular pathway, which is driven by the TEP. The TEP is normally maintained at a positive value, thus the direction of solute-coupled fluid transport is absorptive, from the apical to the basal membrane of the RPE. Decreasing the TEP can reverse the direction of net  $\text{Na}^+$  and fluid flux from absorptive to secretive, which has been suggested to account for the fluid accumulation in the subretinal space observed in central serous retinopathy (CSR) (Edelman and Miller, 1991). This hypothesis is supported by a recent report which indicated that the source of fluid and protein in serous retinal detachments is from choroidal fluid (Takeuchi et al., 1996).

Both the apical and basal membranes of the RPE contain  $\text{K}^+$  conductances. An inwardly rectifying  $\text{K}^+$  channel may be located on the apical membrane, this prediction is based upon the results derived from studies in isolated RPE-choroid preparations

demonstrating that the apical  $K^+$  conductance is more sensitive to  $Ba^{2+}$  than basal  $K^+$  conductance (Joseph and Miller, 1991) as well as on results obtained from this study which show that the inward rectifier  $K^+$  channel is more sensitive to  $Ba^{2+}$  than the delayed rectifier. The voltage-dependent  $K^+$  conductances described here, in cultured rabbit RPE cells, could provide conductive pathways which would support the activities of active  $K^+$  transporters including electrogenic pump and facilitated co-transporter, and contribute to  $[K^+]$  homeostasis in the subretinal space. Decreases in subretinal  $[K^+]$ , following light-induced activation of photoreceptors, transiently hyperpolarize the RPE apical membrane. This hyperpolarization can activate the inward rectifier  $K^+$  current, which would in turn limit the hyperpolarization by clamping the membrane potential around  $E_K$  and increasing  $K^+$  efflux to the subretinal space through this channel. The transient hyperpolarization of the RPE apical membrane also inhibits the  $Na^+-K^+$  pump (Joseph and Miller, 1991) resulting in less active  $K^+$  transport into the cell. The pump inhibition limits the apical membrane hyperpolarization which is in favor of  $K^+$  efflux through the inward rectifier. Subsequent reaccumulation of  $[K^+]$  in the subretinal space and the resulting recovery from membrane hyperpolarization would then decrease the inwardly rectifying  $K^+$  conductance, thereby minimizing  $K^+$  efflux through this channel and allowing the resumption of electrogenic  $K^+$  transport into the cell. This mechanism may contribute to the reaccumulation of  $K^+$  in the subretinal space during phase II of the RPE's response to light onset (see Introduction, section 3.3 & Table 1-1, pp. 19). It may also indirectly influence  $Na^+$  transport across the RPE.

The outwardly rectifying  $K^+$  conductances, which include delayed rectifier and

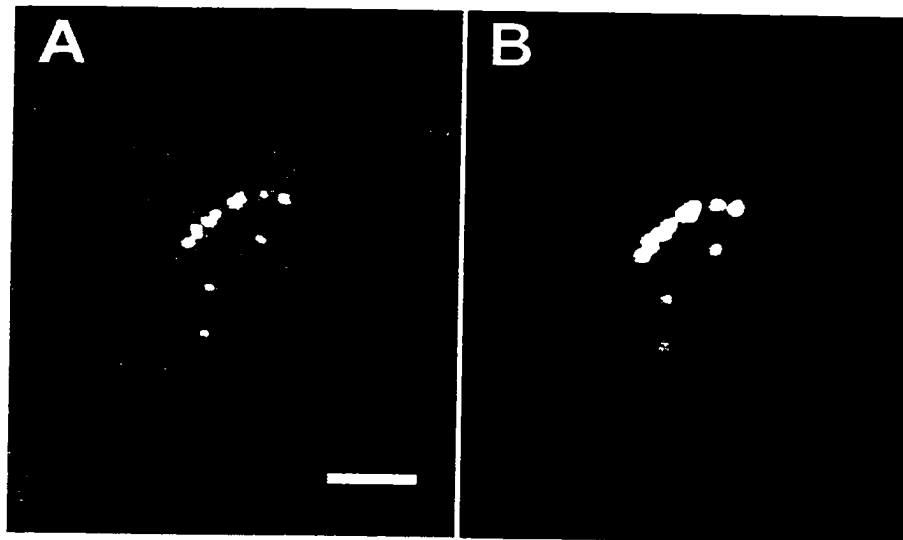


**Fig. 4-2.** Phagocytotic function of cultured rabbit RPE cells is well maintained. Cultured rabbit RPE cells were co-incubated with fluorescent latex beads. After a one-hour incubation, the culture dishes were thoroughly washed with culture media to remove unattached latex beads and the RPE cells were incubated overnight to allow ingestion of the beads. The cells were treated with trypsin/EDTA to ensure the removal of any latex beads which were not ingested by the cells but were simply bound to the cell surface. The cells were then transferred to a new dish, and were viewed using both fluorescent and phase microscopy. (A) Photomicrographs of an isolated rabbit RPE cell incubated with fluorescent latex beads and viewed with fluorescent and phase microscopy. (B) Corresponding photograph viewed using only fluorescence. Bar equals 10  $\mu\text{m}$ .



$\text{Ca}^{2+}$ -activated  $\text{K}^+$  channels, in rabbit RPE cells may provide efflux pathways for  $\text{K}^+$  which enters the cell via electrogenic and facilitated  $\text{K}^+$  transporters. In exocrine cells from other tissues, maxi- $\text{K}_{\text{Ca}}$  channels are integral to the export of  $\text{K}^+$ . However, since the activation threshold for the outwardly rectifying  $\text{K}^+$  current, which is the predominant outward  $\text{K}^+$  conductance observed in rabbit RPE cells, was close to the resting potential measured for these cells in culture, and was considerably depolarized with respect to values measured for the membrane potential of the intact epithelium in several species (Miller and Steinberg, 1977a; Steinberg, Miller and Stern, 1978; Joseph and Miller, 1991), therefore it is unlikely that this current would contribute significantly to  $\text{K}^+$  export at membrane potentials close to the resting membrane potential of the cell. Phagocytosis of shed photoreceptor outer segments is one of the major roles of RPE cells. Activation of outward  $\text{K}^+$  conductances accompanied by membrane hyperpolarization has been demonstrated to contribute to the membrane potential alterations associated with phagocytosis of particles by macrophages (Ince et al., 1987 & 1988). Preliminary results from our experiments (Fig. 4-2) and other published studies (Clark, 1986) demonstrated that the phagocytosis function is well maintained in cultured RPE cells. Thus, it is possible that, in addition to ion transport,  $\text{K}^+$  channels such as the delayed rectifier  $\text{K}^+$  current and the maxi- $\text{K}_{\text{Ca}}$  current may be involved in phagocytic activities of the RPE cells and may also contribute to other cellular functions concerned with the maintenance of photoreceptor cell viability.

## **8. Physiological implications of maxi- $\text{K}_{\text{Ca}}$ channel modulation by $\alpha_1$ -**

### **adrenergic receptors**

A role of maxi- $K_{Ca}$  channels in electrolyte transport has been proposed in a variety of cell types (Bolivar and Cereijido, 1987; Kolb, Paulmichl and Lang, 1987; Marty, 1989). Since both the choroid and the retina vasculature are innervated by sympathetic neurons and intrinsic EPI-containing neurons (amacrine cells) which are responsive to light have been demonstrated in the retina, the modulation of maxi- $K_{Ca}$  channel activity by NE and EPI could provide a mechanism for both the paracrine and endocrine regulation of transepithelial ion and fluid transport, as well as in regulating other functions in the RPE which include phagocytosis. It is demonstrated in this study that maxi- $K_{Ca}$  channels are modulated by  $\alpha_1$ -adrenoreceptor stimulation in rabbit RPE cells. The possible physiological and clinical relevance of this modulation is discussed below.

#### **8.1. Subretinal ion and fluid absorption**

Stimulation of  $\alpha_1$ -adrenoreceptors has been reported to affect transepithelial potential in rabbit and bovine RPE and to increase fluid absorption across the RPE (Frambach, et al. 1988b; Edelman and Miller, 1991; Joseph and Miller, 1992). These earlier findings can be explained by the results obtained in this study.  $\alpha_1$ -Adrenergic receptor stimulation activates apical maxi- $K_{Ca}$  channels causing  $K^+$  efflux, which will in turn, hyperpolarize the apical membrane. An increase in the basolateral  $Cl^-$  conductance upon  $\alpha_1$ -adrenoreceptor stimulation due to a transient increase in  $[Ca^{2+}]_i$ , has also been suggested in both rabbit and bovine RPE (Frambach, et al. 1988b; Edelman and Miller, 1991; Joseph and Miller, 1992). Increasing basolateral  $Cl^-$  conductance will result in

basolateral membrane depolarization. In addition, a  $K^+$  exit coupled with  $Cl^-$  exit has been suggested (Frambach et al., 1988b). This  $K^+$  exit route could be the maxi- $K_{Ca}$  channels. Coupled  $KCl$  efflux will leave the basolateral membrane potential unchanged. The hyperpolarization of the apical membrane will result in increases in TEP ( $TEP = V_{ba} - V_{ap}$ ), the driving force for paracellular  $Na^+$ ,  $K^+$  transepithelial transport. Thus, an overall increase in  $Na^+$ ,  $K^+$  +  $Cl^-$  and solute-coupled fluid absorption across the RPE occurs.

## 8.2. Phagocytosis

Given the fact that phagocytosis is one of the major functions of RPE cells, and the demonstration of a link between maxi- $K_{Ca}$  channel activation and phagocytosis in macrophages (Ince et al., 1987 & 1988), it is conceivable that  $\alpha_1$ -adrenoreceptor modulation of maxi- $K_{Ca}$  channels present in the apical membrane may participate in regulating the phagocytic action of RPE cells. This speculation is supported by the demonstration that phagocytic challenge with rod outer segment (ROS) is associated with an increase in  $IP_3$  generation in normal Long Evans rat RPE (Heth and Marescalchi, 1994), and the phagocytic defect in Royal College of Surgeons (RCS) rat RPE, is related to an abnormality in  $IP_3$  generation (Heth and Marescalchi, 1994; Heth, Marescalchi and Ye, 1995). The RCS rat is a dystrophic rat with a hereditary retinal degeneration caused by a defect in ROS phagocytosis by the RPE. Intracellular  $Ca^{2+}$  is suggested to be the link between the 2 events. However, the specific role of elevated intracellular  $Ca^{2+}$  following  $IP_3$  generation in ROS phagocytosis remains to be identified, since  $Ca^{2+}$  can also serve as a second messenger in the activation of  $Ca^{2+}$ -dependent kinases. Phagocytosis of shed

photoreceptor outer segments by RPE cells is essential for the renewal process of the photoreceptors and the maintenance of normal vision (Bok, 1993). The understanding of the roles which different ion transport pathways including  $K^+$  channels play, and their contribution to phagocytosis and other RPE functions may provide valuable clues towards the treatment of ocular diseases caused by functional deficiencies within the RPE.

**In summary**, viable and pure rabbit RPE cell cultures have been established. The use of in vitro cell models should facilitate further biochemical and molecular biological studies of RPE function. Both whole-cell and single-channel recordings have been routinely made from cultured rabbit RPE cells. Voltage-activated  $K^+$  currents from these cells have been recorded and characterized. Four different  $K^+$  currents have been distinguished on the basis of their voltage dependence, activation and inactivation characteristics,  $Ca^{2+}$  sensitivity and pharmacology. These currents may serve crucial roles in the regulation of the membrane potential, transepithelial ion and fluid transport, and in other vital RPE functions including phagocytosis. Maxi- $K_{Ca}$  channels are modulated by  $\alpha_1$ -adrenergic receptors through the  $IP_3$  signalling pathway, which elevates  $[Ca^{2+}]_i$  by releasing  $Ca^{2+}$  from intracellular stores. Whether other cytosolic second messenger pathways are also involved in the  $\alpha_1$ -adrenergic receptor modulation of maxi- $K_{Ca}$  channels in cultured rabbit RPE cells remains to be examined. The  $\alpha_1$ -adrenergic modulation of maxi- $K_{Ca}$  channels may contribute to the regulation of a variety of RPE functions, including fluid transport and phagocytosis.

# 5

## Future directions

---

### 1. To identify the location of maxi-K<sub>Ca</sub> channels on rabbit RPE cell membranes

The use of the cell-attached patch-clamp recording technique to record from freshly isolated RPE explants or cultured RPE monolayers will enable us to confirm whether maxi-K<sub>Ca</sub> channels are located on the apical membrane of the RPE. This information together with the results obtained from this study can further help our understanding of the role that this type of channel plays in RPE cells.

### 2. To characterize Cl<sup>-</sup> conductances in rabbit RPE cells

Basolateral Cl<sup>-</sup> conductances have been suggested to play important roles in fluid absorption across the RPE and are reported to be subjected to the  $\alpha_1$ -adrenergic modulation in tissue preparation (Joseph and Miller, 1991 & 1992). Whole-cell patch-clamp studies of Cl<sup>-</sup> channels at the single cell level will allow further examination of the role of Cl<sup>-</sup> channels in RPE transport functions and the regulation of these channels by receptor-coupled signalling pathways.

### 3. To define whether other intracellular signalling pathways are involved in $\alpha_1$ -adrenergic modulation

It will be important to determine whether other intracellular signalling pathways distinct from the IP<sub>3</sub> pathway, are involved in  $\alpha_1$ -adrenergic modulation. This can be

achieved by using pharmacological tools to activate or inhibit those pathways which are known to be involved following  $\alpha_1$ -adrenergic receptor activation in other systems.

# 6 Appendices

**The Rockefeller  
University Press**

1114 First Avenue, 4th Floor  
New York, New York 10021  
(212) 327-7938  
Fax (212) 327-8587

4 November 1996

Dear Dr. Tao:

We shall be glad to grant you permission for the reproduction of the material referred to in your letter of 28 October 1996.\*

Our only requirements are that you also obtain permission from the author(s) and give suitable acknowledgment to the source in the following manner: Reproduced from **The Journal of General Physiology** by copyright permission of The Rockefeller University Press.

Sincerely yours,

  
Iris Vallecilla  
Permissions

Dr. Qianping Tao  
Dalhousie University  
Department of Pharmacology  
Halifax, Nova Scotia  
B3H 4H7  
Canada

P.S. Since this article is over 10 years old, the author's permission is waived.

\*JGP-vol:83,213-232,1984 - fig. 8-for Thesis.



**Dalhousie University**  
Department of Pharmacology

**Qianping Tao M.D.**

Faculty of Medicine  
Halifax, Nova Scotia  
B3H 4H7  
Tel:(902) 494-3616  
Fax:(902) 494-1388

**RECEIVED**

Oct. 28, 1996

NOV 04 1996

Academic Press, Inc.  
Orlando, Florida 32887  
USA

**PERMISSIONS DEPARTMENT**

To whom it may concern:

I am writing to request permission to use one of the figures in a book chapter published by Academic Press, Inc. in 1986. The chapter title is "The cell biology of the retinal pigment epithelium" written by Clark, V. M.. The name of the book is "*The retina - a model for cell biology studies, Part II*" edited by R. Adler and D. Farber.

Enclosed are a copy of the front page of the book, a copy of the first page of the chapter, and a copy of the figure (Fig. 2) that I would like to use. I would deeply appreciate if your Inc. could allow me to use this figure for the introduction of my Ph.D. thesis.

Thank you very much for your attention on this matter; I look forward to hearing from you soon.

Sincerely yours,

Qianping Tao  
Ph.D. Candidate

PERMISSION GRANTED, provided that 1) complete credit is given to the source, including the Academic Press copyright notice; 2) the material to be used has appeared in our publication without credit or acknowledgement to another source; and 3) if commercial publication should result, you must contact Academic Press again.

We realize that University Microfilms must have permission to sell copies of your thesis, and we agree to this. However, we must point out that we are not giving permission for separate sale of your article.

---

Shirley P. Bias  
Paralegal  
Academic Press  
Orlando, FL

11/5/96



# 7

## References

---

- Adams, D.J. and Nonner, W., 1990. Voltage-dependent potassium channels: gating, ion permeation and block. In: *Potassium channels: structure, classification, function and therapeutic potential*. N.S. Cook, editor. pp 23-60. Ellis Horwood Ltd., Chichester, UK.
- Adorante, J.S., Hughes, B.A. and Miller, S.S., 1988. Electrogenic NaHCO<sub>3</sub> transport at the apical membrane of the frog retinal pigment epithelium (RPE). *FASEB J.* **2**:A1722
- Adorante, J.S. and Miller, S.S., 1990. Potassium dependent volume regulation in retinal pigment epithelium is mediated by Na,K,Cl cotransport. *J. Gen. Physiol.* **96**:1153-1176
- Alberts, B., Brag, D., Lewis, J. Raff, M., Roberts, K. and Watson, J.D., 1994. Cell Signalling. In: *Molecular biology of the cell*. Third edition, **Ch. 15**, pp 721-787. Garland Publishing, Inc., New York & London.
- Amigorena, S., Choquet, D., Teillaud, J.L., Korn, H. and Fridman, W.H., 1990. Ion channels and B cell mitogenesis. *Mol. Immunol.* **27**(12), 1259-68.
- Armstrong, C.M. and Hille, B., 1972. The inner quaternary ammonium ion receptor in potassium channels of the node of Ranvier. *J. Gen. Physiol.* **59**(4):388-400
- Armstrong, C.M. and Taylor, S.R., 1980. Interaction of barium ions with potassium channels in squid giant axons. *Biophys. J.* **30**, 473-88
- Armstrong, C.M. and Gilly, W.F., 1992. Access resistance and space clamp problems associated with whole-cell patch clamping. In: *Methods in enzymology*. Rudy, B. and Iverson, L.E. eds. **Vol. 207**, section 1, pp.100-122. Academic Press, Inc.
- Aronson, 1983. Human retinal pigment cell culture. *In Vitro* **19**:642-650
- Bernstein, P.S., Law, W.C. and Rando, R., 1987. Isomerization of all-*trans* retinoids to 11-*cis* retinoids in vitro. *Proc. Nat. Acad. Sci. USA* **84**:1849-1853
- Berweck, S., Lepple-Wienhues, A., Stöß, M. and Wiederholt, M., 1994. Large conductance calcium-activated potassium channels in cultured retinal pericytes

- under normal and high-glucose conditions. *Pflügers Arch.* 427:9-16
- Bird, A.C., 1989. Pathogenesis of serous detachment of the retina and pigment epithelium. In: *Retina*, vol. 2. B.M. Glaser and R.G. Michels, editors. pp 99-105. The C.V. Mosby Company, St.Louis, MO.
- Blatz, A.L. and Magleby, K.L., 1987. Calcium-activated K<sup>-</sup> channels. *Trends Neurosci.* 10:463-467
- Bok, D., 1988. Structure and Function of Retinal Pigment Epithelium-Photoreceptor Complex. In: *Retina diseases*. Mark O.M. Tso, editor. pp 3-48. J. B. Lippincott Company, Philadelphia.
- Bok, D., 1993. The Retinal Pigment Epithelium: a Versatile Partner in Vision. *J. Cell Sci. Suppl.* 17:189-195
- Bolivar, J.J. and Cerejido, M., 1987. Voltage and Ca<sup>2+</sup> activated K<sup>-</sup> channel in cultured epithelial cells (MDCK). *J. Membr. Biol.* 97:443-51
- Brown, K.T. and Wiesel, T. N., 1961. Localization of origins of electroretinogram components by intraretinal recording in the intact cat eye. *J. Physiol.* 158:257-280
- Brown, A.M., Yatani, A., Kirsch, G., Okabe, K., vanDongen, A.M.J. and Birnbaumer, L., 1991. Control of K<sup>-</sup> channels by G proteins. *J. Bioenerg. Biomemb.* 23:499-506
- Cahalan, M.D., Chandy, K.G., Decoursey, T.E. and Gupta, S., 1985. A voltage-gated K<sup>-</sup> channel in human T lymphocytes. *J. Physiol.* 358:197-237
- Candida, S., Garcia, M.L. and Latorre, R., 1992. Mode of action of iberiotoxin, a potent blocker of the large conductance Ca<sup>2+</sup>-activated K<sup>-</sup> channels. *Biophys. J.* 63:1-8
- Carl, A. and Sanders, K.M., 1990. Measurement of single channel open probability with voltage ramps. *J. Neurosci. Methods.* 33(2-3):157-163
- Cecchi, X., Alvarez, O. and Wolf, D., 1986. Characterization of a Calcium-activated potassium channel from rabbit intestinal smooth muscle incorporated into planar bilayers. *J Membr. Biol.* 91: 11-18.
- Chader, G.J., Aguirre, G.D. and Sanyal, S., 1988. Studies on Animal Models of Retinal Degeneration. In: *Retina diseases*. Mark O.M. Tso, editor. pp 3-48. J. B. Lippincott Company, Philadelphia.

- Chuang, E.L., Sharp, D.M., Fitzke, F.W., Kemp, C.M., Holden, A.L. and Bird, A.C., 1987. Retinal dysfunction in central serous retinopathy. *Eye*. **1**:120-125
- Clark, V.M., 1986. The cell biology of the retinal pigment epithelium. In: *The Retina-a model for cell biology studies. Part II*. R. Adler and D. Farber, editors. pp 129-132. Academic Press, Inc. London.
- Cole, W.C. and Sanders, K.M., 1989. G protein mediated suppression of Ca<sup>2+</sup>-activated K<sup>+</sup> current by acetylcholine in smooth muscle cells. *Am. J. Physiol.* **257**:c596-c600
- Cooper, K., Rae, J.L., Gates, P. and Dewey, J., 1990. Electrophysiology of cultured human lens epithelial cells. *J. Membrane Biol.* **117**:285-298
- Cooper, K., Rae, J.L. and Dewey, J., 1991. Inwardly rectifying potassium current in mammalian lens epithelial cells. *Am. J. Physiol.* **261**:C115-C123
- Corwin, D.J. and Gown, A.M., 1989. Review of selected lineage-directed antibodies useful in routinely processed tissues. *Arch. Pathol. Lab. Med.* **113**:645-652
- Decoursey, T.E., Chandy, K.G., Gupta, S. and Cahalan, M.D., 1987. Two types of potassium channels in murine T Lymphocytes. *J. Gen. Physiol.* **89**:379-404
- Dowling, J.E. 1987. The Approachable Retina. In: *The Retina: an Approachable Part of the Brain. Chap. 1*. pp 8-11. The Belknap Press of Harvard University Press. Cambridge, MA., USA.
- Dreyer, F., 1990. Peptide toxins and potassium channels. *Rev. Physiol. Biochem. Pharmacol.* **115**:93-136
- Eaton, D.C. and Brodwick, M.S., 1980. Effect of barium on the potassium conductance of squid axon. *J. Gen. Physiol.* **75**:727-750
- Edelman, J. L. and Miller, S. S., 1991. Epinephrine stimulates fluid absorption across bovine retinal pigment epithelium. *Invest. Ophthalmol. Vis. Sci.* **32**:3033-3040
- Edelman, J. L. and Miller, S. S., 1992. Epinephrine (EP) stimulates KCl and fluid absorption across the bovine retinal pigment epithelium (RPE). *Invest. Ophthalmol. Vis. Sci. Suppl.* **33**:1111
- Ernst, S.A., Palacios, J.R. and Siegel, G.J., 1986. Immunocytochemical localization of Na,K,ATPase catalytic polypeptide in mouse choroid plexus. *J. Histochem. Cytochem.* **34**:189-195

- Ford, A.P.D.W., Williams, T.J., Blue, D.R. and Clarke, D.E., 1994.  $\alpha_1$ -Adrenoceptor classification: sharpening Occam's razor. *TIPS*. **15**:167-170
- Fox, J.A., Pfeffer, B. and Fain, G., 1988. Single-channel recordings from cultured human retinal pigment epithelium. *J. Gen. Physiol.* **91**:193-222
- Fox, J.A. and Steinberg, R.H., 1992. Voltage-dependent currents in isolated cells of the turtle retinal pigment epithelium. *Pflügers Arch.* **420**:451-60
- Frambach, D.A. and Marmor, M.F., 1982. The rate and route of fluid reabsorption from the subretinal space of the rabbit. *Invest. Ophthalmol. Vis. Sci.* **22**:292-302
- Frambach, D.A. and Misfeldt, D.S., 1983. Furosemide-sensitive  $\text{Cl}^-$  transport in embryonic chicken retinal pigment epithelium. *Am. J. Physiol.* **244**:F679-685
- Frambach, D.A., Valentine, J. L. and Weiter, J. J., 1988a. Initial observations of rabbit retinal pigment epithelium-choroid-sclera preparations. *Invest. Ophthalmol. Vis. Sci.* **29**:814-817
- Frambach, D.A., Valentine, J.L. and Weiter, J.J., 1988b. Alpha-1-adrenergic receptors on rabbit retinal pigment epithelium. *Invest. Ophthalmol. Vis. Sci.* **29**:737-741
- Frambach, D. A., Fain, G. L., Farber, D. B. and Bok, D., 1990. Beta adrenergic receptors on cultured human retinal pigment epithelium. *Invest. Ophthalmol. Vis. Sci.* **31**:1767-1772
- Fuchs, U., Kivelä, T. and Tarkkanen, A., 1991. Cytoskeleton in normal and reactive human retinal pigment epithelial cells. *Invest. Ophthalmol. Vis. Sci.* **32**:3178-3186
- Fujii, S., Gallemore, R. P., Hughes, B. A. and Steinberg, R. H., 1992. Direct evidence for a basolateral membrane  $\text{Cl}^-$  conductance in toad retinal pigment epithelium. *Am. J. Physiol.* **262**:C374-383
- Fujisawa, K., Ye, J. and Zadunaisky, J.A., 1992. A Na/Ca exchange mechanism in apical membrane vesicles of the retinal pigment epithelium. *Invest. Ophthalmol. Vis. Sci. Suppl.* **33**:911
- Fukushima, Y., 1982. Blocking kinetics of the anomalous potassium rectifier of tunicate egg studied by single channel recording. *J. Physiol.* **331**:311-331
- Gallemore, R.P. and Steinberg, R.H., 1989. Effects of DIDS on the chick retinal pigment epithelium. II. Mechanism of the light peak and other responses originating at the

- basal membrane. *J. Neurosci.* 9(6):1977-19
- Gallin, E.K. and McKinney, L.C., 1988a. Inwardly rectifying whole-cell and single-channel K<sup>+</sup> currents in the murine macrophage cell line J774.1. *J. Memb. Biol.* 103:41-53
- Gallin, E.K. and McKinney, L.C., 1988b. Patch-clamp studies in human macrophages: single channel and whole-cell characterization of two K<sup>+</sup> conductances. *J. Membrane Biol.* 103:55-66
- Giangiaco, K.M., Garcia, M.L. and McManus, O.B., 1992. Mechanism of iberiotoxin block of the large-conductance calcium-activated potassium channel from bovine aortic smooth muscle. *Biochem.* 31:6719-6727
- Giangiaco, K.M., Sugg, E.E., Garcia, C.M., Leonard, R.J., McManus, O.B., Kaozorowski, G.J. and Garcia, M.L., 1993. Synthetic charybdotoxin-iberiotoxin chimeric peptides define toxin binding sites on calcium-activated and voltage-dependent potassium channels. *Biochem.* 32(9):2363-2370
- Gigi, O., Geiger, B., Eshhar, Z., Moll, R., Schmid, E., Winter, S., Schiller, D.L. and Franke, W. W., 1982. Detection of a cytokeratin determinant common to diverse epithelial cells by a broadly cross-reacting monoclonal antibody. *EMBO J.* 1:1429-1437
- Gilly, W.F. and Armstrong, C.M., 1982. Slowing of sodium channel opening kinetics in squid axon by extracellular zinc. *J. Gen. Physiol.* 79:935-964
- Gögelein, H., Capek, K., 1990. Quinine inhibits chloride and nonselective cation channels in isolated rat distal colon cells. *Biochem. Biophys. Acta* 1027:191-198
- Goldstein, S.A. and Miller, C., 1993. Mechanism of charybdotoxin block of a voltage-gated K<sup>+</sup> channel. *Biophys. J.* 65(4):1613-1619
- Graham, R.M., Perez, D.M., Piascik, M.T., Riek, R.P. and Hwa, J., 1995. Characterisation of  $\alpha_1$ -adrenergic receptor subtypes. *Pharmacol. Commu.* 6 (1-3):15-22
- Gregory, C.Y., Abrams, T.A. and Hall, M.O., 1994. Stimulation of A<sub>2</sub> adenosine receptors inhibits the ingestion of photoreceptor outer segments by retinal pigment epithelium. *Invest. Ophthalmol. Vis. Sci.* 35:819-825
- Gribkoff, V.K., Lum-Ragan, J.T., Boissard, C.G., Post-Munson, D.J., Meanwell, N.A., Starrett, J.E. Jr., Kozlowski, E.S., Romine, J.L., Trojnacki, J.T., Mckay,

- M.C., Zhong, J. and Dworetzky, S.I., 1996. Effects of channel modulators on cloned large-conductance calcium-activated potassium channels. *Mol. Pharmacol.* **50**(1): 206-17
- Hadjiconstantinou, M., Cohen, J. and Neff, N.H., 1983. Epinephrine: A potential neurotransmitter in retina. *J. Neurochem.* **41**:1440-1444
- Hadjiconstantinou, M., Mariani, A.P., Panula, P., Joh, T.H. and Neff, N.H., 1984. Immunohistochemical evidence for epinephrine-containing retinal amacrine cells. *Neurosci.* **13**(2):547-551
- Hamill, O.P., Marty, A., Neher, E., Sakmann, B. and Sigworth, F.J., 1981. Improved patch-clamp techniques for high-resolution current recording from cells and cell-free membrane patches. *Pflügers Arch.* **391**:85-100
- Harvey, R.D. and Ten Eick, R.E., 1988. Characterization of the inward rectifier potassium current in cat ventricular myocytes. *J. Gen. Physiol.* **91**(4):593-615
- Heginbotham, L. and MacKinnon, R., 1992. The aromatic binding site for tetraethylammonium ion on potassium channels. *Neuron.* **8**:483-491
- Heth, C.A. and Marescalchi, P.A., 1994. Inositol triphosphate generation in cultured rat retinal pigment epithelium. *Invest. Ophthalmol. Vis. Sci.* **35**(2):409-416
- Heth, C.A. Marescalchi, P.A. and Ye, I., 1995. IP<sub>3</sub> generation increases rod outer segment phagocytosis by cultured Royal College of Surgeons rat retinal pigment epithelium. *Invest. Ophthalmol. Vis. Sci.* **36**:980-989
- Hille, B., 1975. Ionic selectivity of Na<sup>+</sup> and K<sup>+</sup> channels of nerve membranes. In *Membranes: a series of Advances*. G. Eisenman, editor, 3:255-544. Marcel Dekker, New York.
- Hille, B., 1992. *Ionic channels of excitable membranes*. 2nd edition, **Ch. 13.**, pp 337-361. Sinauer Associates Inc., Sunderland, MA, USA.
- Hirsh, J. K. and Quandt, F.N., 1993. Aminopyridine block of potassium channels in mouse neuroblastoma cells. *J. Pharmacol. Exp. Ther.* **267**:604-611
- Hiscott, P.S., Grierson, I. and McLeod, D., 1984. Retinal pigment epithelial cells in epiretinal membranes: an immunohistochemical study. *Br. J. Ophthalmol.* **68**:708-715
- Horn, R. and Marty, A., 1988. Muscarinic activation of ionic currents measured by a

- new whole-cell recording method. *J. Gen. Physiol.* **92**:145-59
- Hoshi, T., Zagotta, W. N., Aldrich, R. W., 1991. Two types of inactivation in shaker K<sup>+</sup> channels: effects of alterations in the carboxy-terminal region. *Neuron.* **7**:547-556
- Hubel, D.H. and Wiesel, T.N., 1961. Integrative action in the cat's lateral geniculate body. *J. Physiol.* **155**:385-398
- Hubel, D.H. and Wiesel, T.N., 1962. Receptive fields, binocular interaction and functional architecture in the cat's visual cortex. *J. Physiol.* **160**:106-154
- Hughes, B.A., Miller, S.S. and Machen, T.E., 1984. Effects of cyclic AMP on fluid absorption and ion transport across frog retinal pigment epithelium: Measurements in the open-circuit state. *J. Gen. Physiol.* **83**:875-899
- Hughes, B.A., Miller, S.S., Joseph, D.P. and Edelman, J.L., 1988. Cyclic AMP stimulates the Na-K pump of the bullfrog retinal pigment epithelium. *Am. J. Physiol.* **254**:C84-98
- Hughes, B.A., Joseph, S.A., Miller, S.S. and Lin, H., 1989. Apical electrogenic NaHCO<sub>3</sub> cotransport: A mechanism for HCO<sub>3</sub><sup>-</sup> absorption across the retinal pigment epithelium. *J. Gen. Physiol.* **94**:125-150
- Hughes B.A., Botchkina, L.M. and Steinberg, R.H., 1990. Whole-cell currents in isolated retinal pigment epithelial (RPE) cells of the normal pigmented rat. *Invest. Ophthalmol. Vis. Sci. Suppl.* **31**:177
- Hughes B.A. and Steinberg, R.H., 1990. Voltage-dependent currents in isolated cells of the frog retinal pigment epithelium. *J. Physiol.* **428**:273-97
- Hurst, R.S., Kavanaugh, M.P., Yakel, J., Adelman, J.P. and North, R.A., 1992. Cooperative interactions among subunits of a voltage-dependent potassium channel. *J. Biol. Chem.* **267**:23742-23745
- Immel, J. and Steinberg, R.H., 1986. Spatial buffering of K<sup>+</sup> by the retinal pigment epithelium. *J. Neurosci.* **6**:3197-3204
- Ince, C., Duijn, B. van, Ypey, D.L., Bavel, E. van, Weidema, F. and Leijh, P.C.J., 1987. Ionic channels and membrane hyperpolarizations in human macrophages. *J. Memb. Biol.* **97**:251-258
- Ince, C., Coremans, J.M.C.C., Ypey, D.L., Leijh, P.C.J., Verveen, A.A., Van Furth, R.,

1988. Phagocytosis by human macrophages is accompanied by changes in ionic channel currents. *J. Cell Biol.* **106**:1873-1878
- Ishikawa, T. and Cook, D.I., 1993. Effects of K<sup>+</sup> channel blockers on inwardly and outwardly rectifying whole-cell K<sup>+</sup> currents in sheep parotid secretory cells. *J. Membr. Biol.* **133**:29-41
- Iwatsuki, N. and Petersen, O.H., 1985. Inhibition of Ca<sup>2+</sup>-activated K<sup>+</sup> channels in pig pancreatic acinar cells by Ba<sup>2+</sup>, Ca<sup>2+</sup>, quinine and quinidine. *Biochem. Biophys. Acta* **819**:249-257
- Jalkh, A.E., Jabbour, N., Avila, M.P., Trempe, C.L. and Schepens, C.L., 1984. Retinal pigment epithelium decompensation. I. Clinical features and natural course. *Ophthalmology.* **91**:1544-1548
- Joseph, D.P. and Miller, S.S., 1991. Apical and basal membrane ion transport mechanisms in bovine retinal pigment epithelium. *J. Physiol.* **435**:439-463
- Joseph, D.P. and Miller, S.S., 1992. Alpha-1-adrenergic modulation of K and Cl transport in bovine retinal pigment epithelium. *J. Gen. Physiol.* **99**:263-290
- Kavanaugh, M.P., Hurst, R.S., Yakel, J., Varnum, M.D., Adelman, J.P. and North, R.A., 1992. Multiple subunits of a voltage-dependent potassium channel contribute to the binding for tetraethylammonium. *Neuron.* **8**:493-497
- Kawamura, S., 1995. Phototransduction, excitation and adaptation. In: *Neurobiology and clinical aspects of the outer retina*. Djamgoz, M.B.A., Archer, S.N. and Vallerger, S. eds. pp 105-132. Chapman & Hall, London.
- Kelly, M.E.M., Dixon, S.J. and Sim, S.M., 1992. Inwardly rectifying potassium current in rabbit osteoclast: A whole-cell and single-channel study. *J. Membr. Biol.* **126**:171-181
- Kenyon, E., Lin, H. and Miller, S.S., 1991. Mechanisms of pH<sub>i</sub> regulation in the apical membrane of human RPE. *Invest. Ophthalmol. Vis. Sci. Suppl.* **32**:671
- Kirsch, G.E., Shieh, C.C., Drewe, J.A., Vener, D.F. and Brown, A.M., 1993. Segmental exchanges define 4-aminopyridine binding and the inner mouth of K<sup>+</sup> pores. *Neuron.* **11**:503-512
- Kolb, H.A., Paulmichl, M. and Lang, F., 1987. Epinephrine activates outward rectifying K channel in Madin-Darby canine kidney cells. *Pflügers Arch.* **408**:584-591



- Konishi, T., 1989. Voltage-dependent K<sup>+</sup> channels in mouse Schwann cells. *J. Physiol.* **411**:115-130.
- Kume, H., Graziano, M.P. and Kotlikoff, M.I., 1992. Stimulatory and inhibitory regulation of calcium-activated potassium channels by guanine nucleotide-binding proteins. *Proc. Natl. Acad. Sci. U.S.A.* **89**:11051-11055
- La Cour, M., Lund-Anderson, H. and Zeuthen, T., 1986. Potassium transport of the frog retinal pigment: autoregulation of potassium activity in the subretinal space. *J. Physiol.* **375**:461-479
- La Cour, M., 1989. Rheogenic sodium-bicarbonate co-transport across the retinal membrane of the frog retinal pigment epithelium. *J. Physiol.* **419**:539-553
- La Cour, M., 1991. Kinetic properties and Na<sup>+</sup> dependence of rheogenic Na<sup>+</sup>-HCO<sub>3</sub><sup>-</sup> co-transport in frog retinal pigment epithelium. *J. Physiol.* **439**:59-72
- Latorre, R. and Miller, C., 1983. Conduction and selectivity in potassium channels. *J. Membr. Biol.* **71**:11-30
- Latorre, R., Bacigalupo, J., Delgado, R. and Labarca, P., 1991. Four cases of direct ion channel gating by cyclic nucleotides. *J. Bioenerg. Biomemb.* **23**:577-597
- Lewis, R.S. and Cahalan, M.D., 1988. Subset-specific expression of potassium channels in developing murine T lymphocytes. *Science* **239**:771-775
- Lin, H. and Miller, S.S., 1991a. pH<sub>i</sub> regulation in frog retinal pigment epithelium: two apical membrane mechanisms. *Am. J. Physiol.* **261**:C132-142
- Lin, H. and Miller, S.S., 1991b. Apical epinephrine modulates [Ca<sup>2+</sup>]<sub>i</sub> in bovine retinal pigment epithelium. *Invest. Ophthalmol. Vis. Sci. Suppl.* **32**:671
- Lin, H. and Miller, S.S., 1992. Basolateral membrane pH<sub>i</sub>-dependent Cl-HCO<sub>3</sub> exchanger helps regulate intracellular pH (pH<sub>i</sub>) in frog retinal pigment epithelium (RPE). *Invest. Ophthalmol. Vis. Sci. Suppl.* **33**:911
- Lindau, M. and Fernandez, J.M., 1986. A patch-clamp study of histamine-secreting cells. *J. Gen. Physiol.* **88**:349-68
- Linsenmeier, R.A. and Steinberg, R.H., 1984. Delayed basal hyperpolarization of cat retinal pigment epithelium, and its relation to the fast oscillation of the DC Electroretinogram. *J. Gen. Physiol.* **83**:213-232

- Liu, C-M. And Hermann, T.E., 1978. Characterization of ionomycin as a calcium ionophore. *J. Biol. Chem.* **253(17)**:5892-5894
- Lu, L., Montrose-Rafizadeh, C., Hwang, T.C. and Guggino, W.B., 1990. A delayed rectifier potassium current in xenopus oocytes. *Biophys. J.* **57**:1117-1123
- Machemer, R. and Laqua, H., 1975. Pigment epithelium proliferation in retinal detachment (Massive periretinal proliferation) *Am. J. Ophthalmol.* **80**:1-23
- MacKinnon, R. and Miller, C., 1988. Mechanism of charybdotoxin block of  $Ca^{2+}$ -activated  $K^+$  channels. *J. Gen. Physiol.* **91**:335-349
- Magleby, K.L. and Pallotta, B.S., 1983. Calcium dependence of open and shut interval distributions from calcium-activated potassium channels in cultured rat muscle. *J. Physiol.* **344**:585-604
- Marmor, M.F., 1989. Mechanisms of normal retinal adhesion. In: *Retina*, vol. 3. B.M. Glaser, R.G. Michels, editors. pp. 71-88. The C.V. Mosby Company, St.Louis.
- Marty, A., 1987. Control of ionic currents and fluid secretion by muscarinic agonists in exocrine glands. *TINS* **10**: 373-377.
- Marty, A., 1989. The physiological role of calcium-dependent channels. *TINS* **12**: 420-424
- Mattioli, M.; Barboni, B. and DeFelice, L.J., 1993. Calcium and potassium currents in porcine granulosa cells maintained in follicular or monolayer tissue culture. *J. Membr. Biol.* **134(1)**:75-83
- Miller, S.S. and Steinberg, R.H., 1977a. Passive ionic properties of frog retinal pigment epithelium. *J. Membr. Biol.* **36**:337-372
- Miller, S.S. and Steinberg, R.H., 1977b. Active transport of ions across frog retinal pigment epithelium. *Exp. Eye Res.* **25**:235-248
- Miller, S.S., Hughes, B.A. and Machen, T.E., 1982. Fluid transport across retinal pigment epithelium is inhibited by cyclic AMP. *Proc. Natl. Acad. Sci. USA* **79**:2111-2115
- Miller, S.S. and Steinberg, R.H., 1982. Potassium transport across the frog retinal pigment epithelium. *J. Membr. Biol.* **67**:199-209
- Miller, C., Moczydlowski, E., Latorre, R. and Phillips, M., 1985. Charybdotoxin, a

- protein inhibitor of single  $\text{Ca}^{2+}$ -activated  $\text{K}^+$  channels from mammalian skeletal muscle. *Nature*. **313**:316-318
- Miller, S.S. and Edelman, J.L., 1990. Active ion transport pathways in the bovine retinal pigment epithelium. *J. Physiol.* **424**:283-300
- Misfeldt, D.S., Hamamoto, S.T. and Pitelka, D.R., 1976. Transepithelial transport in cell culture. *Proc. Natl. Acad. Sci. U.S.A.* **73**:1212-1216
- Moczydlowski, E. and Latorre, R., 1983. Gating kinetics of  $\text{Ca}^{2+}$ -activated  $\text{K}^+$  channels from rat muscle incorporated into planar lipid bilayers. *J. Gen. Physiol.* **82**:511-542
- Nakaoka, H., Perez, D.M., Baek, K.J., Das, T., Husain, A., Misono, K., Im, M.J. and Graham, R.M., 1994.  $G_{\beta}$ : A GTP-binding protein with transglutaminase activity and receptor signalling function. *Science*. **264**:1593-1596
- Neill, J.M. and Barnstable, C.J., 1990. Expression of the cell surface antigens RET-PE2 and N-CAM by rat retinal pigment epithelial cells during development and in tissue culture. *Exp. Eye Res.* **445**:537-548
- Nesselhut, T. and Osborne, N.N., 1982. Is noradrenaline a major catecholamine in the bovine retina? *Neurosci. Lett.* **28**:41-45
- Niemeyer, G., 1976. c-Waves and intracellular responses from the pigment epithelium in the cat. *Bibl. Ophthalmol.* **85**:68-74
- Noell, W.K., 1954. The origin of the electroretinogram. *Am. J. Ophthalmol.* **38**:78-90
- Oakley, B.H. and Green, D.G., 1976. Correlation of light-induced changes in retinal extracellular potassium concentration with the c-wave of the electroretinogram. *J. Neurophysiol.* **39**:1117-1133.
- Oakley, B.H., 1977. Potassium and the photoreceptor dependent pigment epithelial hyperpolarization. *J. Gen. Physiol.* **70**:405-424
- Oakley, B.H. and Steinberg, R.H., 1982. Effects of maintained illumination upon  $[\text{K}^+]_o$  in the subretinal space of the frog retina. *Vision Res.* **22**:767-773
- Ohmori, H., 1978. Inactivation and steady-state current noise in the anomalous rectifier of tunicate egg cell membrane. *J. Physiol.* **281**:77-99

- Ordway, R.W., Clapp, L.H., Gurney, A. M. Singer, J. J. and Walsh, J. V., Jr., 1989. Fatty acids directly activate large conductance, calcium-activated  $K^+$  channels in pulmonary artery smooth muscle cells from rabbit. *J. Gen. Physiol.* **94**:37a
- Osborne, N.N. and Nesselhut, T, 1982. Adrenaline: occurrence in the bovine retina. *Neurosci. Lett.* **39**:33-36
- Owaribe, K., Kartenbeck, J., Rungger-Brändle E. and Franke, W.W. , 1988. Cytoskeletons of retinal pigment epithelial cells: interspecies differences of expression patterns indicate independence of cell function from the specific complement of cytoskeletons proteins. *Cell Tissue Res.* **254**:301-315
- Park, D.H., Teitelman, M.J., Evinger, J.I., Woo, D.A., Ruggiero, D.A. and Albert, V.R., 1986. Phenylethanolamine-*N*-methyltransferase-containing neurons in rat retina: immunohistochemistry, immunochemistry, and molecular biology. *J. Neurosci.* **6**(4): 1108-1113
- Perez, D.M., Young, D. and Graham, R.M., 1993. Coupling of expressed  $\alpha_{1B}$  and  $\alpha_{1D}$ -adrenergic receptors to multiple signalling pathways is both G protein and cell type specific. *Mol. Pharmacol.* **44**:784-795
- Perez, G.J., Toro, L., Erulkar, S. and Stefani, E., 1993. Characterization of large-conductance calcium-activated potassium channels from human myometrium. *Am. J. Obst. Gynecol.* **168**:652-660.
- Petersen, O.H. and Maruyama, Y., 1984. Calcium-activated potassium channels and their role in secretion. *Nature* **307**: 693-696
- Pfeffer, B.A. and Newsome, D.A., 1983. Proliferation and differentiation of human and monkey RPE in culture. *Invest. Ophthalmol. Vis. Sci. Suppl.* **24**:143
- Pino, R.M. and Essner, E., 1981. Permeability of rat choriocapillaris to heme proteins. Restriction of traces by a fenestrated endothelium. *The J. Histochem. & Cytochem.* **29**:281-290
- Pino, R.M., Essner, E. and Pino, L.C., 1982. Permeability of the neonatal rat choriocapillaries to heme proteins and ferritin. *The Am. J. Anatomy.* **164**:334-341
- Poyer, J.F., Ryan J.S. and Kelly, M.E.M., 1996. G protein-mediated activation of a nonspecific cation current in cultured rat retinal pigment epithelial cells. *J. Membr. Biol.* **153**:13-26
- Price, D.T., Chari, R.S., Berkowitz, D.E., Mevers, W.C. and Schwinn, D.A., 1994.

- Expression of  $\alpha_1$ -adrenergic receptor subtype mRNA in rat tissues and human SK-N-MC neuronal cells: implication for  $\alpha_1$ -adrenergic receptor subtype classification. *Mol. Pharmacol.* **46**(2):221-226
- Quinn, R.H. and Miller, S.S., 1992. Ion transport mechanisms in native human retinal pigment epithelium. *Invest. Ophthalmol. Vis. Sci.* **33**:3513-3527
- Rae, J.L. and Levis, R.A., 1984. Patch voltage clamp of lens epithelial cells: theory and practice. *Mol. Physiol.* **6**:115-162
- Rae, J.L., 1993. Ion channels in ocular epithelia. *Invest. Ophthalmol. Vis. Sci.* **34**:2608-2612
- Rasmusson, R.L., Zhang, Y., Campbell, D.L. Comer, M.B., Castellino, R.C., Liu, S. and Strauss, H.C., 1995. Bi-stable block by 4-aminopyridine of a transient  $K^+$  channel (Kv1.4) cloned from ferret ventricle and expressed in *Xenopus* oocytes. *J. Physiol.* **485**(1):59-71
- Rodieck, R.W., 1972. Components of the electroretinogram--A reappraisal. *Vis. Res.* **12**:773-780
- Rudy, B., 1988. Diversity and ubiquity of K channels. *Neurosci.* **25**:729-749
- Saari, J.C., 1990. Enzymes and proteins of the mammalian visual cycle. In: *Progress in Retinal Research*. Osborne N. and Chader G., eds. pp: 363-82. Oxford: Pergamon Press.
- Sakmann, B. and Trube, G., 1984. Conductance properties of single inwardly rectifying potassium channels in ventricular cells from guinea-pig heart. *J. Physiol.* **347**:641-657
- Schneider, M.J., Rogowski, R.S., Krueger, B.K. and Blaustein, M.P., 1989. Charybdotoxin blocks both Ca-activated K channels and Ca-independent voltage-gated K channels in rat brain synaptosomes. *FEBS.* **250**(2): 433-436
- Schwinn, D.A., Page, S.O., Middleton, J.P. Lorenz, W., Liggett, S.B., Yamamoto, K., Lapetina, E.G., Caron, M.G., Lefkowitz, R.J. and Cotecchia, S., 1991. The  $\alpha_{1c}$ -adrenergic receptor: characterization of signal transduction pathways and mammalian tissue heterogeneity. *Mol. Pharmacol.* **40**:619-626
- Standen, N.B. and Stanfield, P.R., 1978. A potential- and time-dependent blockage of inward rectification in frog skeletal muscle fibres by barium and strontium ions. *J. Physiol.* **280**:169-191

- Standen, N.B. and Stanfield, P.R., 1979. Potassium depletion and sodium block of potassium currents under hyperpolarization in frog sartorius muscle. *J. Physiol.* **294**:497-520
- Stanfield, P.R., 1983. Tetraethylammonium ions and the potassium permeability of excitable cells. *Rev. Physiol. Biochem. Pharmacol.* **97**:1-67
- Starr, M.S., 1977. Prospective neurotransmitters in vertebrate retina, in *Essays in Neurochemistry and Neuropharmacology, Vol. 2*. Youdin, M.B.H., Lovenberg, W., Sharmas, D.F. and Langnado, J.R., eds, pp. 151-174. John Wiley & Sons, New York.
- Steinberg, R.H., Schmidt, R. and Brown, K.T., 1970. Intracellular responses to light from cat pigment epithelium: origin of the electroretinogram c-wave. *Nature* **227**:728-730
- Steinberg, R.H., Miller, S.S. and Stern, W.H., 1978. Initial observations on the isolated retinal pigment epithelium-choroid of the cat. *Invest. Ophthalmol. Vis. Sci.* **17**: 675-678
- Steinberg, R.H. and Miller, S.S., 1979. Transport and membrane properties of the retinal pigment epithelium. In: *The retinal pigment epithelium*. K.M. Zinn, M.F. Marmor, editors. pp 205-225. Harvard University Press, Cambridge, MA.
- Steinberg, R.H., Oakley, B.H. and Neimeyer, G., 1980. Light-evoked changes in  $[K^+]_o$  in retina of the intact cat eye. *J. Neurosci.* **44**:897-921
- Steinberg, R.H., Linsenmeier, R.A. and Griff, E.R., 1983. Three light-evoked responses of the retinal pigment epithelium. *Vis. Res.* **11**:1315-1323
- Steinberg, R.H., 1986. Research update: report from a workshop on cell biology of retinal detachment. *Exp. Eye Res.* **43**:695-706
- Steinberg, R.H., 1988. Electrical interactions between the RPE and the photoreceptors. In: *Retina diseases*. Mark O. M. Tso, editor. pp 60-79. J. B. Lippincott Company, Philadelphia.
- Strauß, O. and Weinrich, M., 1992. Retinal pigment epithelial cells from the rat in culture: Whole-cell recordings of membrane currents. *Invest. Ophthalmol. Vis. Sci.* **33**(suppl):1103
- Strauß, O., Richard, G. and Weinrich, M., 1993. Voltage-dependent potassium currents in cultured human retinal pigment epithelial cells. *Biochem. Biophys. Res. Comm.*

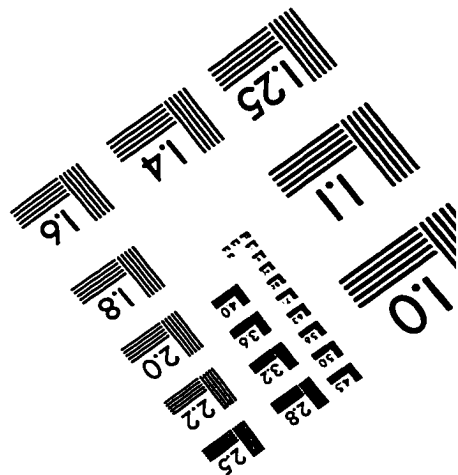
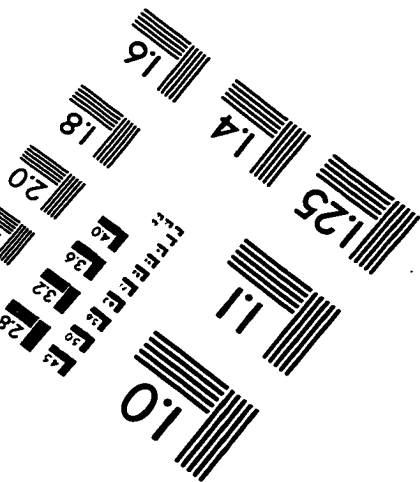
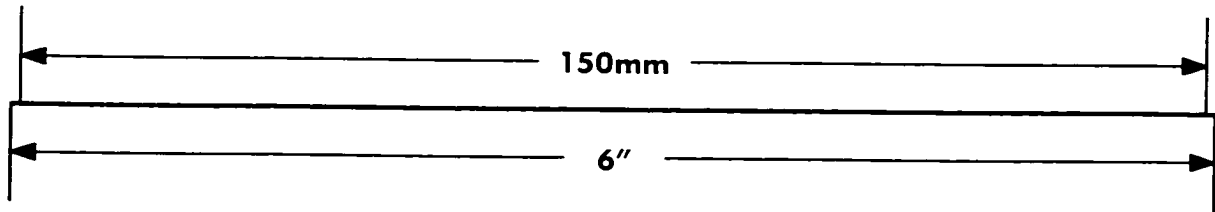
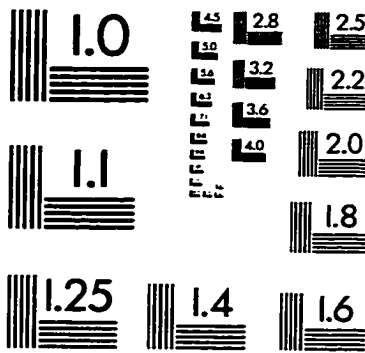
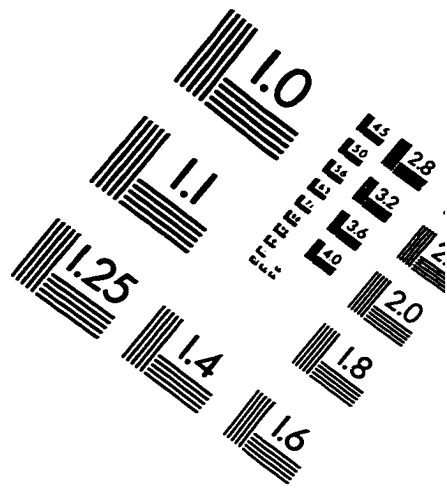
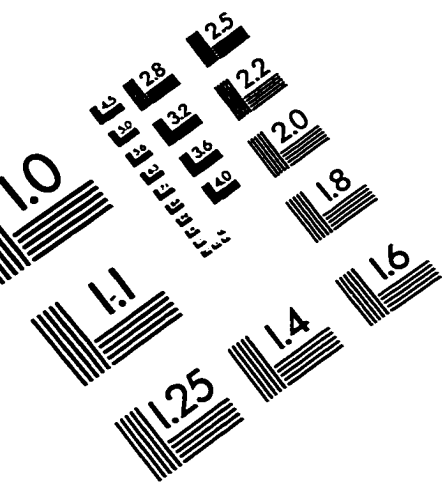
191:775-781

- Strauß, O. and Weinrich, M., 1994. TTX-sensitive  $Ca^{2+}$  channels in cultured retinal pigment epithelial cells. *Invest. Ophthalmol. Vis. Sci.* **35**(suppl):2127
- Sun, T-T., Eichner, R., Nelson, W.G., Tseng, S.C.G., Weiss, R.A., Jarvinen, M. and Woodcock-Mitchell, J., 1983. Keratin classes: molecular markers for different types of epithelial differentiation. *J. Invest. Dermatol.* **81** (1 Suppl):109s-115s
- Takeuchi, A., Kricorian, G., Wolfensberger, T.J. and Marmor, M.F., 1996. The source of fluid and protein in serous retinal detachments. *Curr. Eye Res.* **15**(7):764-767
- Topping, T.M., Abrams, G.W. and Macheimer, R., 1979. Experimental double-perforating injury of the posterior segment in rabbit eyes. *Arch. Ophthalmol.* **97**:735-742
- Toro, L., Ramos-Franco, J. and Stefani, E., 1990. GTP-dependent regulation of myometrial  $K_{Ca}$  channels incorporated into lipid bilayers. *J. Gen. Physiol.* **96**:373-394
- Toro, L. and Stefani, E., 1991. Calcium-activated  $K^+$  channels: metabolites regulation. *J. Bioenerg, Biomemb.* **23**(4):561-576
- Travo, P., Weber, K. and Osborn, M., 1982. Co-existence of vimentin and desmin type intermediate filaments in a subpopulation of adult rat vascular smooth muscle cells growing in primary culture. *Exp. Cell Res.* **139**:87-94
- Tseng, S.C.G., Jarvinen, M., Nelson, W.G., Huang, J-W., Woodcock-Mitchell, J. and Sun, T-T., 1982. Correlation of specific keratins with different types of epithelial differentiation: Monoclonal antibody studies. *Cell.* **30**:361-372
- Tso, Mark O.M. 1988. Comparison of pathologic changes in retinal photic injury and age-related macular degeneration. In: *Retinal diseases*. Mark O.M. Tso, editor. pp 207-208. J. B. Lippincott Company, Philadelphia.
- Tsuboi, S., Manabe, R. and Iisuka, S., 1986. Aspects of electrolyte transport across isolated dog retinal pigment epithelium. *Am. J. Physiol.* **250**:F781-784
- Ueda, Y. and Steinberg, R.H., 1993. Voltage-operated calcium channels in fresh and cultured rat retinal pigment epithelial cells. *Invest. Ophthalmol. Vis. Sci.* **34**:3408-3418
- Wade, G.R. and Sims, S.M., 1993. Muscarinic stimulation of tracheal smooth muscle

- cells activates a large-conductance  $\text{Ca}^{2+}$ -dependent  $\text{K}^+$  channel. *Am. J. Physiol.* **265**:C658-C665.
- Wen, R., Lui, G.M. and Steinberg, R.H., 1993. Whole-cell  $\text{K}^+$  currents in fresh and cultured cells of the human and monkey retinal pigment epithelium. *J. Physiol.* **465**:121-147
- Williams, D.S. and Fisher, S.K., 1987. Prevention of rod disk shedding by detachment from the retinal pigment epithelium. *Invest. Ophthalmol. Vis. Sci.* **28**:184-187
- Wu, S.M., 1988. Electrical interactions between the neuronal cells of the retina: encoding of visual images in the vertebrate retina. In: *Retina diseases*. Mark O.M. Tso, editor. pp 112-121. J. B. Lippincott Company, Philadelphia.
- Wu, D., Katz, A., Lee, C.H. and Simon, M.I., 1992. Activation of phospholipase C by  $\alpha_1$ -adrenergic receptors is mediated by the  $\alpha$  subunits of  $G_q$  family. *J. Biol. Chem.* **267**(36):25798-25802
- Ypey, D.L. and Clapham, D.E., 1984. Development of a delayed outward-rectifying  $\text{K}^+$  conductance in cultured mouse peritoneal macrophages. *Proc. Natl. Acad. Sci. USA.* **81**:3083-3087
- Zauberman, H., 1979. Adhesive forces between the retinal pigment epithelium and sensory retina. In: *The retinal pigment epithelium*. K.M. Zinn, M.F. Marmor, editors. pp 192-202. Harvard University Press, Cambridge, MA.
- Zinn, K.M., Benjamin-Henkind, J.V., 1979. Anatomy of the human retinal pigment epithelium. In: *The retinal pigment epithelium*. K.M. Zinn, M.F. Marmor, M.F. editors. pp3-27. Harvard University Press, Cambridge, MA.



# IMAGE EVALUATION TEST TARGET (QA-3)



**APPLIED IMAGE, Inc**  
 1653 East Main Street  
 Rochester, NY 14609 USA  
 Phone: 716/482-0300  
 Fax: 716/288-5989

© 1993, Applied Image, Inc., All Rights Reserved